

**A STUDY INTO THE MECHANISM OF CRYSTAL
GROWTH RATE DISPERSION**

Miss Pareena Pantaraks

**A Thesis Submitted in Partial Fulfillment of the Requirements for the
Degree of Doctor of Philosophy in Chemical Engineering**

Suranaree University of Technology

Academic Year 2004

ISBN 974-533-342-5

การศึกษากลไกการกระจายของอัตราการใช้ของผลึก

นางสาวปาริณา พันธรักษ์

วิทยานิพนธ์นี้เป็นส่วนหนึ่งของการศึกษาหลักสูตรปริญญาวิศวกรรมศาสตรดุษฎีบัณฑิต

สาขาวิศวกรรมเคมี

มหาวิทยาลัยเทคโนโลยีสุรนารี

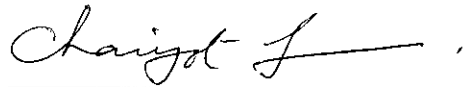
ปีการศึกษา 2547

ISBN 974-533-342-5

**A STUDY INTO THE MECHANISM OF CRYSTAL
GROWTH RATE DISPERSION**

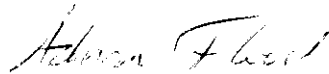
Suranaree University of Technology has approved this thesis submitted in partial fulfillment of the requirements for the Degree of Doctor of Philosophy.

Thesis Examining Committee



(Assoc. Prof. Dr.Chaiyot Tangsathitkulchai)

Chairperson



(Asst. Prof. Dr.Adrian Flood)

Member (Thesis Advisor)



(Assoc. Prof. Dr.Kenneth Haller)

Member



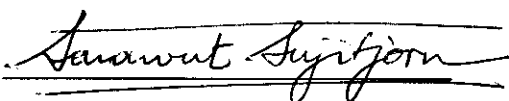
(Dr.Teerasut Sookumnerd)

Member



(Dr.Sopark Sornwai)

Member



(Assoc. Prof. Dr.Sarawut Sujitjorn)

Vice Rector for Academic Affairs



(Assoc. Prof. Dr.Vorapot Khompis)

Dean of Institute of Engineering

ปาริณา พันธรักษ์ : การศึกษากลไกการกระจายของอัตราการโตของผลึก (A STUDY INTO THE MECHANISM OF CRYSTAL GROWTH RATE DISPERSION)
 อาจารย์ที่ปรึกษา: ผู้ช่วยศาสตราจารย์ ดร.เอเดรียน ฟลัด, 122 หน้า. ISBN 974-533-342-5

การกระจายของอัตราการโตของผลึก/ จีอาร์ดี/ ความขรุขระของผิวผลึก

จุดมุ่งหมายหลักของวิทยานิพนธ์นี้คือเพื่อเข้าใจในปรากฏการณ์การกระจายของอัตราการโตของผลึก (จีอาร์ดี) ให้ดีขึ้น ซึ่งแสดงถึงผลึกที่มีลักษณะเหมือนกันและอยู่ในสภาวะเงื่อนไขเดียวกัน แต่กลับโตด้วยอัตราการโตที่แตกต่างกัน วิทยานิพนธ์นี้ได้ทำการศึกษาว่า (ก) กลไกการโตใดที่เป็นสาเหตุให้มีการกระจายตัวของอัตราการโตของผลึก (การแพร่ผ่าน และ/หรือการรวมตัวของผิว) (ข) สาเหตุของแต่ละกลไกที่ทำให้เกิดการกระจายตัวของอัตราการโตของผลึก และ (ค) เครื่องตกลึกที่ประดิษฐ์ใช้ในการทดลองมีผลกระทบต่อการวัดอัตราการกระจายตัวของผลึกในการวิจัยทั่วไปหรือไม่

การศึกษาอัตราการโตและอัตราการละลายของผลึกน้ำตาลภายใต้สภาวะหยุดนิ่ง และสภาวะที่มีการไหลเวียนในเครื่องตกลึกสามชนิด ได้แก่ เครื่องตกลึกขนาดเล็ก เครื่องตกลึกแบบท่อ และเครื่องตกลึกขนาด 2 ลิตร ให้ผลแสดงว่า สิ่งประดิษฐ์ของเครื่องตกลึกขนาดเล็กทำให้เกิดจีอาร์ดีสูงกว่าเครื่องตกลึกอีกสองชนิดประมาณ 1.2-1.5 เท่าภายใต้สภาวะที่มีการไหลเวียน ผลที่เกิดจากสิ่งประดิษฐ์คือ ในเครื่องตกลึกขนาดเล็กภายใต้สภาวะที่มีการไหลเวียน ผลึกต่างกันจะประสบกับสภาวะการไหลเวียนของสารละลายต่างกัน

จากการศึกษาพบว่ามีผลที่แสดงให้เห็นว่ามีความเป็นไปได้สำหรับการกระจายตัวของอัตราการโตทั้งในขั้นตอนการแพร่ผ่านและการรวมตัวของผิว ผลศึกษานี้ได้มาจากการศึกษาอัตราการโตและอัตราการละลายของผลึกน้ำตาลและผลึกเฮกซะเมทิลีนเตตระมีน หรือ ผลึกเอชเอ็มที ในสภาวะหยุดนิ่ง การโตของผลึกเอชเอ็มทีถูกควบคุมด้วยกลไกการแพร่ผ่าน ในขณะที่การโตของผลึกน้ำตาลบางส่วนถูกควบคุมด้วยกลไกการรวมตัวของผิว ในที่ที่มีอัตราการไหลเวียนสูง การโตของผลึกทั้งน้ำตาลและ เอชเอ็มทีถูกควบคุมด้วยกลไกการรวมตัวของผิว ทั้งผลึกน้ำตาลและผลึกเอชเอ็มที แสดงการกระจายตัวของอัตราการโต และอัตราการละลายของผลึกอย่างมีนัยสำคัญ ภายใต้สภาวะหยุดนิ่งและสภาวะที่มีการไหลเวียน ซึ่งแสดงให้เห็นเด่นชัดถึงการกระจายตัวของอัตราการโตในทั้งกลไกการแพร่ผ่าน และกลไกการรวมตัวของผิว

การกระจายตัวของอัตราการโตของกลไกการแพร่ผ่าน เกิดจากความแตกต่างของตำแหน่งของผลึกที่สัมพันธ์กับการไหลเวียนของสาร ซึ่งผลดังกล่าวมีนัยสำคัญมากในระบบที่ผลึกมีการกำหนดตำแหน่งของผลึก และจะมีความเป็นนัยสำคัญน้อยในเครื่องตกลึกแบบแวนลอย ที่ซึ่งผลึกมีการเปลี่ยนตำแหน่งในระบบอย่างต่อเนื่อง

การกระจายตัวของอัตราการใช้ของกลไกการรวมตัวของผิว เกิดจากความแตกต่างในโครงสร้างผิวของผลึกที่ต่างกันในระบบ โครงสร้างผิวของผลึกโดยเฉพาะความขรุขระผิวที่เห็นชัดในระดับมองด้วยกล้องจุลทรรศน์มีความสัมพันธ์กับประวัติการใช้ของผลึก โดยที่ผลึกที่โตในสารละลายอิ่มตัวยิ่งยวดมากกว่าจะมีความขรุขระของผิวว่าผลึกที่โตในสถานะที่สารละลายมีความอิ่มตัวยิ่งยวดน้อยกว่า ปรากฏการณ์ดังกล่าวจะเกิดในสารละลายอิ่มตัวยิ่งยวดที่มีระดับมากกว่าระดับวิกฤต ซึ่งเกี่ยวข้องไปถึงภาวะการเปลี่ยนแปลงลำดับความขรุขระผิว ภาวะการเปลี่ยนแปลงลำดับความขรุขระผิวขึ้นอยู่กับค่าพลังงานเชิงผิวของผลึก ดังนั้นผลึกที่มีค่าพลังงานเชิงผิวสูงกว่าจะมีค่าภาวะการเปลี่ยนแปลงลำดับความขรุขระผิวต่ำกว่า

PAREENA PANTARAKS : A STUDY INTO THE MECHANISM OF
CRYSTAL GROWTH RATE DISPERSION. THESIS ADVISOR : ASST.
PROF. ADRIAN FLOOD, Ph.D. 122 PP. ISBN 974-533-342-5

GROWTH RATE DISPERSION/ GRD/ SURFACE ROUGHNESS

The major aim of this work is to obtain the better understanding of growth rate dispersion (GRD), whereby seemingly identical crystals grow at different rates under identical conditions. The study investigated; (a) which growth mechanisms (diffusion and/or surface integration) are responsible for GRD; (b) the causes of GRD in each mechanism; and (c) whether experimental artifacts affect measurements of GRD in common research crystallization units.

Investigation of growth and dissolution rates of sucrose crystals under stagnant and convection conditions in three types of crystallizer including the small-cell, the pipe-cell, and the 2-L batch crystallizers showed that an artifact of the small-cell crystallizer appeared to generate GRD of 1.2-1.5 times higher magnitude than the other two crystallizers under convection conditions. The reason for the artifact is that in the small cell crystallizer, under convection conditions, different crystals experience different hydrodynamic conditions in the cell.

It has been shown that there is potential for rate dispersion in both the diffusion step and the integration step of crystal growth. This was determined by studying the crystal growth and dissolution rates of sucrose and hexamethylene tetramine (HMT) crystals. In stagnant conditions the crystal growth of HMT is mass transfer controlled, whilst the crystal growth of sucrose is partly controlled by the surface integration step. At very high solution flow the growth of both types of crystal

is surface integration rate controlled. Both sucrose and HMT displayed significant growth rate and dissolution rate dispersion, both in stagnant and flow conditions, and thus dispersion in rate in both mechanisms is evident.

The dispersion in the rates of diffusion in the system is due to differences in the orientation of crystals with respect to the flow. This is most significant in systems where the crystal has a fixed orientation, and will be far less significant in suspension crystallizers, where crystals reorient in the suspension continuously.

The dispersion in the rates of the surface integration step is due to variations in the surface structure of different crystals in the system. The surface structure of the crystal, in particular the degree of surface roughness evident on a microscopic scale, is related to the growth history of the crystal, with crystals having a history of high growth in high supersaturation environments having a significantly rougher surface than similar crystals with a more benign history. This phenomenon only occurs at supersaturations higher than a critical level, which is referred to as the roughening transition. The roughening transition is dependent on the surface energy of the crystals, with crystals having a higher surface energy also having a lower roughening transition.

School of Chemical Engineering

Academic Year 2004

Student's Signature _____

Advisor's Signature _____

Acknowledgement

This thesis could not have been accomplished without a great help from Asst. Prof. Dr. Adrian Flood, my thesis advisor. I am grateful to him for all of his supporting information and valuable advice, as well as his kindness, which helped me pass through my difficult times. I also thank him for his tireless effort in correcting my English grammar, and encouraging me to complete my work.

I am grateful to Prof. Masakuni Matsuoka, who not only acted as a good thesis co-advisor, but also as a loving parent when I was in Japan. I thank him very much for his patience, for his supporting information, and useful materials. His suggestions also deserve a special mention as my major source of inspiration.

Special thanks go to Assoc. Prof. Dr. Kenneth Haller for his suggestions and questions driving me to generate new ideas for further study. Great acknowledgement is also given to Assoc. Prof. Chaiyot Tangsathitkulchai and Dr. Teerasut Sookumnerd for their useful advice and their patience in answering my questions.

I am grateful to Miss Jaruan Tangtongsakulwong for assistance with the CFX program for CFD modeling of crystallizer systems.

I owe a debt of gratitude to the Thailand Research Fund for their support through the RGJ Ph.D. program. I am also grateful to Suranaree University of Technology and Tokyo University of Agriculture and Technology where I studied and conducted my research.

Miss Pareena Pantaraks

Contents

Page

Thai Abstract.....	I
English Abstract.....	III
Acknowledgement	V
Contents	VI
List of Tables	X
List of Figures	XII
Symbols and Abbreviations	XX

Chapter

1 Introduction.....	1
1.1 Background.....	1
1.2 Objectives	5
1.3 Scope of work	5
1.4 Output	6
2 Theory and Literature Review	7
2.1 Theory.....	7
2.1.1 Supersaturation	7
2.1.2 Crystal nucleation	10
2.1.3 Crystal growth.....	14

Contents (Cont.)

	Page
2.2 Literature Review.....	26
2.2.1 Growth rate dispersion (GRD).....	26
2.2.2 Proposed mechanism for GRD	30
3 Apparatus, Materials, and Methods	37
3.1 Apparatus	37
3.1.1 Small-cell crystallizer	37
3.1.2 Batch crystallizer	39
3.1.3 Pipe-cell crystallizer.....	41
3.2 Materials	42
3.2.1 Sucrose.....	42
3.2.2 Hexamethylene tetramine (HMT).....	43
3.2.3 Potassium aluminium phosphate (potash alum)	44
3.2.4 Potassium dihydrogen phosphate (KDP).....	45
3.3 Methods.....	46
3.3.1 Comparison of the average growth rate data obtained from different types of crystallizer	46
3.3.2 Study of which growth mechanism or mechanisms (diffusion and surface integration step) is responsible for GRD	50

Contents (Cont.)

	Page
3.3.3 Determination of the possible causes of GRD in the growth mechanism	51
4 Results and Discussion	57
4.1 Comparison of the average growth rate data obtained from different types of crystallizer	58
4.1.1 Growth and dissolution rates results of sucrose crystals	58
4.1.2 GRD and DRD results	65
4.2 Study of which growth mechanism or mechanisms (diffusion and surface integration step) is responsible for GRD	70
4.2.1 Average crystal growth and dissolution rates of HMT and sucrose crystals.....	70
4.2.2 GRD and DRD of sucrose crystals	73
4.2.3 GRD and DRD of HMT crystals	75
4.3 Determination of the possible causes of GRD in the growth mechanism	78
4.3.1 Cause of GRD in diffusion step.....	78
4.3.2 Cause of GRD in surface integration step.....	77
5 Conclusions and Recommendations.....	101
5.1 Conclusions.....	101
5.2 Recommendations.....	104

Contents (Cont.)

	Page
References	106
Appendices	110
A Solubility Data	110
B Determination of Surface Energy (γ)	113
C CD of Experimental Data.....	120
C.1 Growth and dissolution rates of sucrose crystals obtained from three types of crystallizer	
C.2 Growth and dissolution rates of sucrose and HMT crystals	
C.3 Growth rate history of sucrose, potash alum, KDP crystals	
C.4 CSD of potash alum, KDP, K ₂ SO ₄ crystals	
C.5 Growth rate of sucrose at different flow rates obtained from three types of crystallizer	
Biography	122

List of Tables

Table	Page
2.1 Proposed equations used to calculate the surface entropy	21
2.2 Prediction of growth mechanism <i>via</i> estimation of α factor	25
2.3 GRD in crystallization system	28
3.1 Number of crystals and the solution flow rate used in each type of crystallizer.....	47
3.2 The conditions used in the growth rate history experiments	54
4.1 Average growth and dissolution rates ($\mu\text{m}\cdot\text{min}^{-1}$) of sucrose crystals obtained from the three crystallizers; small-cell crystallizer, pipe-cell crystallizer and batch crystallizer experiments.....	61
4.2 Growth and dissolution rates models of sucrose crystals under stagnant and convection conditions (29 °C).....	64
4.3 Average growth (\bar{G}) and dissolution rates (\bar{D}), standard deviation (σ) and coefficient of variation (C.V.) of sucrose crystals obtained from the small-cell and the pipe-cell crystallizers	66
4.4 Average growth and dissolution rates of HMT and sucrose crystals at various agitation speed of the batch crystallizer	71

List of Tables (Cont.)

Table	Page
4.5 The effect of crystal growth history on current crystal growth rates of sucrose	85
4.6 Coefficient of variation (C.V.) values of CSD of sucrose, potash alum and KDP grown in low (1.50%) and high (5.00%) supersaturation	97
A.1 Solubility of HMT (g) in 100 g of solution.....	111
A.2 Solubility of Potash alum in water (g of anhydrous per 100 g of water).....	111
A.3 Solubility of KDP in water (g of anhydrous compound per 100 g of water).....	112
A.4 Solubility of K ₂ SO ₄ in water (g of anhydrous compound per 100 g of water).....	112
B.1 Primary nucleation rate (B) of potash alum and KDP crystals as a function of relative supersaturation levels	116
B.2 Physical properties of potash alum and KDP crystals for surface energy calculations.....	117

List of Figures

Figure	Page
2.1 The solubility diagram representing the metastable zone (Mullin, 2001)	8
2.2 The solubility diagram represents the difference of ΔC and ΔT	9
2.3 Classification of nucleation mechanism	11
2.4 Crystal growth phenomena at various levels of magnification.....	15
2.5 The two-step crystal growth process, and a model representation of the concentration driving force	16
2.6 The model representing the integration of solute molecules as a step, a flat, and a kink sites at the molecular level.....	19
2.7 Crystal surface structure in molecular level (a) rough surface (b) slightly rough surface (c) smooth surface (Randolph and Larson, 1988)	23
2.8 Screw dislocation	24
2.9 The spread in sizes after a growth experiment (White and Wright, 1971)	26
2.10 Schematic diagram of photomicroscopic cell used to observe secondary nucleation: (1) solution, (2) parent crystal, (3) contact rod, (4) support rod, (5) cover glasses, (6) constant temperature water, (7) water inlet and outlet, (8) thermostat	31

List of Figures (Cont.)

Figure	Page
2.11 Two models accepted for describing GRD (a) the Constant Crystal Growth (CCG) model; (b) the Random Fluctuation (RF) model	32
3.1 Schematic diagram of small-cell crystallizer (a) Top view, (b) Side view; (1) Glass cover-slip, (2) solution inlet and outlet, (3) thermometer, (4) crystals, (5) cover glasses, (6) constant temperature water.....	38
3.2 The 2-L batch crystallizer	39
3.3 A 300-mL batch crystallizer	40
3.4 Schematic diagram of the pipe-cell crystallizer.....	41
3.5 Chemical structure of sucrose.....	42
3.6 Sucrose crystal (a) Monoclinic habit (b) SEM photograph of sucrose seed crystals used in this study.....	43
3.7 Chemical structure of hexamethylene tetramine (HMT).....	44
3.8 HMT crystal (a) Rhombic dodecahedron habit (b) SEM photograph of HMT seed crystals used in this study	44
3.9 Potash alum crystal (a) Octahedral habit (b) SEM photograph of potash alum seed crystals used in this study	45
3.10 KDP crystal (a) Tetragonal habit (b) SEM photograph of KDP seed crystals used in this study.....	46

List of Figures (Cont.)

Figure	Page
3.11 Average crystal growth rates for sucrose grown from aqueous solution at various solution flow rates in (a) the small-cell crystallizer, (b) the pipe-cell crystallizer (c) the 2-L batch crystallizer; ● $\sigma = 2.20\%$; ○ $\sigma = 3.60\%$ relative supersaturation	48
3.12 Change of the positions of the crystals in the small- cell crystallizer.....	49
3.13 Crystal held on the holder to study the effect of hydrodynamic on its facial growth rate.....	52
3.14 The method to study the effect of growth rate history.....	54
4.1 Size of individual sucrose crystals vs time in the small-cell crystallizer (a) 3.60 percent relative supersaturation in stagnant condition (b) 3.60 percent relative undersaturation in stagnant condition.....	59
4.2 Size of individual sucrose crystals vs time in the pipe-cell crystallizer (a) 3.60 percent relative supersaturation in stagnant condition (b) 3.60 percent relative undersaturation in stagnant condition.....	59
4.3 Growth of sucrose crystals in 3.60 percent relative supersaturation under convection condition in the 2-L batch crystallizer (a) Crystal size distribution (b) Mean crystal size of the CSD vs time.....	60
4.4 Dissolution of sucrose crystals in 3.60 percent relative undersaturation under convection condition in the 2-L batch crystallizer (a) Crystal size distribution (b) Mean crystal size of the CSD vs time.....	61

List of Figures (Cont.)

Figure	Page
4.5 Velocity gradient of sucrose-water solutions above the glass-cover slip used in the small-cell crystallizer.....	64
4.6 Velocity gradient of sucrose-water solution passing three sucrose crystals above the glass-cover slip in the small-cell crystallizer	68
4.7 Change of the positions of the crystals in the small-cell crystallizer (a) Position 1 (b) Position 2	69
4.8 Average crystal growth and dissolution rates for HMT grown from aqueous solution. Filled symbols indicate growth rates, and hollow symbols indicate dissolution rates, ● $\sigma = 0.11\%$; ■ $\sigma = 0.22\%$	72
4.9 Average crystal growth and dissolution rates for sucrose grown from aqueous solution. Filled symbols indicate growth rates, and hollow symbols indicate dissolution rates, ● $\sigma = 2.20\%$; ■ $\sigma = 3.60\%$	72
4.10 Crystal growth rate dispersion (GRD) and dissolution rate dispersion (DRD) for sucrose in 2.20% relative supersaturation. Filled symbols indicate growth rates, and hollow symbols indicate dissolution rates.....	74
4.11 Crystal growth rate dispersion (GRD) and dissolution rate dispersion (DRD) for sucrose in 3.60% relative supersaturation. Filled symbols indicate growth rates, and hollow symbols indicate dissolution rates.....	74

List of Figures (Cont.)

Figure	Page
4.12 Growth rate distribution and dissolution rate distribution of sucrose in 3.60% relative supersaturation under 500 rpm of agitation speed. Filled symbols indicate growth rates, hollow symbols indicate dissolution rates	75
4.13 Crystal growth rate dispersion (GRD) and dissolution rate dispersion (DRD) for HMT in 0.11% relative supersaturation. Filled symbols indicate growth rates, and hollow symbols indicate dissolution rates	76
4.14 Crystal growth rate dispersion (GRD) and dissolution rate dispersion (DRD) for HMT in 0.22% relative supersaturation. Filled symbols indicate growth rates, and hollow symbols indicate dissolution rates	76
4.15 Growth rate distribution and dissolution rate distribution of HMT in 0.22% relative supersaturation under 350 rpm of agitation speed. Filled symbols indicate growth rates, hollow symbols indicate dissolution rates	77
4.16 Facial growth of a HMT crystal when the flow direction of $0.25 \text{ cm}\cdot\text{s}^{-1}$ solution flow was changed from (a) Direction 1 to (b) Direction 2.....	79
4.17 The effect of supersaturation during crystal growth on the surface roughness of sucrose crystals (a) before growth, (b) after growth	82

List of Figures (Cont.)

Figure	Page
4.18 SEM photographs of the surface of a sucrose crystal (a) after growth at 2.20% relative supersaturation (b) after growth at 5.00% relative supersaturation.....	83
4.19 SEM photographs of the surface of a potash alum crystal (a) after growth at 2.60% relative supersaturation (b) after growth at 7.50% relative supersaturation.....	83
4.20 SEM photographs of the surface of a KDP crystal (a) after growth at 2.00% relative supersaturation (b) after growth at 5.00% relative supersaturation	83
4.21 50×50 μm area of the surface of potash alum (a) after growth at 2.60% relative supersaturation (b) after growth at 7.50% relative supersaturation. Plots of the height of roughness at each width distance of each crystal are also shown.....	84
4.22 The effect of growth history of sucrose crystals on their current crystal growth. Previous crystal growth under; ● 5.00% supersaturation; ○ 2.20% supersaturation.....	86
4.23 Growth rate of sucrose crystals at 2.20% supersaturation. Previous crystal growth under; ● 5.00% supersaturation; ○ 2.20% supersaturation	86

List of Figures (Cont.)

Figure	Page
4.24 The effect of the growth history of potash alum crystals; (b) KDP on their current crystal growth. Previous crystal growth under; ● 5.00% supersaturation; ○ 2.20% supersaturation.....	87
4.25 Crystal growth behavior of sucrose under varying conditions of supersaturation (a) Crystal size vs time (b) Growth rate vs time.....	88
4.26 The healing period of sucrose crystals demonstrated by three jumps in relative supersaturation (a) crystal size vs time and (b) growth rate during the healing period	91
4.27 30 × 30 μm area of the surface of potash alum scanned by AFM (a) initial surface 7.50% (b) surface after growth in 2.50% for 30 minutes (c) surface after growth in 2.50% for 1 hour	92
4.28 Height of roughness of the surface of potash alum scanned by AFM (a) initial surface 7.50% (b) surface after growth in 2.50% for 30 minutes (c) surface after growth in 2.50% for 1 hour	93
4.29 The relative difference of the growth rates of crystals that were initially grown in 2.20% and in 5.00% supersaturation.....	95
4.30 CSD of (a) sucrose crystals (b) potash alum crystals (c) KDP crystals at 2.20% relative supersaturation; ● Initial time; ○ final time.....	99
4.31 CSD of (a) sucrose crystals (b) potash alum crystals (c) KDP crystals at 5.00% relative supersaturation; ● Initial time; ○ final time.....	100

List of Figures (Cont.)

Figure	Page
B.1 Number of potash alum nuclei from primary nucleation experiment as a function of time.....	118
B.2 Number of KDP nuclei from primary nucleation experiment as a function of time.....	118
B.3 Plots of $\ln B + 3 \ln \ln(x/x_s)$ and $\ln^{-2}(x/x_s)$ for potash alum and KDP.....	119

Symbols and Abbreviations

A_c	=	Surface area of the crystal (m^2)
B	=	Nucleation rate ($\# \cdot m^{-3} \cdot s^{-1}$)
B^0	=	Secondary nucleation rate ($\# \cdot m^{-3} \cdot s^{-1}$)
C	=	Solute concentration ($kmol \cdot m^{-3}$)
C^0	=	Solute concentration of crystal-solution interface ($kmol \cdot m^{-3}$)
C'	=	Solute concentration at interface between solution and adsorbed layer ($kmol \cdot m^{-3}$)
$(C.V.)_G$	=	Coefficient of variation of growth rate data (-)
$(C.V.)_D$	=	Coefficient of variation of dissolution rate data (-)
c^*	=	Saturation concentration ($g \cdot g \text{ solution}^{-1}$)
c	=	Solution concentration ($g \cdot g \text{ solution}^{-1}$)
d	=	Height of molecular step (m)
D	=	Dissolution rate of an individual crystal ($m^2 \cdot s^{-1}$)
\bar{D}	=	Mean dissolution rate ($m \cdot s^{-1}$)
D_f	=	Diffusion coefficient ($m^2 \cdot s^{-1}$)
i	=	Modeling constant of equation (2.8)
G	=	Growth rate of an individual crystal ($m \cdot s^{-1}$)

Symbols and Abbreviations (Cont.)

\bar{G}	=	Mean growth rate ($\text{m}\cdot\text{s}^{-1}$)
$\bar{G}_{1.5}$	=	Growth rate of the crystals previous grown in 1.50% supersaturation ($\mu\text{m}\cdot\text{min}$)
$\bar{G}_{5.0}$	=	Growth rate of the crystals previous grown in 5.00% supersaturation ($\mu\text{m}\cdot\text{min}$)
k	=	Boltzman constant ($1.3085 \times 10^{-23} \text{ J}\cdot\text{K}^{-1}$)
k_d	=	Diffusion rate constant ($\text{m}\cdot \text{m}^{3.i}\cdot\text{kmol}^{-i}\cdot\text{s}^{-1}$)
k_r	=	Surface integration rate constant ($\text{m}\cdot \text{m}^{3.z}\cdot\text{kmol}^{-z}\cdot\text{s}^{-1}$)
k_x	=	Liquid phase mass transfer coefficient ($\text{m}^2\cdot\text{s}^{-1}$)
K_G	=	Overall crystal growth coefficient ($\text{m}\cdot \text{m}^{3.n}\cdot\text{kmol}^{-n}\cdot\text{s}^{-1}$)
\bar{L}	=	Rate of increase characteristic dimension ($\text{m}\cdot\text{s}^{-1}$)
M	=	Molecular weight ($\text{g}\cdot\text{mol}^{-1}$)
M_g	=	Magma density ($\text{kg}\cdot\text{m}^{-3}$)
n	=	Modeling constant of equation (2.12)
N_A	=	Flux of solute to the growing crystals ($\text{mol}\cdot\text{m}^{-2}\cdot\text{s}^{-1}$)
N_o	=	Avogadro number ($6.023 \times 10^{23} \text{ mol}^{-1}$)
r_c	=	Critical radius of nuclei (m)
R	=	Gas constant ($8.314 \text{ J}\cdot\text{K}^{-1}\cdot\text{mol}^{-1}$)
R_d	=	Diffusion rate ($\text{mol}\cdot\text{s}^{-1}$)

Symbols and Abbreviations (Cont.)

R_r	=	Surface integration rate ($\text{mol}\cdot\text{s}^{-1}$)
S	=	Supersaturation ratio (-)
T	=	Temperature (K)
\bar{V}	=	Rate of increase of the crystal volume ($\text{m}^3\cdot\text{s}^{-1}$)
x	=	Mole fraction of solute in supersaturation solution (-)
x_s	=	Mole fraction of solute in saturation solution (-)
z	=	Modeling constant of equation (2.9)
Δf	=	Internal free energies of solute and solid ($\text{J}\cdot\text{mol}^{-1}$)
ΔH_f	=	Heat of fusion ($\text{J}\cdot\text{mol}^{-1}$)
α	=	Surface entropy factor (-)
β	=	Crystal structure geometric factor (-)
δ	=	Thickness of stagnant film (m)
ϕ_{ff}	=	Bond energies for fluid-fluid neighbor bonds (J)
ϕ_{sf}	=	Bond energies for solid-fluid neighbor bonds (J)
ϕ_{ss}	=	Bond energies for solid-solid neighbor bonds (J)
γ	=	Surface energy ($\text{J}\cdot\text{m}^{-2}$)
γ_e	=	Edge free energy ($\text{J}\cdot\text{m}^{-1}$)
σ	=	Relative supersaturation (-)
σ_G	=	Standard deviation of growth rate data ($\mu\text{m}\cdot\text{min}^{-1}$)
σ_D	=	Standard deviation of dissolution rate data ($\mu\text{m}\cdot\text{min}^{-1}$)

Symbols and Abbreviations (Cont.)

ρ	=	Solid density ($\text{kg}\cdot\text{m}^{-3}$)
ω	=	Agitation speed (rpm)
ε	=	Potential energy change per solid fluid bond (J)
v	=	Molecular volume ($\text{m}^3\cdot\text{mol}^{-1}$)
ξ	=	Crystallographic factor (-)

Chapter 1

Introduction

1.1 Background

Growth rate dispersion (GRD) is a phenomenon, known as a problem in the crystalline product industries, where individual crystals of the same initial sizes do not grow at the same rate even when they are subjected to identical temperatures, supersaturation levels and hydrodynamic conditions (Mitrovic et al., 1997). The phenomenon has a significant effect on the crystal size distribution from industrial crystallizers, with significant decrease in product quality. It was first shown experimentally for sucrose, an industrially significant product grown primarily in batch crystallizers (White and Wright, 1971). In the thirty years since this initial study a large amount of research has been conducted to determine the causes and mechanisms of GRD and to model its effects. A better understanding of GRD is important for various reasons. Since it provides information about the growth process taking place at the crystal surface, the nature and magnitude of the GRD may give information about the growth mechanism. This will substantially benefit users of industrial crystallizers and improve the capability of crystallizer modeling as well as the design of higher performance crystallizers.

While a number of significant advances have been made, the mechanisms of GRD are still not fully elucidated. The origin of GRD known from the literature lies in the surface integration step of crystal growth since the well-known law namely

McCabe's ΔL Law stated that each crystals should have the same linear crystal growth rate under the same conditions and the validity is evident for systems that are controlled by mass transfer (McCabe, 1929). Current speculations on GRD have centered around the belief of two concepts; variation of the density of dislocation steps on the crystal's surface of each crystal, and differences in the crystal perfection (internal lattice strain) of each crystal. The first concept was proposed based on the classical theory of Burton, Cabrera, and Frank, which describes the influence of screw dislocations on crystal growth. With the idea that higher amounts of surface dislocations give a higher growth rate, it is the most obvious way to explain why the individual crystals grow at different rates with no apparent reason. However, several works demonstrated the results suggesting no correlation between GRD and a variable number of dislocations (Herden and Lacmann, 1997). The concept of varying degrees of 'internal crystal perfection' in terms of 'strain in the crystal lattice' has been focused on recently to explain the mechanism behind GRD. A clear tendency for a reduction in growth rate with increasing amount of overall lattice strain has been revealed by the experimental work of Ristić et al. (1988). The subsequent studies by Mitrović (1995) and Zacher and Mermann (1995) also demonstrated agreement with these results, but the works of Harding et al. (1992) and Harden and Lacmann (1997) disagreed with their conclusions. Harden and Lacmann suggested that there is no correlation between face-specific growth rates of KNO_3 , and Laue quality. The difficulty in correlating Laue quality with growth rates may be explained by the fact that the Laue quality is determined for the whole crystal, while the growth rate is face-specific, and related to surface features only. The influence of the Laue quality is therefore possible, but it is not enough to fully explain GRD.

Two well-known crystallizers have been used for GRD study including mass crystallizers and cell crystallizers. The mass crystallizers are the batch crystallizer, mixed seed mixed product removal (MSMPR) crystallizer, and fluidized bed crystallizer. All of them can represent the actual crystallization processes but their investigations can only determine the average data for whole system, for example, in the batch crystallizer, crystal size distribution (CSD) are analyzed to yield the mean crystal size by the method Zumstein and Rousseau (1987). The cell crystallizer or Photomicroscopic cell initially used by the group of Larson has been used to observe the growth rates of individual crystals. Using the cell, the individual crystals which grow over the glass cover slip are monitored directly throughout the experiment so their inherent growth rates can be observed. The limitation of this technique is that only two visible dimensions of each crystal can be measured, because a side of each crystal is attached to the glass cover slip. These two techniques produce strong experimental evidence that GRD can occur in the growth of crystals or nuclei produced either by primary nucleation or secondary nucleation. It is however quite important to determine why the magnitude of dispersion determined from the cell crystallizer is generally larger than that characterized from the mass crystallizer (Tavare, 1985). The difference between the growth rate data from the two techniques not only provides different information but also leads to a difficulty in data interpretation. The reason of their differences therefore should be considered.

Based on the derivation of McCabe's ΔL law with an assumption of mass transfer as a rate limiting step, all crystals should grow at the same rate, or equivalently, there should be no GRD. It has recently been shown by Fabian et al. (1996) that sucrose crystals display significant dissolution rate dispersion (DRD) in

stagnant conditions. It is not understood why dissolution, apparently a process generally considered to follow first-order kinetics with respect to undersaturation and believed to be mass transfer controlled (Mullin, 2001), displays a dispersion phenomena. In their Photomicroscopic-cell experiments, the plots of the growth rate results and supersaturation levels show GRD and DRD phenomena at all growth conditions. This work possibly indicates that GRD might also occur in the diffusion step of crystal growth.

Wang et al. (1990) observed the growth rates of potash alum ($\text{KAl}(\text{SO}_4)_2 \cdot 12\text{H}_2\text{O}$) under high solution flow, representing a surface integration controlled process, when the supersaturation levels were pulse changed as $\sigma_1 : \sigma_2 : \sigma_1$ (with σ_2 more than or less than σ_1). The results showed that the growth rate decreases with decreasing σ_2 , and increases with increasing σ_2 , but it does not return to the previous value after the second supersaturation change (returning σ_1) in a short-time period. Tanneberger et al. (1996) repeated these experiments and found the same results. Both works concluded (in a similar way) that the variation in growth rates found were possibly caused by a change of the surface structure at each supersaturation level. Although no experiments have been performed to verify their suggestions, it is noticed that this effect should be taken into account as a cause of GRD in the surface integration step. The variation of supersaturation levels in the system can be found either in the nucleation period or in the growth period. In the nucleation period, the initial nuclei must form at a higher supersaturation than later nuclei, which may relate to differences in initial growth rates for apparently identical nuclei. In addition, if local levels of supersaturation vary, this will have an effect on the inherent crystal growth rate dispersion, in addition to displaying random fluctuations in growth rate.

As discussed above, the crystal growth rate results obtained from the different types of the crystallizer should be compared to conclude which growth rate measurement technique can provide the most reliable results. The causes of GRD based on the growth mechanism (diffusion and surface integration mechanism) should also be considered. In this study, the cause of GRD in surface integration focuses on differences in the crystal surface structure of the crystals. If there is GRD in the mass transfer (diffusion) process, differences in the thickness of the boundary layer formed around the crystal will be investigated as a cause of mass transfer rate dispersion.

1.2 Objectives

1.2.1 To compare the average growth rate data obtained from different types of crystallizer.

1.2.2 To study which growth mechanism or mechanisms (mass transfer and surface integration step) is responsible for GRD.

1.2.3 To determine the possible causes of GRD in the growth mechanism.

1.3 Scope of Work

1.3.1 The growth rate data of sucrose crystals will be compared in three types of crystallizers; a 2-L batch crystallizer, a small-cell crystallizer and a pipe-cell crystallizer.

1.3.2 To study whether there is growth rate dispersion in the diffusion step, the growth rate of hexamethylene tetramine (HMT) in HMT-water system will be determined under stagnant (no flow) and low solution flow conditions. It has been known from the literature that the growth rate of HMT in aqueous solution under stagnant solution is controlled by the diffusion step (Bourne and Davey, 1976a).

1.3.3 The work for the third objective depends on the results from the study of the second objective. If there is rate dispersion in mass transfer, the possible factor is the difference in flow velocity around different crystals. The investigation of the mechanism of GRD in the surface integration step will focus on the difference in surface structure at the microscopic level (where the size range is of the order of one to ten micron).

1.4 Output

The better understanding on GRD phenomena will be achieved for describing the cause of and the main factors influencing GRD. This will assist researchers attempting to understand mechanisms of crystal growth, and will also assist industrial users of crystallization processes, by suggesting methods to minimizing GRD, and methods to better design processes to take GRD into account.

Chapter 2

Theory and Literature Review

2.1 Theory

It has been said that “crystallization from solution is usually the result of two processes; crystal nucleation and crystal growth. These two processes can proceed either consecutively (in series) or simultaneously (in parallel) throughout the whole, or during only part, of the crystallization period depending on supersaturation levels” (Mullin, 2001). In this chapter, the concepts of supersaturation will be described first to illustrate the region that the crystals can or cannot grow and nucleate in the system. The nucleation and the growth processes will then be described in detail.

2.1.1 Supersaturation

The state of supersaturation is an essential requirement for all crystallization operations. Supersaturation refers to a solution that contains more dissolved solid than that represented by the equilibrium or saturation condition (Mullin, 2001). The terms labile and metastable supersaturation were first introduced to classify supersaturated solutions in which spontaneous nucleation would or would not occur, respectively. The diagram representing the labile and the metastable zone is demonstrated in a solubility diagram as shown in Figure 2.1.

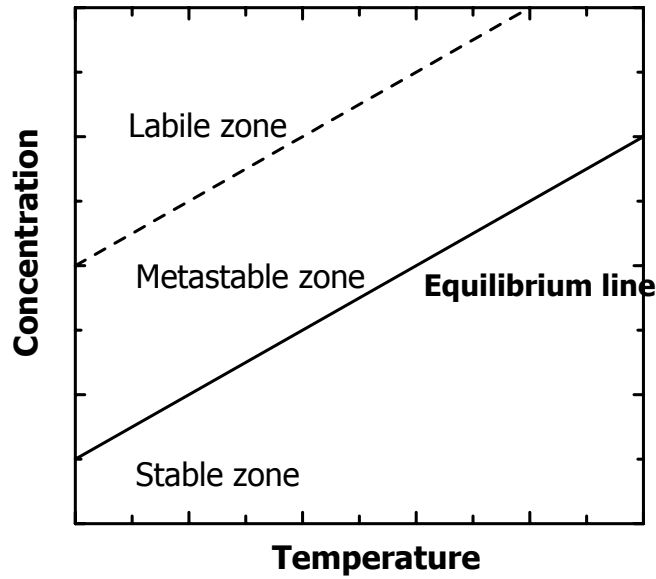


Figure 2.1 The solubility diagram representing the metastable zone (Mullin, 2001)

Above the equilibrium line (solid line), the solutions are at supersaturated conditions. Crystal growth occurs in the metastable zone, in which the crystal growth rate increases with increasing solute concentration at constant temperature. In the labile zone, nuclei formation can occur spontaneously which is called primary nucleation. In the metastable zone, no nucleation occurs though the breakage of the seed crystals can be found.

The supersaturation of a system may be expressed in a number of different ways. Among the most common expressions of supersaturation are the concentration driving force, Δc , the supersaturation ratio, S , and a quantity sometimes referred to as the absolute or relative supersaturation, σ , or percentage supersaturation, 100σ . These quantities are defined by (Söhnel and Garside, 1992)

$$\Delta c = c - c^* \quad (2.1)$$

$$S = \frac{c}{c^*} \quad (2.2)$$

$$\sigma = \frac{\Delta c}{c^*} = S - 1 \quad (2.3)$$

where

- c = Solution concentration ($\text{g}\cdot\text{g solution}^{-1}$)
- c^* = Saturation concentration ($\text{g}\cdot\text{g solution}^{-1}$)
- S = Supersaturation ratio
- σ = Relative supersaturation or supersaturation

Of the above three expressions for supersaturation, it is essential to quote the temperature, T , when expressing the supersaturation of a system, since the equilibrium saturation concentration is temperature dependent. In some situation the supersaturation can be described by a temperature gradient, ΔT , for instance when the equilibrium is a monotonic function with temperature as shown as in Figure 2.2.

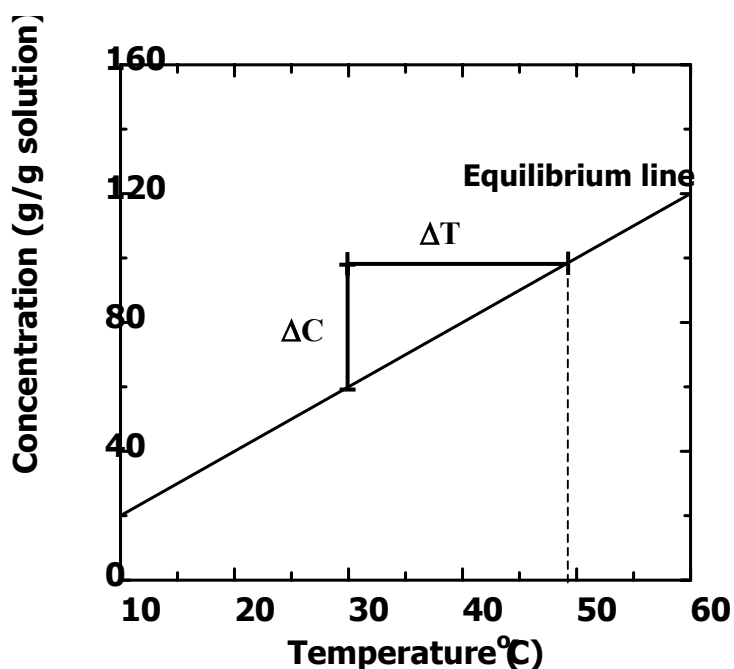


Figure 2.2 The solubility diagram represents the difference of ΔC and ΔT

The explanation of the supersaturation level in terms of ΔC and ΔT in Figure 2.2 is that decreasing the temperature from saturation at 48 °C to 30 °C ($\Delta T = 18$ °C) can represent the same supersaturation as at 30 °C with the given ΔC as the

driving force. It is preferable to use ΔC as a driving force because the solubility line is not always monotonic, and in this case a particular point on the diagram will not have a unique value of ΔT .

2.1.2 Crystal nucleation

The theoretical description of nucleation depends on the mechanism responsible for nucleus formation. The conditions required for the various mechanisms can be schematically represented as shown in Figure 2.3 (Söhnel and Garside, 1992). Three main categories of nucleation can be distinguished, primary homogeneous, primary heterogeneous and secondary heterogeneous. The primary homogeneous nucleation is where the formation of the solid phase is not brought about by the presence of any solid phase. It thus requires very high supersaturation conditions such as in the labile zone. The heterogeneous is where the formation of new solid phase particles is catalyzed by the presence of a foreign solid phase. Secondary nucleation is the most common nucleation event in industrial crystallization, and is the mechanism by which formation of the solid phase is initiated by the presence of solid phase of the crystallizing material itself. This type of nucleation can therefore be found even in the metastable zone where the crystals seemingly only grow. With the different mechanisms governing these three types of nucleation, the resulting rate equations have correspondingly different forms and their relative importance varies with the particular crystallization operation (Garside, 1985a).

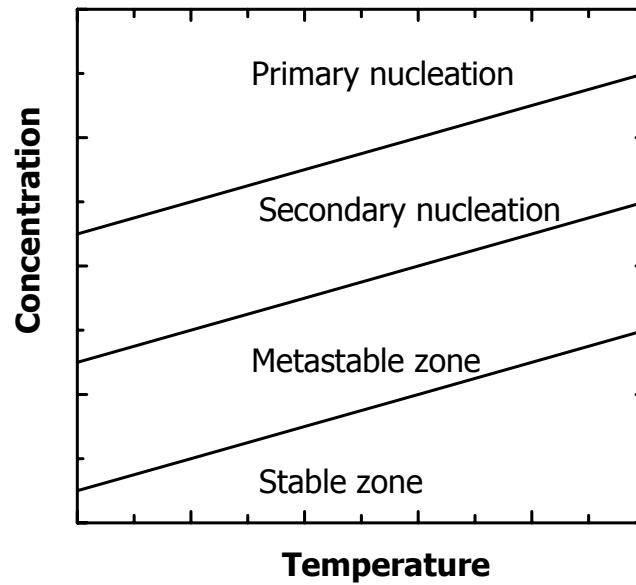


Figure 2.3 Classification of nucleation mechanism

2.1.2.1 Primary nucleation

The mechanism of nucleation that has been most widely studied theoretically is homogeneous nucleation. This is by no means the most common nucleation mechanism and true homogeneous nucleation can usually only be attained under carefully controlled laboratory conditions (Mullin, 2001).

The classical theory of nucleation, stemming from the work of Gibbs, Volmer, Becker and Döring and others is based on the condensation of a vapor to a liquid and this treatment may be extended to crystallization from solutions (Mullin, 2001). The rate of primary nucleation, the number of nuclei formed per unit time per unit volume, in the supersaturated solution is expressed as (Bourne and Davey, 1976b)

$$B = g_k \cdot \exp \left[\frac{-\beta N_o M^2 \gamma^3}{R^3 \rho^2 T^3 \ln^2(x/x_s)} \right] \quad (2.4)$$

$$g_k = k \cdot \ln^{-3}(x/x_s) \quad (2.5)$$

where	B	= Nucleation rate ($\# \cdot \text{m}^{-3} \cdot \text{s}^{-1}$)
	β	= Crystal structure geometric factor of crystal (-)
	N_o	= Avogadro number ($6.023 \times 10^{23} \text{ mol}^{-1}$)
	M	= Molecular weight ($\text{g} \cdot \text{mol}^{-1}$)
	γ	= Surface energy ($\text{J} \cdot \text{m}^{-2}$)
	R	= Gas constant ($8.314 \text{ J} \cdot \text{K}^{-1} \cdot \text{mol}^{-1}$)
	ρ	= Solid density ($\text{kg} \cdot \text{m}^{-3}$)
	T	= Temperature (K)
	x	= Mole fraction of solute in supersaturation solution (-)
	x_s	= Mole fraction of solute in saturation solution (-)
	k	= Modeling constant

Equation (2.4) indicates that the primary nucleation rate is highly nonlinear in solution supersaturation, being near-zero for low values of supersaturation but increasing extremely rapidly when the supersaturation increases. It also describes the importance of three parameter, temperature, degree of supersaturation, and surface energy of solid, on the rate of nucleation.

Once the nuclei form in the process, which occur very rapidly, they can only continue in local regions of very high supersaturation and may also simply redissolve because they are extremely unstable. If nucleus grows beyond a certain critical size, it becomes stable under the average conditions of supersaturation obtained in the bulk of the fluid. The size of the critical nuclei can be determined by the relationship between the surface energy and the supersaturation as follows:

$$r_c = \frac{2\gamma v}{kT \ln(x/x_s)} \quad (2.6)$$

where	r_c	= Critical radius of nuclei (m)
	γ	= Surface energy ($\text{J}\cdot\text{m}^{-2}$)
	v	= Molecular volume ($\text{m}^3\cdot\text{mol}^{-1}$)
	k	= Boltzman constant ($1.3085 \times 10^{-23} \text{ J}\cdot\text{K}^{-1}$)
	T	= Temperature (K)
	x	= Mole fraction of solute in supersaturation solution (-)
	x_s	= Mole fraction of solute in saturation solution (-)

Most primary nucleation that occurs in practice is likely to be heterogeneous which is induced by surfaces of foreign particles. It therefore requires significantly lower supersaturations than homogeneous nucleation. The rate equation appears to be of similar form to that of homogeneous nucleation but the supersaturation required is lower (Dirksen and Ring, 1991).

2.1.2.2 Secondary nucleation

Secondary nucleation can occur in systems where crystals of the solute are already present or added. The three main sources of secondary nucleation are nucleation by fracture, attrition and contact nucleation. Nucleation by contact nucleation has been more widely studied than the other categories. The source of this nucleation is the contacts between a growing crystal and walls of the container, the stirrer or pump impeller, or the other crystals. The work of Bennett, Fiedelman, and Randolph (as quoted by Söhnel, 2001) has shown that the nucleation rate can also be correlated with the degree of agitation as expressed by the tip speed of

a pump impeller or vessel agitator. For design and analysis purposes, an empirical correlation has been successfully used as follows (Dirksen and Ring, 1991):

$$B^0 = k(T)\omega^b M_g^j S^k \quad (2.7)$$

where B^0 = Secondary nucleation rate ($\# \cdot m^{-3} \cdot s^{-1}$)
 $k(T)$ = Constant
 ω = Agitation speed (rpm)
 M_g = Suspension density ($kg \cdot m^{-3}$)
 S = Supersaturation ratio (-)
 b, j, k = Modeling constant

Typical values of k lie between 0.5 and 2.5. The influence of suspension density points directly to the importance of particle concentration. Most values of j are close to unity and the value of b is between approximately 2 and 4 (Garside, 1985a).

2.1.3 Crystal growth

2.1.3.1 Fundamental of crystal growth

The process of crystal growth can be described at several different levels of magnification, various theories having evolved to represent the processes taking place at three different size levels; molecular, microscopic and macroscopic as illustrated in Figure 2.4 (Garside, 1985a).

At the molecular scale, “growth units” diffuse to the crystal surface and attach themselves to the surface of the crystals. When observed at the microscopic scale, step bunches can be seen. These are many hundreds of atomic dimensions in height and are made up of groups of smaller steps that have become bunched together.

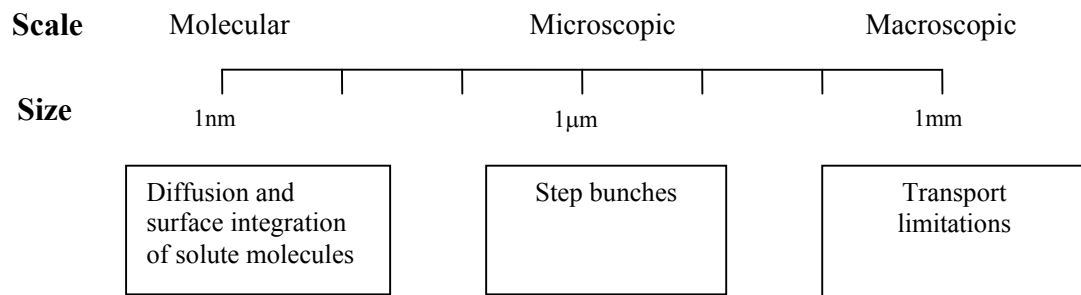


Figure 2.4 Crystal growth phenomena at various levels of magnification

At the macroscopic scale, the mass transport limitations on the growth rate of crystals play important role. Macroscopic concentration gradients influence the surface concentration profile which can lead to growth instabilities at the surface. With the link between each scale, theoretical derivation has often been focused in the molecular scale, by consideration of the diffusion and integration of solute molecules on the crystal's surface. The derivative equations have then been applied for the larger scales. In the theory of crystal growth, the two successive mechanisms are a diffusion step and a surface integration step (Randolph and Larson, 1988). The first step (diffusion) is where the transfer of molecules from the bulk solution to the crystal surface occurs, and the second step concerns the insertion of molecules into the surface (a reaction step), as shown in Figure 2.5.

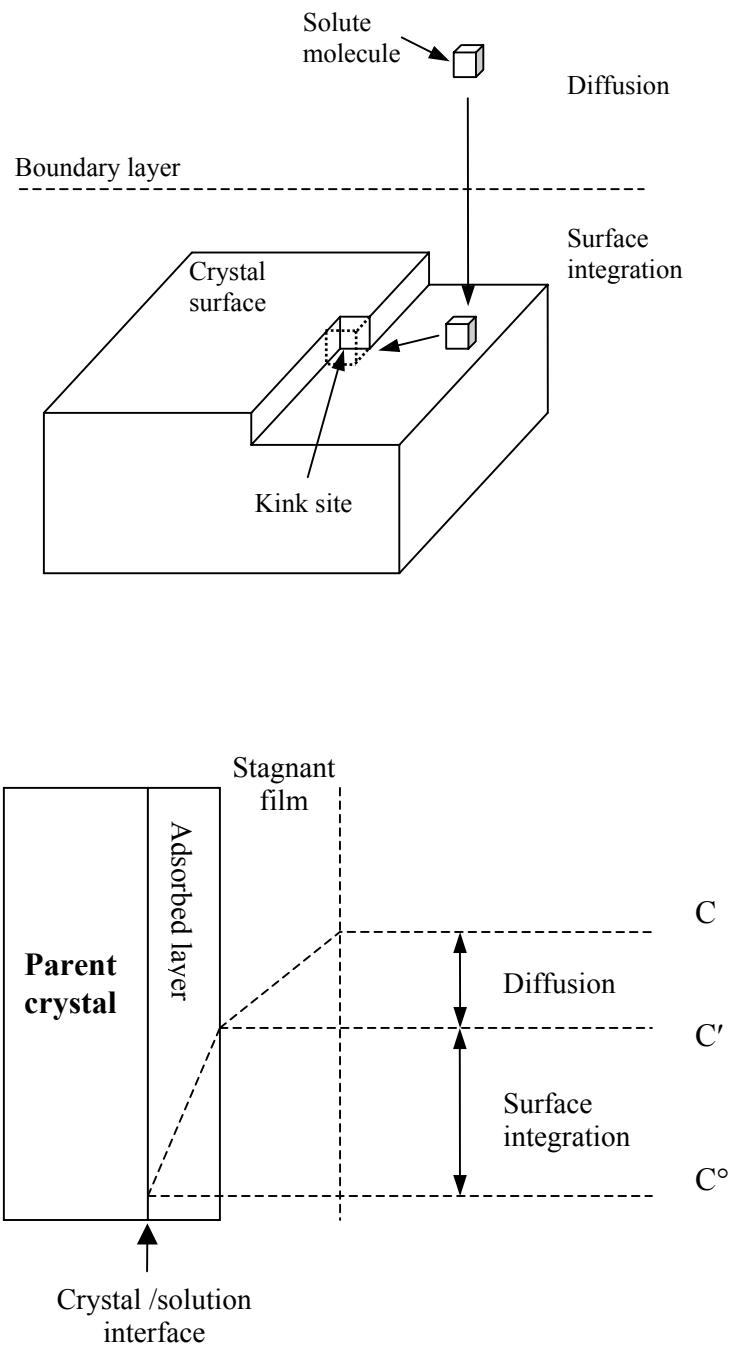


Figure 2.5 The two-step crystal growth process, and a model representation of the concentration driving force

Models for the growth rate based on the diffusion step and on the surface integration step of crystal growth have been proposed as shown in Equation (2.8) and Equation (2.9).

$$R_d = k_d (C - C')^i \quad (2.8)$$

$$R_r = k_r (C' - C^0)^z \quad (2.9)$$

where

- R_d = Diffusion rate ($\text{m} \cdot \text{kmol}^i \cdot \text{s}^{-1} \cdot \text{m}^{-3 \cdot i}$)
- k_d = Diffusion rate constant ($\text{m} \cdot \text{m}^{3 \cdot i} \cdot \text{kmol}^{-i} \cdot \text{s}^{-1}$)
- C = Solute concentration ($\text{kmol} \cdot \text{m}^{-3}$)
- C' = Solute concentration at interface between solution and adsorbed layer ($\text{kmol} \cdot \text{m}^{-3}$)
- R_r = Surface integration rate ($\text{m} \cdot \text{kmol}^z \cdot \text{s}^{-1} \cdot \text{m}^{-3 \cdot z}$)
- k_r = Surface integration rate constant ($\text{m} \cdot \text{m}^{3 \cdot z} \cdot \text{kmol}^{-z} \cdot \text{s}^{-1}$)
- C^0 = Solute concentration of crystal-solution interface ($\text{kmol} \cdot \text{m}^{-3}$)
- i, z = Modeling constant

In general, the diffusion step is considered to be linearly dependent on the concentration deriving force ($i = 1$) by using the assumption of a thin film of liquid adjacent to the growing crystal face, through which molecule of the solute would have to diffuse. Equation (2.8) thus can be written as Equation (2.10). As an approximation, the diffusion rate coefficient, k_d , is a function of diffusion coefficient, D , and thickness of stagnant film, δ which can be noted that it would

obviously depend on the relative solid-liquid velocity, i.e. on the degree of agitation of the system (Mullin, 2001).

$$R_d = k_d(C - C') \quad (2.10)$$

$$k_d = \frac{D_f}{\delta} \quad (2.11)$$

where D_f = Diffusion coefficient ($m^2 \cdot s^{-1}$)

δ = Thickness of stagnant film (m)

Equation (2.8) to equation (2.10) are not easy to apply in practice because they involve interfacial concentrations that are difficult to measure. It is usually more convenient to eliminate the term C' by considering an “overall” concentration driving force, $C - C^o$, which is quite easily measured. A general equation for crystallization based on this overall driving force can be written as:

$$R_G = K_G(C - C^o)^n \quad (2.12)$$

where K_G = Overall crystal growth coefficient

n = Modeling constant

The exponent n is usually referred to as the order of the overall crystal growth process. The value of n is in a range of 1 to 2. In the simplest case where $n = 1$, the term C' (the interfacial concentration) can be eliminated in order to obtain the following expression (Randolph and Larson, 1988):

$$R_G = \frac{k_d k_r}{k_d + k_r} (C - C^o) \quad (2.13)$$

Since the diffusion and reaction processes occur in series it is obvious that the slower process controls the total growth rate. This fact means that if

$k_r \ll k_d$, the overall growth process is controlled by the surface reaction and vice versa if $k_r \gg k_d$. These two extreme situations can be obtained under particular conditions of growth temperature or solution stirring. When diffusion is the controlling mechanism, the crystal growth rate increases as the velocity of supersaturated solution is increased relative to the crystal surface. When further increases in velocity no longer increase growth rate, the growth is controlled by the surface integration step (Mullin, 2001).

2.1.3.2 Crystal surface structure

The growth process of crystal involves the surface integration step in which the solute molecules incorporate in the flat, or step, or kink sites of the crystal surface as illustrated in Figure 2.6.

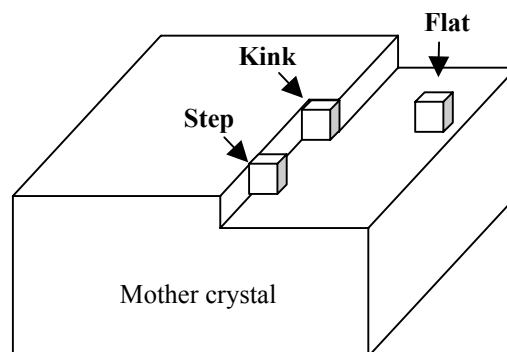


Figure 2.6 The model representing the integration of solute molecules as a step, a flat, and a kink sites at the molecular level

As illustrated in Figure 2.6, the integration of solute molecules on the surface of crystal depends on the crystal surface structure. If the surface of the crystal is very smooth, the solute molecule must incorporate in a flat type and, on the other hand, on a very rough surface crystal a lot of kink sites can be found for

integration. Therefore, it has been noted that the crystal surface structure is an important parameter in crystal growth process.

Jackson et al. (1967) first defined a surface entropy factor, α , to characterize the state of the crystal surface or interface structure at the molecular level. The developed α is defined by

$$\alpha = \frac{4\varepsilon}{kT} \quad (2.14)$$

$$\varepsilon = \frac{1}{2}(\phi_{ff} + \phi_{ss}) - \frac{1}{2}\phi_{sf} \quad (2.15)$$

where	α	= Surface entropy factor
	ε	= Potential energy change per solid fluid bond (J)
	ϕ_{ff}	= Bond energies for fluid-fluid neighbor bonds (J)
	ϕ_{ss}	= Bond energies for solid-solid neighbor bonds (J)
	ϕ_{sf}	= Bond energies for solid-fluid neighbor bonds (J)
	k	= Boltzman constant ($1.3085 \times 10^{-23} \text{ J}\cdot\text{K}^{-1}$)
	T	= Temperature (K)

Jackson has also suggested that the value of α is related to the expected degree of surface roughness on a crystal face, with larges values of α relating to smoother surfaced crystals. By considering the definition of α , increases in the value of temperature leading to lower α values, and so to a rougher surface. The same results will also be found if the value of ε decreases. The term ε is related to the bond interactions between crystal-crystal, solvent-solvent and crystal-solvent. It is quite interesting that if the interaction between crystal (solute) and solvent is high the ε value becomes small resulting in low α value (which refers to a rough surfaced

crystal). Approximate equations to calculate α have also been suggested by several authors, as shown in Table 2.1.

Table 2.1 Proposed equations used to calculate the surface entropy factor

Authors	Proposed model for α	Equation
Jackson (1967)	$\alpha = \frac{4\varepsilon}{kT}$ $\varepsilon = \frac{1}{2}(\phi_{ff} + \phi_{ss}) - \frac{1}{2}\phi_{sf}$	(2.14)
Bourne and Davey (1976b)	$\alpha = \frac{4\gamma_e}{RT}$ $\gamma_e = d\gamma$	(2.16)
	$\alpha = \frac{\xi\Delta H_f}{RT}$	(2.17)
	$\alpha = \xi\left(\frac{\Delta H_f}{RT} - \ln x_s\right)$	(2.18)
Bennema and Van der Eerden (1977)	$\alpha = \xi(1 - x_s)^2 (\Delta f - \ln x_s)$	(2.19)

where

- γ_e = Edge free energy ($\text{J}\cdot\text{m}^{-1}$)
- γ = Surface free energy ($\text{J}\cdot\text{m}^{-2}$)
- d = Height of molecular step (m)
- ΔH_f = Heat of fusion ($\text{J}\cdot\text{mol}^{-1}$)
- Δf = Internal free energies of solute and solid ($\text{J}\cdot\text{mol}^{-1}$)
- R = Gas constant ($8.314 \text{ J}\cdot\text{K}^{-1}\cdot\text{mol}^{-1}$)

T = Temperature (K)

x_s = Mole fraction of solute in saturation solution (-)

ξ = Crystallographic factor (-)

Based on the work of Bourne and Davey (1976b), the α values calculated from different equations were compared to suggest which equation gave the most accurate data. The results suggested that the α values calculated from equation (2.16) are the most accurate. A general attempt to use the α value to characterize the surface of crystal has been made by Bourne and Davey (1976b) who suggested as follows (the models for each surface are illustrated in Figure 2.7).

- a) $\alpha < 3$ Rough surface
- b) $3 < \alpha < 4$ Slightly rough surface
- c) $\alpha > 4$ Smooth surface

Three growth models have also been proposed to represent the growth of each type of surface. The models for the rough surface, slightly rough surface, and smooth surface are the continuous growth model, the birth and spread model and the Burton-Caberra-Frank (BCF) model, respectively (Randolph and Larson, 1988).

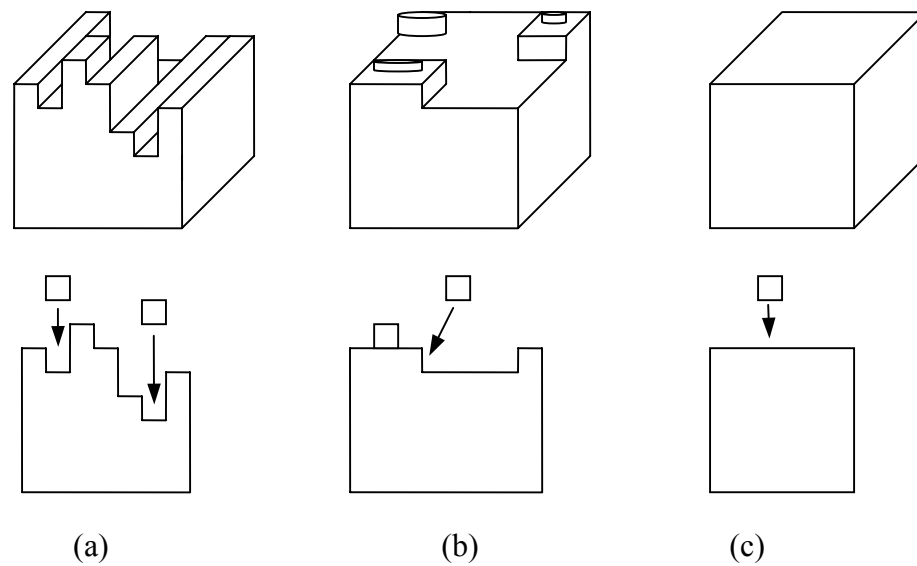


Figure 2.7 Crystal surface structure in molecular level (a) rough surface (b) slightly rough surface (c) smooth surface (Randolph and Larson, 1988)

If α is less than 3 the surface is sufficiently rough, as shown in Figure 2.7(a) for any molecules diffusing to the surface of the crystal to immediately integrate. The continuous growth model assumes the growth units can integrate continuously at the kink site, where they have the lowest energy for its integration. The growth rate will then be linear in supersaturation, as in Equation (2.20).

$$G = A\sigma \quad (2.20)$$

where

- G = Growth rate of an individual crystal($\text{m}\cdot\text{s}^{-1}$)
- A = Constant at maximum growth rate for a given system
- σ = Supersaturation

The birth and spread model is proposed for the system which has α in the range of 3 to 4, referring to a slightly rough surface (Figure 2.7 (b)). This

model describes the growth rate that is controlled by the frequency of formation of two dimensional nuclei on the smooth face of a growing crystal. Surface nucleation is the controlling step, and it is followed by the spread of the birth unit around the nucleus. The equation derived for this model is

$$G = A_1 \sigma^{5/6} \exp(-A_2 / \sigma) \quad (2.21)$$

where G = Growth rate of an individual crystal($\text{m}\cdot\text{s}^{-1}$)
 σ = Supersaturation
 A_1, A_2 = Constant values

For crystal surfaces with values of α greater than about 4, or smooth surfaced crystals (Figure 2.7 (c)), the Burton-Caberra-Frank (BCF) model describes how an otherwise flat crystal surface grows by addition of growth units to kink sites in an infinite (Figure 2.8).

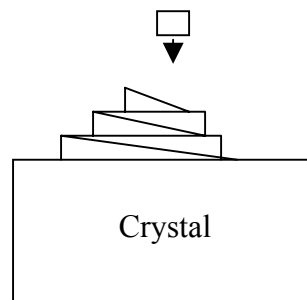


Figure 2.8 Screw dislocation

Screw dislocations have been found on etched surfaces. The growth units not only add in the kink site but also create another, which is favorable to growth. The general form of this model is in equation (2.22)

$$G = A_1 \sigma^2 \tanh(A_2 / \sigma) \quad (2.22)$$

where G = Growth rate of an individual crystal ($\text{m}\cdot\text{s}^{-1}$)

σ = Supersaturation

A_1, A_2 = Constant values

The α values of some systems are known, and can be compared to their crystal growth mechanism. This information is summarized in Table 2.2.

Table 2.2 Prediction of growth mechanism via estimation of α factor (Garside, 1985b)

Material	Solvent(s)	α	Mechanisms
Sucrose	Water	4	BCF
Hexamethylenetetramine	Water	0.5	Continuous growth
	Ethanol	5	BCF
	Water/acetone	0.9	B+S
n-C ₂₈ H ₅₈	Petroleum ether	6.2	BCF
n-C ₃₆ H ₇₄	Petroleum ether	3.6	B+S

BCF: Burton-Caberra-Frank, B+S: Birth and spread

2.2 Literature Review

2.2.1 Growth rate dispersion

Growth rate dispersion or GRD, a phenomenon where the individual crystals of the same initial size grow at different rates under identical conditions of supersaturation, temperature and hydrodynamics, was first seen by White and Wright (1971) in sucrose batch crystallization. Their results demonstrated that when seed crystals with a narrow size range were grown for a period of time, product crystals showed a distinct spread of sizes.

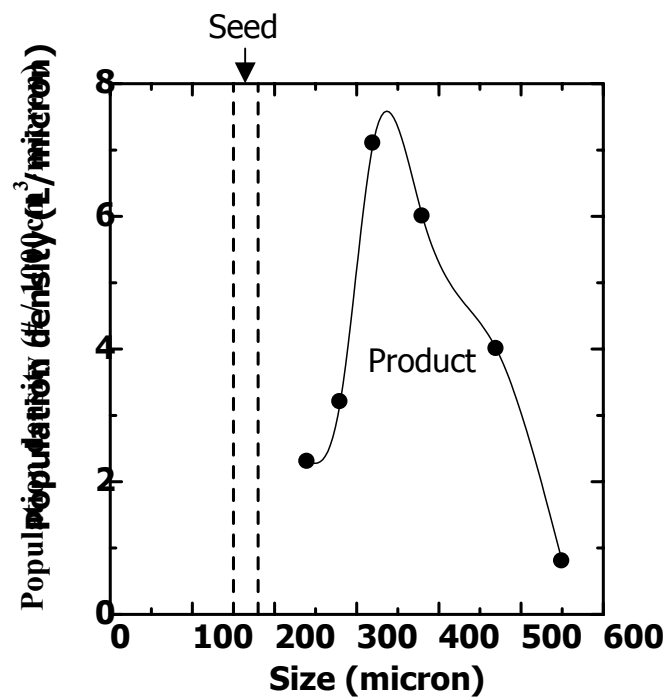


Figure 2.9 The spread in sizes after a growth experiment. (White and Wright, 1971)

As the supersaturation was kept the same for all crystals the only reasonable explanation is that crystals of one size exhibit a spread in growth rates. White and Wright called the spread in sizes “size dispersion”. Janse and De Jong (1976) also found the same results in the fluidized bed crystallization of $K_2Cr_2O_7$

crystals, and showed that the narrow size distribution of seed crystals broaden to the wide size distribution during the growth experiment and they called this phenomenon “growth dispersion”. The GRD in the other systems with different types of materials and crystallizers found by several researchers are summarized in Table 2.3.

From Table 2.3, it is noted that GRD can be found in the systems where the seed crystals were produced from either primary or secondary nucleation and also found in many types of crystallizer. Many GRD studies were carried out in the single crystals in Photomicroscopic cell as illustrated in Figure 2.10, which was initially used by the group of Larson (Garside and Larson, 1978). This technique can provide a lot of results related to the individual crystals, and hence they are applied in the model of mass crystallizers. The works of Garside, however, suggested that the magnitude of dispersion determined from single crystals is generally larger than those characterized from crystal population (Garside, 1979).

Table 2.3 GRD in crystallization systems

Material	System investigated	Crystallizer	Reference
Sucrose	Population of small crystals (150-180 μm)	Batch	White and Wright (1971)
	- Population of small crystals (90-120 μm) - Small single crystals (90-120 μm)	- Batch - small-cell	Liang, Hartel and Berglund (1987)
	- Large single crystals (500-1300 μm)	Small-cell	Fabian, Hartel and Ulrich (1996)
$\text{K}_2\text{Cr}_2\text{O}_7$	Population of small crystals	Fluidized bed	Janse and De Jong (1976)
$(\text{NH}_4)_2\text{SO}_4$	- Population of small crystals ($< 600 \mu\text{m}$) - Primary nucleation	Batch	Westhoff et al. (2002)
KDP	- Small single crystals (0.02-0.2 mm)	Small-cell	Mitrović et al. (1999)
ADP	- Small single crystals (10-100 μm) - Primary nucleation	Small-cell	Garside and Ristić (1983)

Table 2.3 GRD in crystallization systems (Cont.)

Material	System investigated	Crystallizer	Reference
Potash alum	- Small single crystals (1-15 μm) - Secondary nucleation	Small-cell	Garside and Larson (1978)
	- Small single crystals (5-50 μm) - Secondary nucleation	Small-cell	Wang, Mersmann Kind (1990)
	- Large single crystals (1-3 mm)	Flow- cell	Lacmann and Tanneberger (1995)
Rochelle salt	- Small single crystals (0.06-0.1 mm) - Primary nucleation	Small-cell	Mitrović (1987)
KNO_3	- Small single crystals	Small-cell	Herden and Lacmann (1997)
Ammonium sulphate	- Population of small crystals (< 600 μm) - Primary nucleation	Batch	Westhoff et al. (2002)
Ammonium alum	- Small single crystals (8-60 μm) - Secondary nucleation	Small-cell	Teodossiev (1987)
NaNO_3	- Small single crystals - Secondary nucleation	Small-cell	Jones and Larson (1999)

2.2.2 Proposed mechanism for GRD

Because the occurrence of the variations of growth rate of the uniform sized crystals affects the CSD of the product crystals and hence product quality, a large amount of research has been conducted to determine the cause and mechanism of GRD. While a number of significant advances have been made, the mechanisms of GRD are still not fully elucidated. Only two models have been found to describe experimental data, the Constant Crystal Growth model (CCG) and Random Fluctuation model (RF). The CCG model describes the constant growth rate of each crystal along the growth periods, which might differ even for crystals of the same size growing under identical conditions, and the RF model postulates the random time fluctuation of the growth rate of single crystals, however assuming that the average growth of each crystal is the same. The relationship between the crystal sizes and time of each model is illustrated in Figure 2.11.

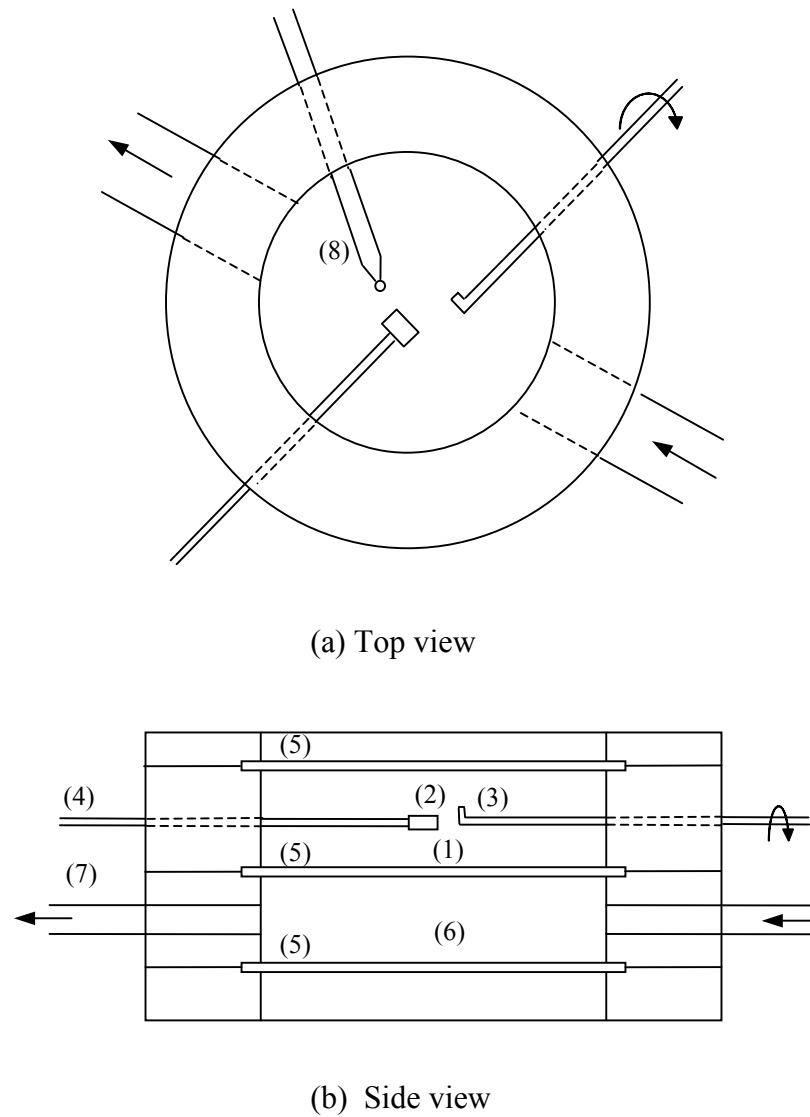


Figure 2.10 Schematic diagram of photomicroscopic cell used to observe secondary nucleation: (1) solution, (2) parent crystal, (3) contact rod, (4) support rod, (5) cover glasses, (6) constant temperature water, (7) water inlet and outlet, (8) thermostat

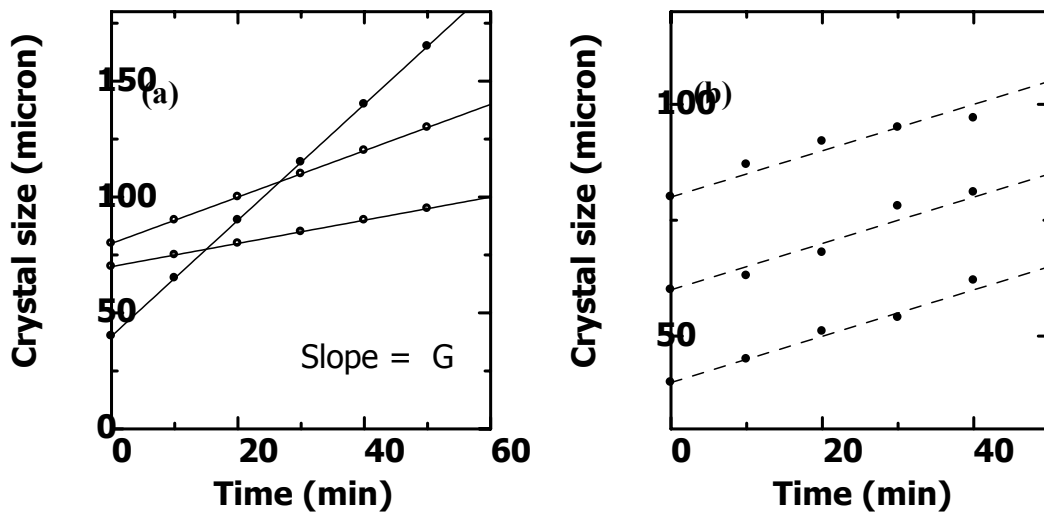


Figure 2.11 Two models accepted for describing GRD (a) the Constant Crystal Growth (CCG) model (b) the Random Fluctuation (RF) model.

Studies of mechanism of GRD have been focused on the difference in the surface integration of crystal growth rather than in the diffusion step. The reason is that there is a well known “law” of crystallization namely McCabe’s ΔL law which states that if any two crystals of the same species grow at the same conditions, the two crystals must have the same increase in a characteristic linear dimension with time, and thus have the same linear crystal growth rate (McCabe, 1929). The validity of the law may be easily proved if we consider the flux of the solute towards the growing crystal:

$$N_A = k_x (x - x_i) \quad (2.23)$$

where

- N_A = Flux of solute to the growing crystals ($\text{mol}\cdot\text{m}^{-2}\cdot\text{s}^{-1}$)
- k_x = Liquid phase mass transfer coefficient ($\text{m}^2\cdot\text{s}^{-1}$)
- x = Mole fraction of the solute in the bulk liquid (-)
- x_i = Mole fraction of the solute at the interface (-)

The total molar solute deposition rate is the molar flux multiplied by the interfacial area, which is the surface area of the crystal. Thus, the rate of increase of the crystal volume is:

$$\bar{V} = \frac{M}{\rho} A_c k_x (x - x_i), \quad (2.24)$$

where \bar{V} = Rate of increase of the crystal volume ($\text{m}^3 \cdot \text{s}^{-1}$)
 M = Molecular weight of crystals ($\text{kg} \cdot \text{kgmol}^{-1}$)
 ρ = Density of the crystal ($\text{kg} \cdot \text{m}^{-3}$)
 A_c = Surface area of the crystal (m^2)

The rate of increase of the linear characteristic dimension, such as the spherical average diameter, L , is the rate of volumetric increase divided by the surface area:

$$\bar{L} = \frac{M}{\rho} k_x (x - x_i) \quad (2.25)$$

where \bar{L} = Rate of increase of characteristic dimension ($\text{m} \cdot \text{s}^{-1}$)

From Equation 2.25, the linear growth rate thus is a function of the supersaturation field (related to the term in brackets) and a set of constants, but not related to the surface area (or size) of the crystal. According to the study of GRD in the surface integration step, three major causes of GRD have been suggested by several workers as follows:

2.2.2.1 Dislocation density at the surface of crystals

A study on the variation of the concentration of dislocation step sources at the crystal surface has been performed based on the classical theory of Burton, Cabrera, and Frank, which suggests that higher concentrations of dislocation

steps should result in higher numbers of growth sectors for integration, resulting in higher growth rates. The dislocation density of the crystal surface can be measured and observed using etch pit density (EDP) measurement. In the work of Tanneberger et al. (1996), it was found that the face specific growth rate of potash alum increases by a factor of two with increasing etch pit density. This result, however, was not used to make any conclusion. Several studies demonstrated no relationship between GRD and dislocation density. In the work of Ristić and Sherwood (1990), it was found that GRD in potash alum was not due to variation in the number of dislocations in the propagation growth sectors and Herden and Lacmann (1997) also showed that there was no correlation between etch pit density and crystal growth rates.

2.2.2.2 Crystal surface quality

Ulrich and Kruse (1990) performed a study on crystal surface quality and its effect on GRD by comparing the growth of crystals with fragmented and perfect surfaces in different size ranges. This work agreed well with the several works suggesting that crystals with fragmented surfaces grow faster than crystal of the same size with perfect surfaces. In the experiment, Ulrich and Kruse used KNO_3 and K_2SO_4 crystals as the case study, and the main results suggested that for KNO_3 crystals with a size lower than 100 μm , perfect crystals grew faster than the fragment crystals. For K_2SO_4 crystals, it appeared that the fragmented crystals grew faster. Lacmann and Tanneberger (1995) also studied the growth rate dispersion of single potassium aluminum alum crystals by considering the crystal surface quality. Individual face-specific growth rates of hurt and unhurt crystals, with diameters of 1-3 mm, were directly determined at different supersaturations [$\sigma = 0.5\text{-}5\%$]. In their experiments, the unhurt crystal faces grew at a constant velocity over the entire

duration of the experiment. The hurt crystal faces, on the other hand, grew with very high velocity in the first 20 minutes (the healing period) and then the growth rate decreased until it reached a constant value. The main conclusion of the study is that the face-specific growth rates of unhurt crystals are lower than those of hurt crystals.

Wang et al. (1999) performed an experiment to study the growth rate of potash alum when the supersaturation was pulse changed; $\sigma_1:\sigma_2: \sigma_1$ ($\sigma_1 \neq \sigma_2$). Their results showed that the growth rate of potash alum at the second period of σ_1 was not the same as at the first period. The suggestion for this situation was the change of the surface structure of the crystals. Harden and Lacmann (1997) also found the same results, but did not investigate the mechanism involved.

2.2.2.3 Overall lattice strain in crystal structure

The current understanding of GRD is focused on the overall lattice strain in crystal or crystalline perfection. X-ray diffraction analysis (by the Laue method) has been carried out to study the internal crystal perfection. The Laue diffraction patterns revealed considerable distortions and strain in the crystal lattice indicated by a high mosaic spread. The correlation between crystal growth rates and their mosaic spread was proposed. Mitrović (1987) has demonstrated the inverse relation of growth rate and mosaic spread of Rochelle salt. The same results were presented in the work of Ristić et al (1990) and Zacher and Mersmann (1995), who studied the growth of sodium chlorate and the growth of potassium alum, respectively. Their results, however, are in opposition to earlier observations in which crystals that grew faster but, under different external conditions, displayed more defects. A study by Herden and Lacmann (1997) showed no correlation between the growth rates of potassium nitrate crystals and their mosaic spread. This

study corresponded to the criticisms on the work of Ristić et al. (1988), which studied the role of the lattice strain in GRD using synchrotron radiation techniques. Harding et al. (1992) suggested, however, that X-radiation damage could have occurred in the samples and they could find no correlation between the strain and growth rate.

Chapter 3

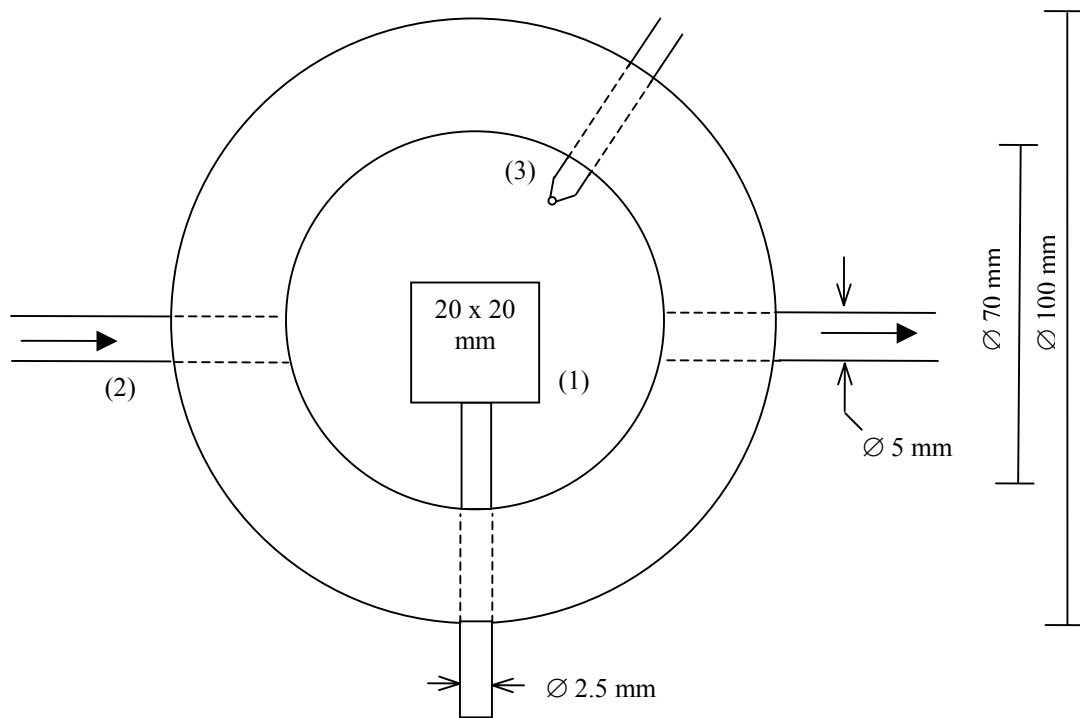
Apparatus, Materials, and Methods

3.1 Apparatus

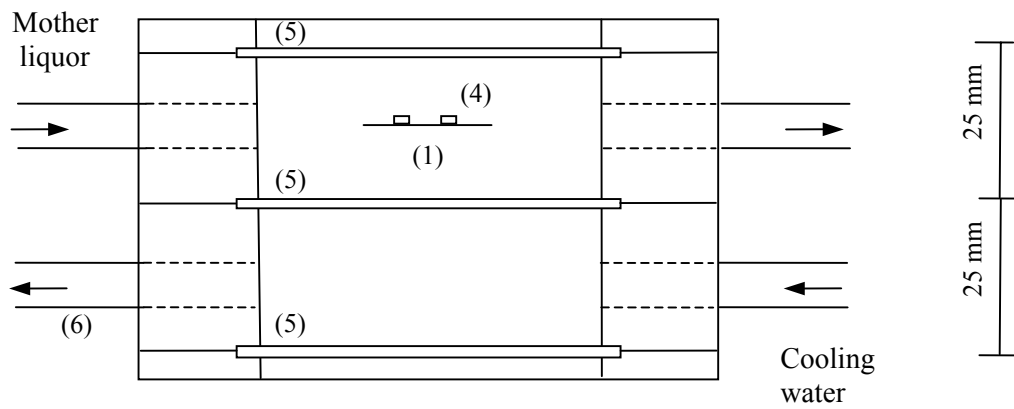
Three types of crystallizers were used in the research; the small-cell crystallizer, the batch crystallizer and the pipe-cell crystallizer. The batch crystallizer investigate growth of crystals in a suspension similar to industrial crystallization. The small-cell crystallizer investigates growth of contact nuclei whereas the pipe-cell crystallizer can investigate growth of individual crystals in a certain defined environment.

3.1.1 Small-cell crystallizer

A schematic diagram of the small cell crystallizer is shown in Figure 3.1. The top cell is for mother liquor, and contains a glass cover slip upon which the crystals grow; the bottom cell, which is separated from the growth section with an acrylic plate, is used for circulation of constant temperature water from a water bath maintained to within ± 0.05 °C. A variable speed peristaltic pump is used to provide a quantitative solution flow rates in experiments involving convection. Crystal size is monitored directly throughout the experiment by the use of a compound microscope. Measurement of the crystal size is enhanced through the use of scaling factor in the lens of the microscope, with the scale calibrated by measurement of wire. In the experiment, the two visible dimensions of the crystal are measured to obtain two facial growth and dissolution rates of each crystal.



(a) Top view



(b) Side view

Figure 3.1 Schematic diagram of small-cell crystallizer (a) Top view, (b) Side view;

- (1) Glass cover-slip, (2) solution inlet and outlet, (3) thermometer, (4) crystals, (5) cover glasses, (6) constant temperature water

3.1.2 Batch crystallizers

The batch crystallizer is a 2-L glass vessel with a sealed glass lid to reduce solvent evaporation as shown in Figure 3.2. The crystallization slurry is agitated at each speed by a centrally located, four-blade impeller driven by an overhead mixer. The crystallizer temperature is maintained at a constant temperature by immersion of a heating coil containing flow of a constant temperature coolant from a water bath maintained at ± 0.05 °C.

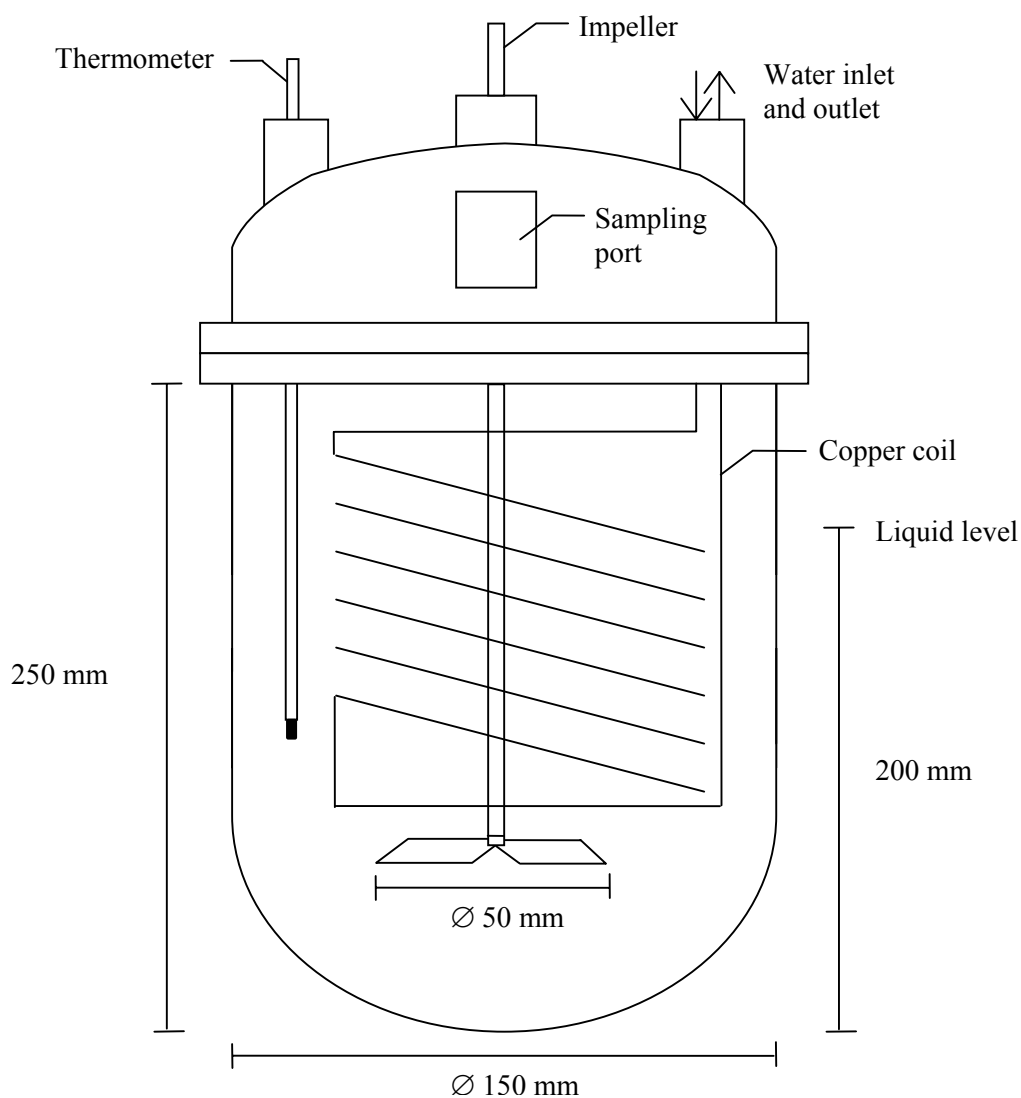


Figure 3.2 A 2-L batch crystallizer

Two convenient methods were used to measure the crystal size; image analysis method and the coulter counter method. The direct measurement method is for large crystals (> 100 micron in length) and the Coulter Counter method is for small sized crystals. In all experiments, direct measurement method was used. More than 30 crystals were retrieved from the crystallizer at each time interval to measure their sizes.

Another batch crystallizer used in this study is a 300-mL batch crystallizer equipped with water-flow jacket as depicted in Figure 3.3. A magnetic stirrer was used to provide high solution flow rate around the crystal grown in the solution.

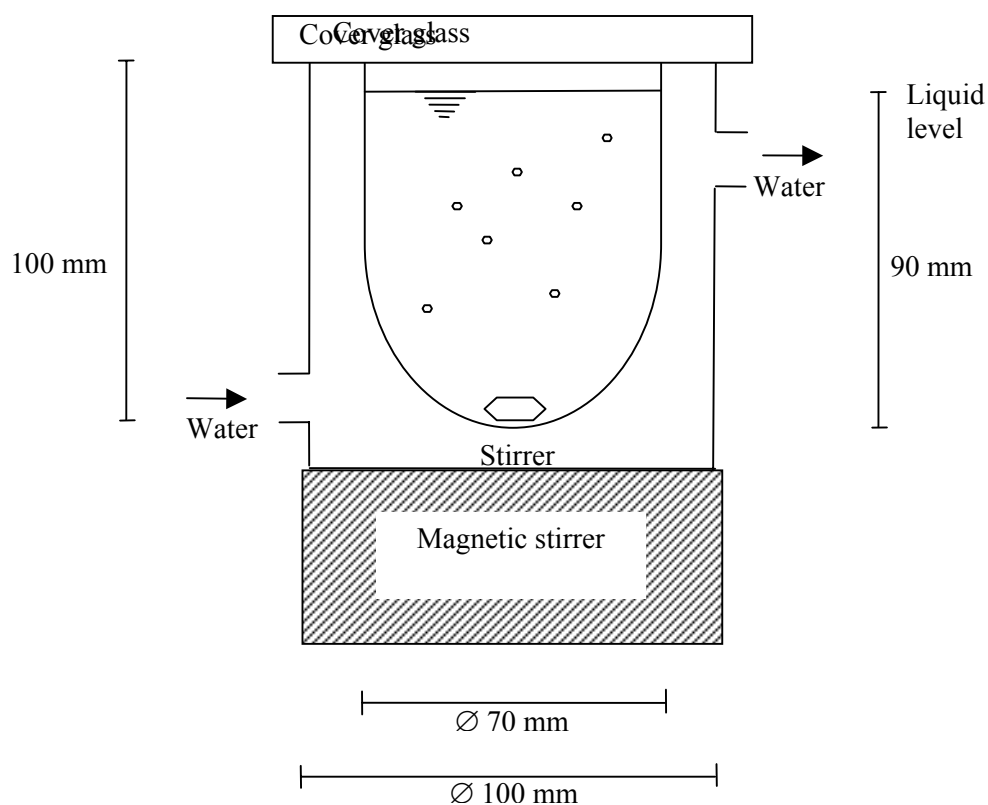


Figure 3.3 A 300-mL batch crystallizer

3.1.3 Pipe-cell crystallizer

A new growth cell has been designed to observe the growth rate of a single crystal. The cell is made from two acrylic tubes connected as in a concentric tube heat exchanger. The inner tube is for solution flow and the outer is for water from a constant temperature bath for temperature control. A crystal is set in the inner tube using a special crystal holder, which consists of holder mounted in a cock. The crystal is held on the holder by two pins and the cock allows the crystal to be removed from the solution and its size measured using a micrometer, and also to be oriented in the solution. The growth rate of the crystal can also be measured during the experiment without taking the crystal out from the cell, by taking its picture using a digital camera attached to a magnification lens.

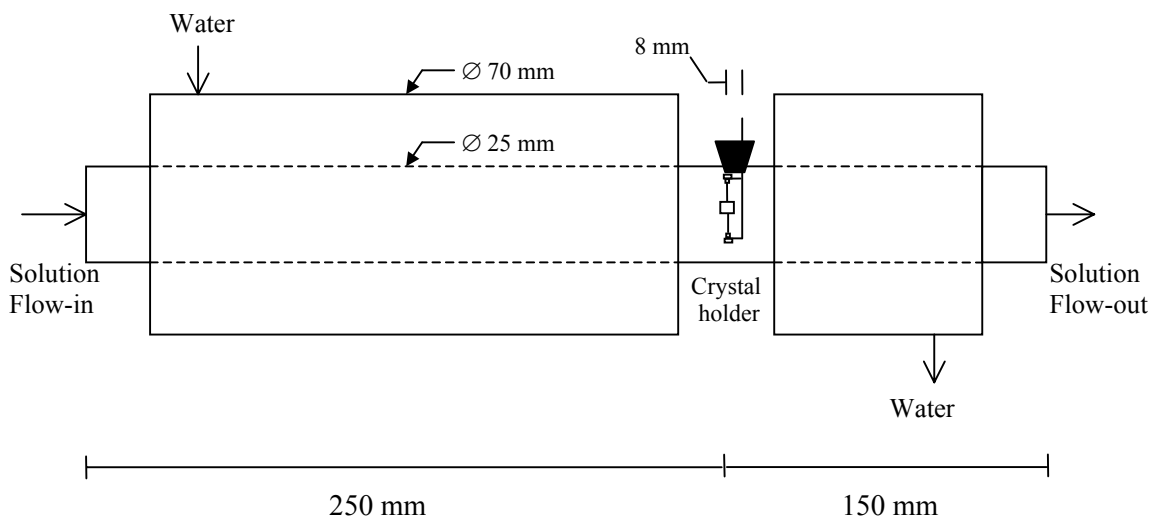


Figure 3.4 Schematic diagram of the pipe-cell crystallizer

3.2 Materials

3.2.1 Sucrose

Sucrose (α -D-glucopyranosyl β -D-fructofuranoside) is a disaccharide sugar with a two ring structure as shown in Figure 3.5. Sucrose is currently one of the highest production crystalline products. Sucrose is particularly significant to the study of growth rate dispersion because much of the production is still performed in batch crystallizers.

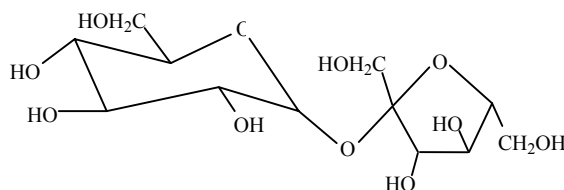


Figure 3.5 Chemical structure of sucrose

Sucrose is an anhydrous monoclinic crystal form, with a large number of crystallographically different faces appearing on the surface of crystals. The typical habit of a sucrose crystal grown from aqueous solution is shown in Figure 3.6 (a). In this study, sucrose crystals grown from aqueous solution were investigated. The seed crystals were taken directly from commercial grade white sugar of approximately 99.9 percent purity (Mitr Phol, Thailand) with a size range of 500-1000 μ m. A SEM photograph of the sucrose seed crystals is illustrated in Figure 3.6 (b). The solubility data of sucrose in aqueous solution as a function of temperature are shown in Appendix A.

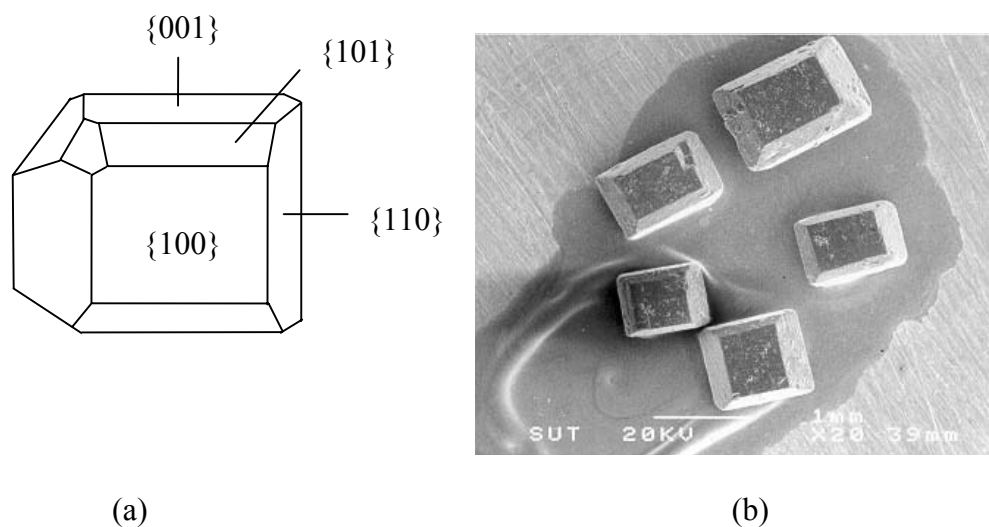


Figure 3.6 Sucrose crystal (a) Monoclinic habit (b) SEM photograph of sucrose seed crystals used in this study

3.2.2 Hexamethylene tetramine (HMT)

Hexamethylene tetramine (HMT, $C_6H_{12}N_4$) or hexamine is a nearly spherical molecule (See in Figure 3.7) that crystallizes in a cubic space group, as a rhombic dodecahedron with only the $\{110\}$ set of faces exposed to the solution in the system as shown in Figure 3.8 (a).

HMT grown from aqueous solutions results in a surface entropy factor < 3 , and thus was used to study whether there is GRD in the diffusion step of crystal growth. The seed crystals were obtained from recrystallization of ACS grade HMT with 99 percent purity (ICN chemical industries). The shape of the HMT crystal is shown in Figure 3.8 (b). The solubility data used for preparing the solution are shown in Appendix A (White, 1967).

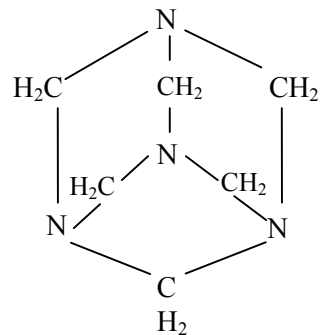


Figure 3.7 Chemical structure of hexamethylene tetramine (HMT)

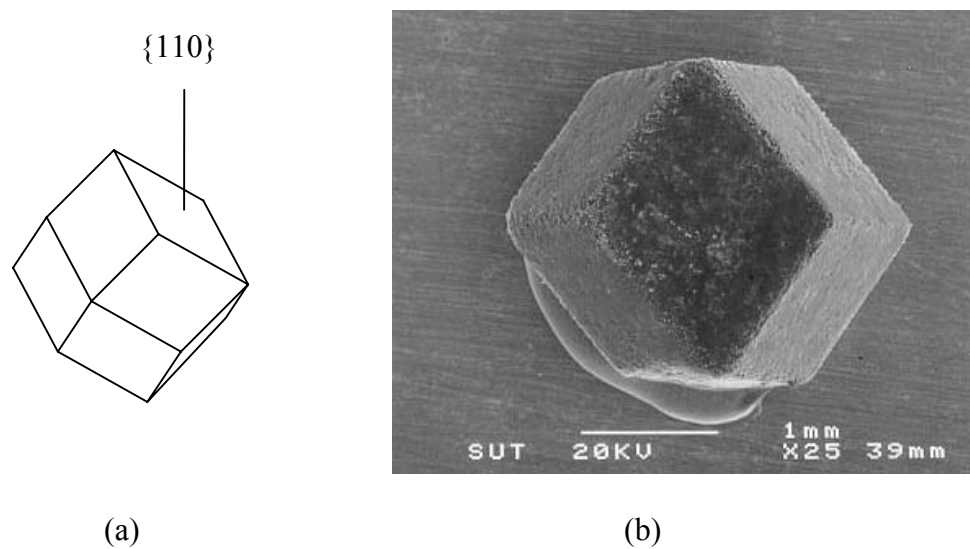


Figure 3.8 HMT crystal (a) Rhombic dodecahedron habit (b) SEM photograph of a HMT seed crystal used in this study

3.2.3 Potassium aluminium phosphate (potash alum)

Potassium aluminium phosphate or potash alum ($\text{KAl}(\text{SO}_4)_2 \cdot 12(\text{H}_2\text{O})$) is an inorganic material with a hexagonal crystal structure. In Figure 3.9 (a), there are two distinct types of face present but in general the face $\{100\}$ is rarely found in the system. This type of crystal is often selected as a case study due to the fact that a

well-formed crystal possesses a symmetric structure. The size of the face $\{111\}$ can be easily measured for finding the facial growth rate of the crystal.

The growth of potash alum crystals was studied in the potash alum-water system. Solutions were produced from 99.5 percent purity potash alum (Wako Industries) and distilled water. The solubility data of potash alum in water are in Appendix A (Mullin, 2001). The size of seed crystals from recrystallizing the crystal in aqueous solution was in a range of 550-1000 μm .

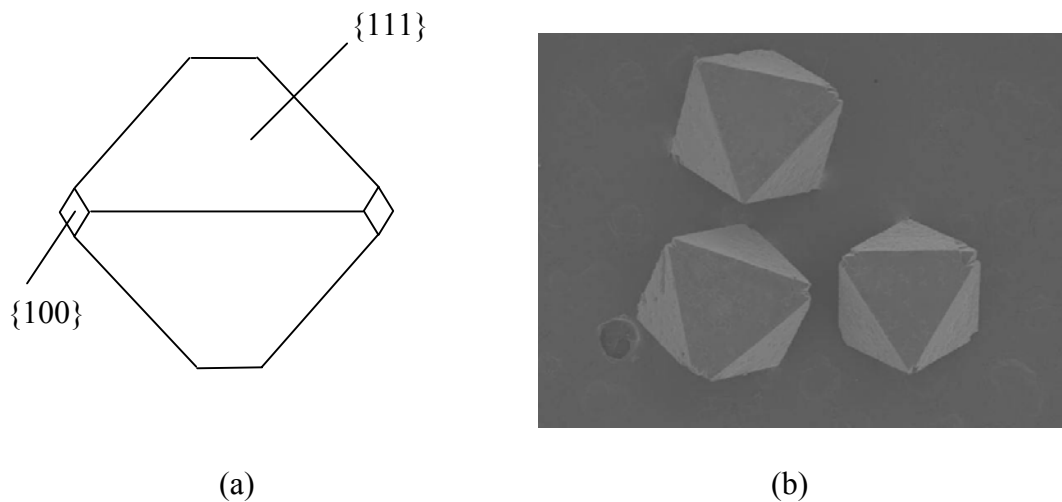


Figure 3.9 Potash alum crystal (a) Rhombic dodecahedron habit (b) SEM photograph of potash alum seed crystals used in this study

3.2.4 Potassium dihydrogen phosphate (KDP)

Potassium dihydrogen phosphate or KDP (KH_2PO_4) is the other type of inorganic material used in this study. The crystal structure of KDP being recrystallized from aqueous solution is tetragonal as depicted in Figure 3.10(a).

Solution of KDP in aqueous solution were prepared from 99.5% percent purity (Wako Industries) and distilled water. The solubility data of KDP in

water are in Appendix A (Mullin, 2001). The size of seed crystals was measured by using the relationship of $\sqrt{S_1 S_2}$ with the size range of 850-1500 μm . A SEM photograph of KDP crystals used in the experiment is shown in Figure 3.10 (b).

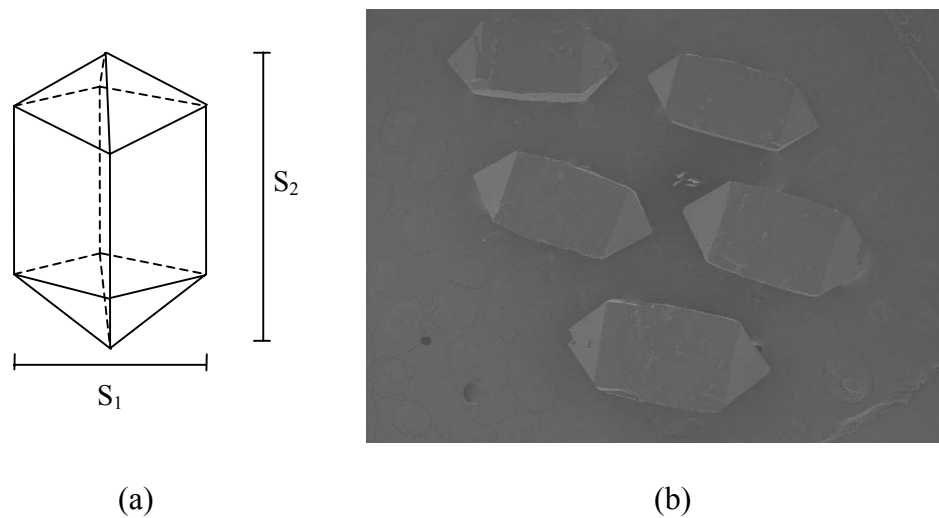


Figure 3.10 KDP crystal (a) Tetragonal habit (b) SEM photograph of KDP seed crystals used in this study

3.3 Methods

With the three objectives of this study, the methods to approach each objective are described below.

3.3.1 Comparison of the average growth rate data obtained from different types of crystallizer

The average growth and dissolution rates of sucrose crystals obtained from three types of crystallizer, including the small-cell, the 2-L batch and the pipe-cell crystallizers were measured and were compared under the same experimental

conditions. The temperature used in all experiments was set constant at 29.0 °C. Two levels of supersaturation as well as two level of undersaturation were used. The supersaturations for growth were 2.20% and 3.60% and the undersaturations for dissolution were 2.20% and 3.60%. The hydrodynamic conditions were varied; stagnant and convection where surface integration was expected to dominate. To ensure that the mass transfer rate does not effect on the crystal growth rates, the measurement of growth rates of sucrose crystal as a function of solution flow rate of each type of crystallizer was also performed as shown in Figure 3.11. The number of crystals and the solution flow rate used in each crystallizer are shown in Table 3.1.

Table 3.1 Number of crystals and the solution flow rate used in each type of crystallizer

Type of crystallizer	Number of crystals per run	Solution flow rate	
		Stagnant	Convection
Small-cell	10	No flow	150 mL·min ⁻¹
Pipe-cell	1	No flow	200 mL·min ⁻¹
Batch	30	100 rpm*	500 rpm ⁺

* Not stagnant, but a small degree of agitation was required to ensure crystals did not become stationary at the base of the crystallizer and agglomerate. ⁺ Sufficient for surface integration limited growth.

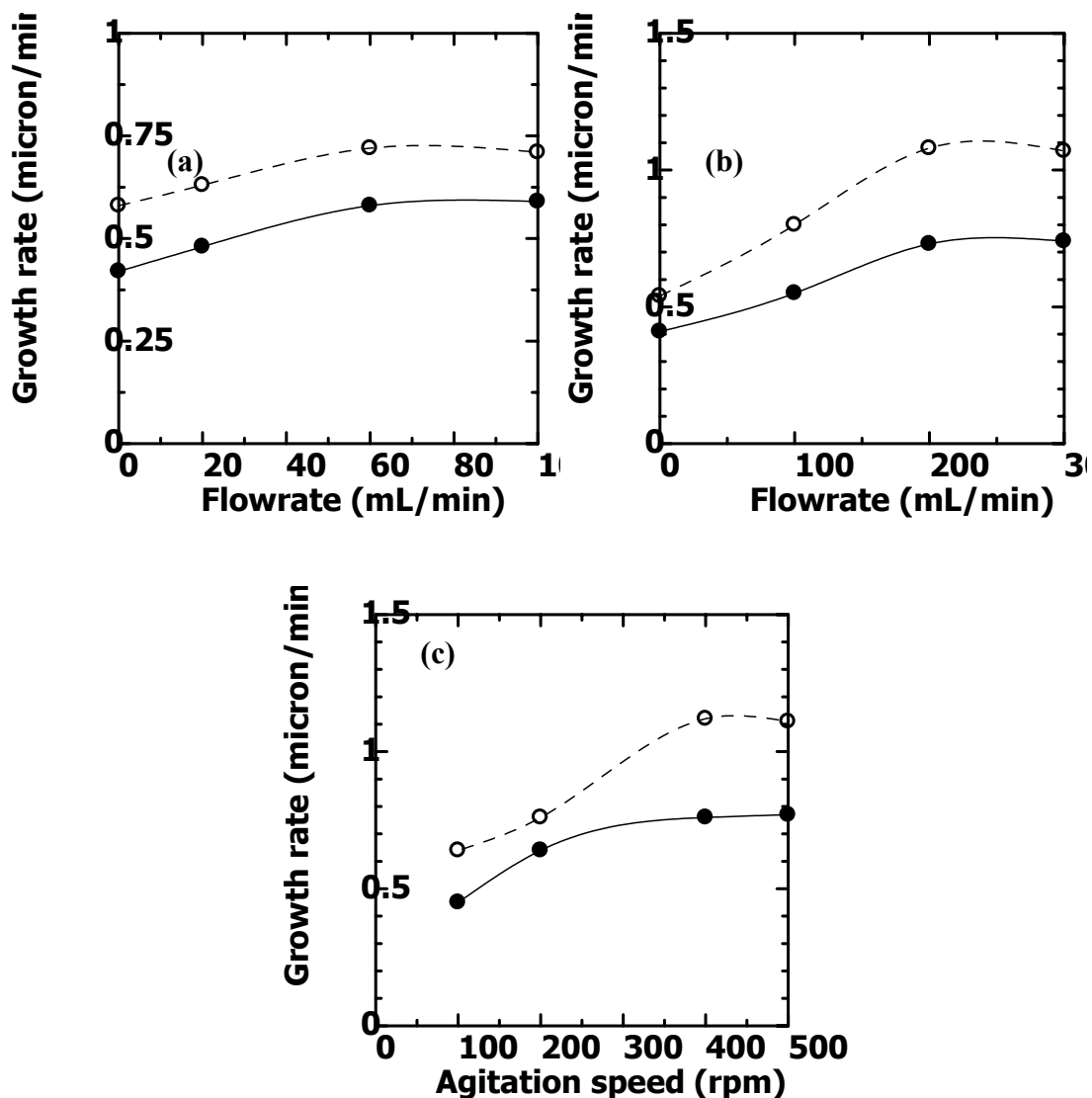


Figure 3.11 Average crystal growth rates for sucrose grown from aqueous solution at various solution flow rates in (a) the small-cell crystallizer (b) the pipe-cell crystallizer and (c) the 2-L batch crystallizer ; ● $\sigma = 2.20\%$; ○ $\sigma = 3.60\%$ relative supersaturation

The method used to measure the size of crystals for each technique is the direct measurement method, by the use of a compound microscope containing a calibrated scale in the lens. Calibration of the scale was performed by measuring

crystals and a standard wire that had previously been measured with a three-decimal digital micrometer. Relative errors from the measurement of the scale of microscope were about 1 percent which produced the error in growth and dissolution rates around $\pm 0.05 \mu\text{m} \cdot \text{min}^{-1}$.

According to comment of Garside (1979) stating that the magnitude of GRD in the small-cell crystallizer is larger than the other systems, a hypothesis was proposed that the hydrodynamic condition around the crystals on over the glass cover slip is not uniform. Thus, a study of the artifact of the small-cell crystallizer was also performed to study the hydrodynamic conditions of the small-cell crystallizer. In the experiment, the growth rates of sucrose crystals at two different positions on the cover slip in the small cell crystallizer were investigated. Because the crystals grown in the small-cell crystallizer are attached on the glass cover slip, the method to change the positions of the crystal in the cell is to change the orientation of the glass cover slip by 90° as depicted in Figure 3.12. Crystal 1 is at the same position but the orientation of the crystal faces relative to the solution flow changes, while crystals 2 and 3 change both their positions, and the orientation of the crystal faces relative to the solution flow.

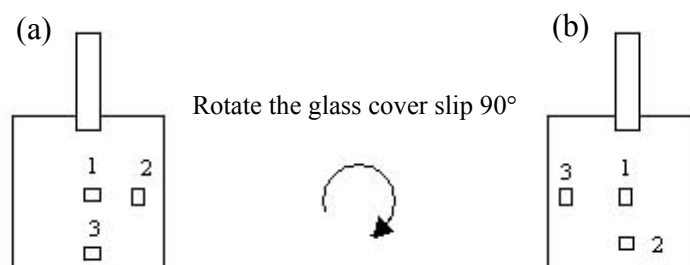


Figure 3.12 Change of the positions of the crystals in the small-cell crystallizer

3.3.2 Study of which growth mechanism or mechanisms (mass transfer and surface integration step) is responsible for GRD

3.3.2.1 Study of GRD in the diffusion step

Growth rates and dissolution rates of HMT crystals were investigated under stagnant and convection conditions. HMT has a very low value of the surface entropy factor, indicating that crystal growth in stagnant solutions is almost certainly controlled by diffusion. This has been confirmed and discussed in a series of papers on HMT growth from the group of Bourne and Davey (1976). The growth and dissolution of HMT was then studied as a means to confirm whether either, or both, the rate dispersions could be attributed to dispersion in rates of mass transfer.

In the stagnant case, experiments were carried out in the pipe-cell crystallizer. The growth rates of the crystals in convection case were observed in the 2-L batch crystallizer. The agitation speeds used in this case were varied at 100, 200, 350 and 500 rpm. The supersaturation and undersaturation were equivalent at $\pm 0.11\%$ and $\pm 0.22\%$ in each solution flow rates

3.3.2.2 Study of GRD in the surface integration step

Growth rates and dissolution rates of sucrose crystals were investigated under stagnant and convection conditions in the 2-L batch crystallizer. The growth rates of sucrose crystals in stagnant conditions were observed in the pipe-cell crystallizer whereas the batch crystallizer was employed in the convection cases. The agitation speeds were varied at 200, 400 and 500 rpm. The two equivalent supersaturations and undersaturations used were $\pm 2.20\%$ and $\pm 3.60\%$.

3.3.3 Determination of the possible causes of GRD in the growth mechanism

3.3.3.1 Possible cause of GRD in the diffusion step

A study of the possible cause of GRD in the mass transfer process was focused on the effect of different flow orientation around crystal. The study of flow orientation around the crystal was performed in the pipe-cell crystallizer. With the crystal holder, a crystal set in the cell was able to be rotated at any angle to the flow of solution. The hypothesis of this study was that if there was an effect of solution flow around the crystal, the facial growth rates of each face of the crystal were not the same even though the faces are crystallographically equivalent. In other words, each face of the same crystal should grow at different rates. The face that faces into the flow of solution should grow faster than the opposite face (at the back of the crystal). In the experiment, the HMT crystals were grown in the pipe-cell crystallizer with a very low solution flow rate. By considering a single HMT crystal's shape in Figure 3.13, HMT crystal consists of twelve faces, six pairs of parallel opposite faces. To compare the growth rate of each face of a crystal (facial growth rate), the crystal was held on the crystal holder as illustrated in Figure 3.13. The facial growth rate was obtained from the increase of size of each two faces (Face 1 and Face 2) of the crystal. By using image analysis, images of the crystal were captured using a digital camera at several time intervals. The initial size of each face was measured from the middle point of the crystal to each face. The increase in size of each crystal's face was also measured from the same initial point and was plotted with time to obtain their facial growth rates.

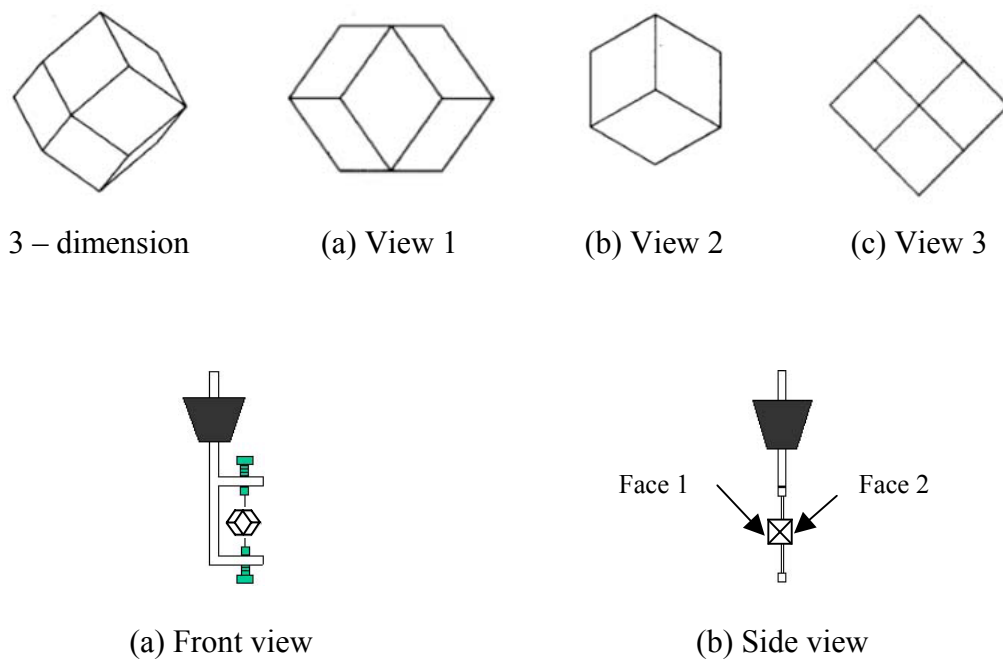


Figure 3.13 Crystal held on the holder to study the effect of hydrodynamic on its facial growth rate

3.3.3.2 Possible cause of GRD in surface integration step

The surface roughness observed in microscopic scale was expected to be a major cause of GRD in the surface integration step of crystal growth. The method to study was divided into five main parts as shown below.

a) Determination of the effect of supersaturation levels on the crystal surface

Experiments were performed by observing the surface of each sucrose crystal grown under different supersaturation. Growth experiments took place in both the pipe-cell and the batch crystallizer. The crystals were grown at 1.50%, 2.20%, 3.60% and 5.00% percent relative supersaturation at conditions where the growth rate was integration controlled. The photographs of the individual crystals

before and after growth were taken by a digital camera under a microscope. SEM photographs were also prepared for the product crystals (after growth). The surfaces of the other crystals including potash alum and KDP were also observed after growth at low and high supersaturation by using a Scanning Electron Microscope (SEM). To produce the same history for the seed crystals, all types of seed crystals were first dissolved with a low undersaturated solution, followed by further growth in a low supersaturated solution for a short period.

b) Determination of effect of growth history on the current crystal growth

Experiments for three crystals; sucrose, potash alum and KDP were carried out in the batch crystallizer under isothermal conditions. In all cases, two groups of 200 crystals were each initially grown at low different supersaturations to produce a different growth history. The crystals in each group were then separated into equal batches to subsequently grow in various supersaturations. For example, a group of 200 sucrose crystals grown for 2 hours in 1.5% relative supersaturation were separated into 4 groups, which were subsequently grown for 2 hours at 1.50, 2.20, 3.60 and 5.10% relative supersaturation.

The diagram of the method is illustrated in Figure 3.14. The values of ΔC_1 , ΔC_2 and ΔC_3 for each type of crystal and the temperature used in the experiments are summarized in Table 3.2.

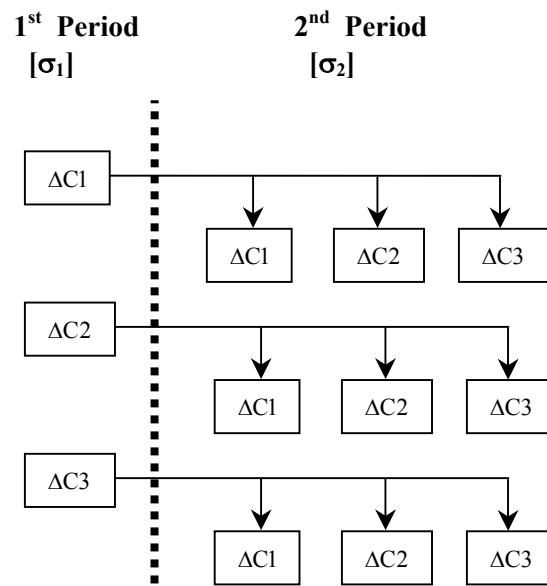


Figure 3.14 The method to study the effect of growth rate history

Table 3.2 The conditions used in the growth rate history experiments

Type of crystals	Temperature (°C)	Supersaturation (%)			
		$\Delta C1$	$\Delta C2$	$\Delta C3$	$\Delta C4$
Sucrose	29	1.50	2.20	3.60	5.00
Potash alum	24.3	3.50	5.90	7.60	-
KDP	24.3	2.50	3.80	5.00	-

To measure the average growth rates, all crystals were retrieved by filtration using a vacuum pump every 30 minutes in order to take photographs for size measurement.

c) Study of the growth rate of sucrose crystals when the supersaturation was pulse changed

These experiments were carried out in the pipe-cell crystallizer. A single sucrose crystal was grown for 3 hours under an initial supersaturation (σ_1), followed by growth at a second supersaturation (σ_2), after which the supersaturation was returned to the initial supersaturation (σ_1). The value of the initial supersaturation was fixed at 0.70 percent relative supersaturation; intermediate values were varied at 1.50, 3.60 and 5.00 percent relative supersaturation.

Another experiment was performed to study the effect of growth time for each supersaturation. In the experiment, the individual sucrose crystals were grown in a series of supersaturations σ_1 : σ_2 : σ_1 : σ_2 . Three similar experiments were performed, but the growth time for each supersaturation was varied at 1, 2 and 3 hours, respectively.

d) Observation of the surface of a potash alum crystal during growth, by using Atomic Force Microscopy (AFM)

Ex-situ observation of the surface of potash Alum during growth under low (2.60%) and high (7.50%) supersaturations was performed by using high performance equipment, Atomic Force Microscopy (AFM). The crystal was removed from the solution at each time period and washed by ethanol before scanning. A small area (about $50 \times 50 \mu\text{m}$) of the crystal's surface was scanned and analyzed.

The observation of the surface of potash alum was also performed when the supersaturation was changed from 7.50% relative supersaturation (at high supersaturation producing a rough surface) to 2.50% relative supersaturation. The AFM scans of the initial surface of crystal (crystallized from 7.50% relative

supersaturation), and the surface of the crystal after growing in 2.50% relative supersaturation for 30 minutes and 1 hour were taken.

e) Study of the relationship between GRD and crystal surface energy (γ)

This study was done to find the link between the crystal's parameter such as surface energy (γ) and the magnitude of GRD. The experiment was performed by comparing the magnitude of GRD during growth of crystals which have different surface energy factors. Three types of crystal were selected including potash alum, KDP and Potassium sulphate (K_2SO_4). As reported in Söhnel (2001), the surface energy of potash alum, KDP and K_2SO_4 is $2.5 \text{ erg}\cdot\text{cm}^{-2}$, $12\text{-}16 \text{ erg}\cdot\text{cm}^{-2}$ and $24 \text{ erg}\cdot\text{cm}^{-2}$, respectively. To ensure the surface energy data reported in the reference are reliable, determinations of the surface energy of each crystal were also performed. The method to determine the surface energy is present in Appendix B.

The growth experiments were carried out in a batch crystallizer. In each experiment, about 200 crystals were retrieved at every 1 hour for size measurement. The crystal size distributions were plotted at each time interval to analyze the magnitude of GRD.

Chapter 4

Results and Discussion

As the major aim of this thesis is to understand the possible reasons of growth rate dispersion, three main works were developed for the study: 1) which mechanisms (the diffusion and/or the surface integration step) are responsible for GRD; 2) the possible causes of GRD in each mechanism; and 3) whether the artifacts of the experimental technique also appear to be a cause of GRD. In the experiments, the artifacts of techniques were studied by comparing the growth and dissolution rate of sucrose crystals obtained from three types of crystallizers, the small-cell, the pipe-cell and the 2-L batch crystallizers. The results of the final study are first discussed in this chapter to demonstrate which technique gives the most accurate growth and dissolution rate results.

The study of which mechanisms are responsible GRD are then reported and described. The results were analyzed from the growth and dissolution rate at equivalent relative supersaturation and undersaturation of sucrose and HMT crystals under stagnant and convection conditions. The growth rate results demonstrate the rate dispersion either in the diffusion step (stagnant conditions) or in the surface integration step (high convection conditions). The rate dispersion in the diffusion step can also be shown if there is rate dispersion in the dissolution rate of crystals.

A possible cause of GRD in the diffusion step was studied based on a belief in the variation of mass transfer rates of each crystal due to the difference of flow

orientation around the crystals. This study investigated the effect of flow orientation around a single HMT crystal on its facial growth rate. The possible cause of GRD in the surface integration step will be demonstrated and discussed last. This study focused on the effect of microscopic roughness due to the variation of supersaturation levels. This work evidently showed that the difference in microscopic roughness is a major cause of GRD in the surface integration step rather than the effect of internal structure (which might be seen as mosaic spread) as suggested by other studies.

4.1 Comparison of Average Growth Rate Data Obtained From Different Types of Crystallizer

4.1.1 Growth and dissolution rates results of sucrose crystals

The size of individual crystals grown and dissolved in the small-cell and the pipe-cell crystallizers was measured and plotted at each time interval. Either in stagnant conditions or where there was the convection flows, all crystals were found to grow and dissolve as a linear function of time (correlation coefficients of linear regression greater than 0.99) as shown in Figure 4.1 (for the small-cell), and Figure 4.2 (for the pipe-cell). It was also found that the growth and dissolution rates of the individual crystals were different and not dependent on their initial sizes. This was in agreement with the constant crystal growth (CCG) model and constant crystal dissolution model (CCD). The growth rate and dissolution rate results of this work are similar to those in the work of Fabian et al. (1996).

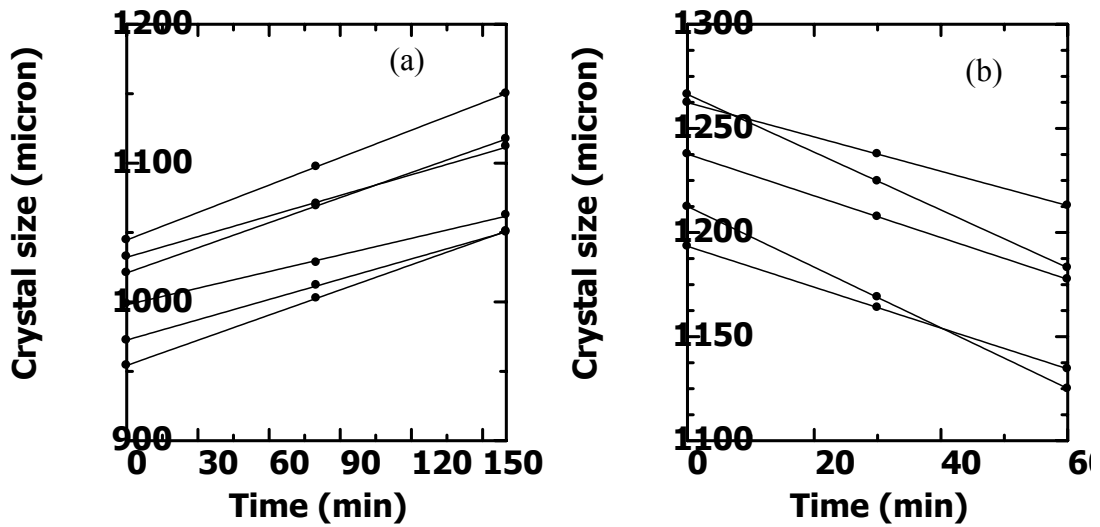


Figure 4.1 Size of individual sucrose crystals vs time in the small-cell crystallizer

(a) 3.60 percent relative supersaturation in stagnant condition

(b) 3.60 percent relative undersaturation in stagnant condition

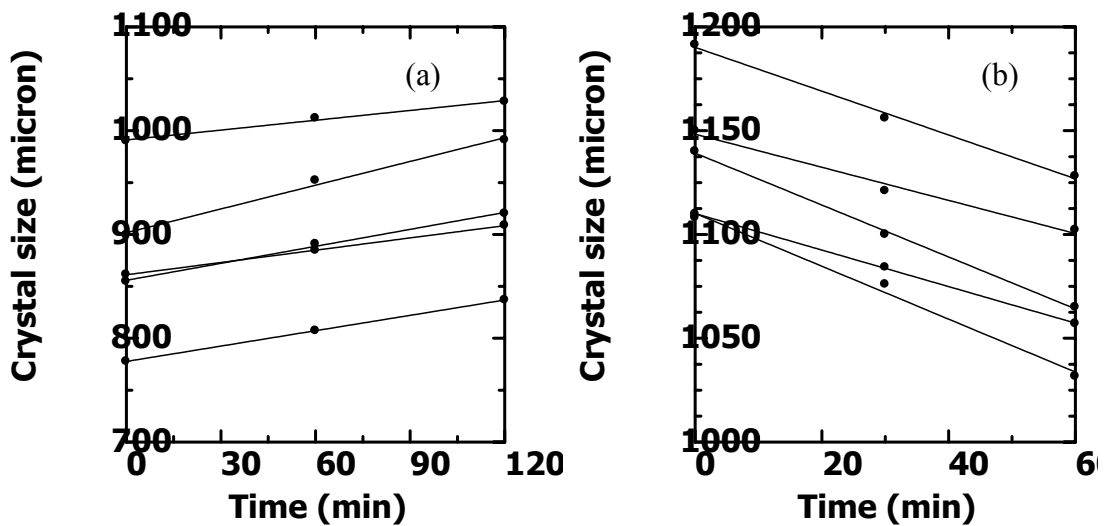


Figure 4.2 Size of individual sucrose crystals vs time in the pipe-cell crystallizer

(a) 3.60 percent relative supersaturation in stagnant condition

(b) 3.60 percent relative undersaturation in stagnant condition

In the batch experiment, the mean size of all crystals in the growth and dissolution experiments can be obtained by the crystal size distribution (CSD). The mean crystal size was found to increase and decrease linearly as depicted in Figure 4.3 (for the growth process) and Figure 4.4 (for the dissolution process). As shown in Figure 4.3 (a), it was found that there was an increase in the width of the CSD when the growth time increased which demonstrates GRD in the growth process. The spread of CSD was also seen in the dissolution process as illustrated in Figure 4.4 (a). The magnitude of the rate dispersion found in the system will be discussed in the following section.

Average growth and dissolution rates of sucrose crystals obtained from each technique at each growth and dissolution condition are summarized in Table 1.

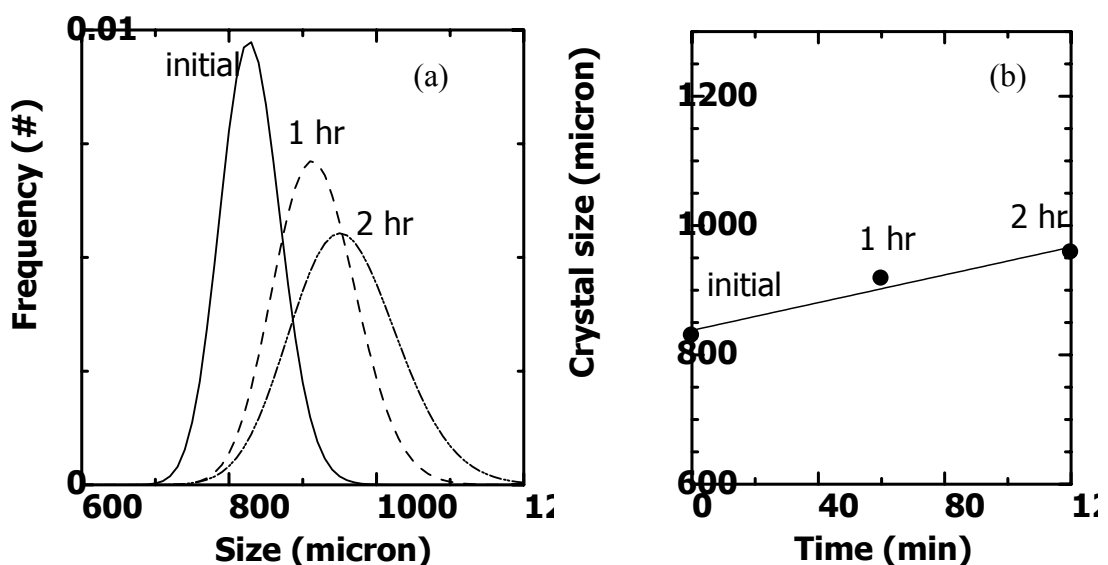


Figure 4.3 Growth of sucrose crystals in 3.60 percent relative supersaturation under convection conditions in the 2-L batch crystallizer

(a) Crystal size distribution (b) Mean crystal size of the CSD vs time

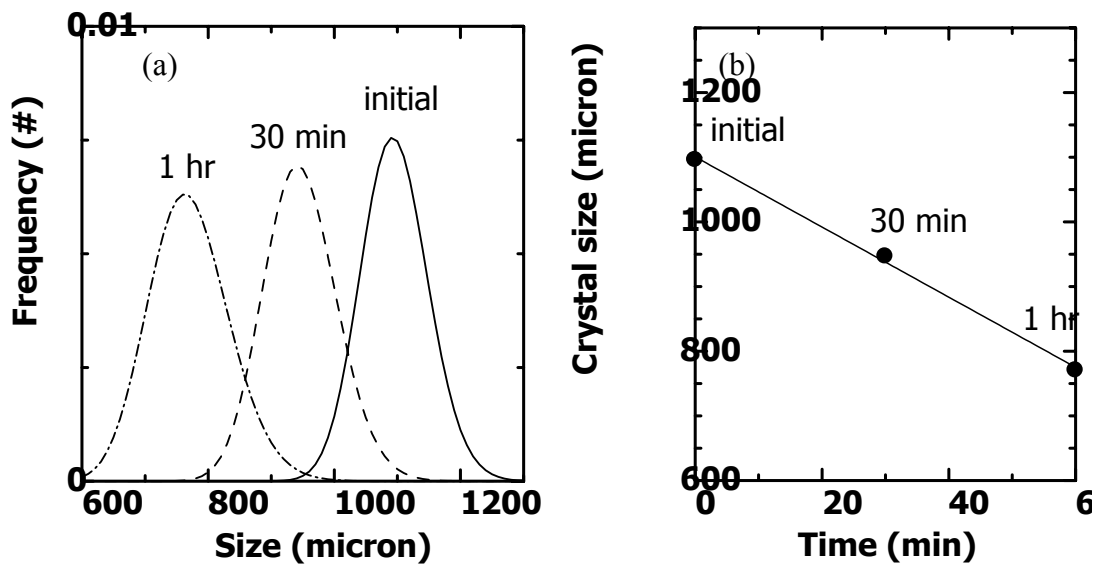


Figure 4.4 Dissolution of sucrose crystals in 3.60 percent relative undersaturation under convection conditions in the 2-L batch crystallizer

(a) Crystal size distribution (b) Mean crystal size of the CSD vs time

Table 4.1 Average growth and dissolution rates ($\mu\text{m}\cdot\text{min}^{-1}$) of sucrose crystals

obtained from the three crystallizers; the small-cell crystallizer, the pipe-cell crystallizer, and the batch crystallizer

Type of crystallizer	Average growth rate (\bar{G})				Average dissolution rate (\bar{D})			
	Stagnant		Convection		Stagnant		Convection	
	2.20%	3.60%	2.20%	3.60%	2.20%	3.60%	2.20%	3.60%
Small-cell	0.41	0.54	0.59	0.66	0.57	1.10	0.73	1.98
Pipe-cell	0.41	0.55	0.73	1.08	0.59	1.07	2.39	4.53
Batch	0.45	0.64	0.75	1.27	0.68	1.35	2.71	5.51

In stagnant conditions, mean growth rate results obtained from the small-cell crystallizer were quite similar to those obtained from the pipe-cell crystallizer. Deviation of the results of the batch crystallizer from the other techniques is probably owing to the speed of agitation in the crystallizer. Use of slow agitation in the stagnant cases in the batch crystallizer is necessary to avoid the crystals attaching to the bottom of the crystallizer and also to stop the crystals agglomerates in the system. The greater mass transfer resistance to crystal growth under the stagnant conditions thus existed in the small-cell and the pipe-cell crystallizers. It is however believed that, in the absence of agitation system, results in good agreement will also be obtained from batch crystallizer. Similar trends were also found in the dissolution rate results. Mean dissolution rates of sucrose in each undersaturation obtained from the small-cell and pipe-cell crystallizer were close whereas there were some positive deviations found in the mean dissolution rates obtained from the batch technique. With very high magnitude of the deviation in dissolution, it may suggest that in the dissolution process, which is controlled by mass transfer, the solution flow rate around the crystals is very significant. Slightly increased agitation speeds, therefore, may cause large change in the dissolution rates.

In the case of high convection, both growth and dissolution rates of sucrose crystals in the pipe-cell and batch crystallizers were very close. Slight differences in the dissolution rates are probably caused by the differences in how crystals are suspended in the two crystallizers. In the batch crystallizer, crystals freely move along the crystallizer (they are suspended by the flow of mother liquor), but in the pipe-cell crystallizer, position of the crystals was fixed by the holder. Hence, the crystals in the batch must have a larger mass transfer area, enabling the molecule

diffusing more than those in the pipe-cell. Average growth and dissolution rates at very high solution flow observed in the small-cell technique showed very large disagreement with the other two crystallizers. The average growth and dissolution rates from the pipe-cell and the batch crystallizers were nearly a factor of two and three, respectively, greater than those from small-cell crystallizer. The small values of growth and dissolution rates in this case are possibly due to the effect of artifact of the small-cell crystallizer. In the small-cell experiment, all crystals were grown on the glass-cover slip, which has a no-slip boundary condition. A computation fluid dynamic (CFD) simulation model run using CFX 5.5.1 confirms this explanation by showing that solution velocity passing the glass cover-slip approaches zero at the solid-liquid interface (Figure 4.5). The simulation result appears to show that the velocity profile of the solution does not change along the glass-cover slip. The fluid velocity near the top surface at the same distance as the top face of a crystal on the slip is only approximately 20% of the mean velocity in the cell.

The growth and dissolution rate models of sucrose crystals under stagnant and convection conditions in each crystallizer as a function of percent super- and undersaturation (σ) can be expressed as shown in Table 4.2. The growth rates can be modeled as a linear function of percent relative supersaturation in all conditions of all three techniques, while the dissolution rates can be modeled as power law functions of percent undersaturation. As discussed earlier, dissolution is a process purely controlled by the diffusion step, where the growth rate and supersaturation relationship of a crystal should be linear. The power function equations of dissolution rate results in this study are unusual, but these results are in agreement the work of Fabian et al. (1996).

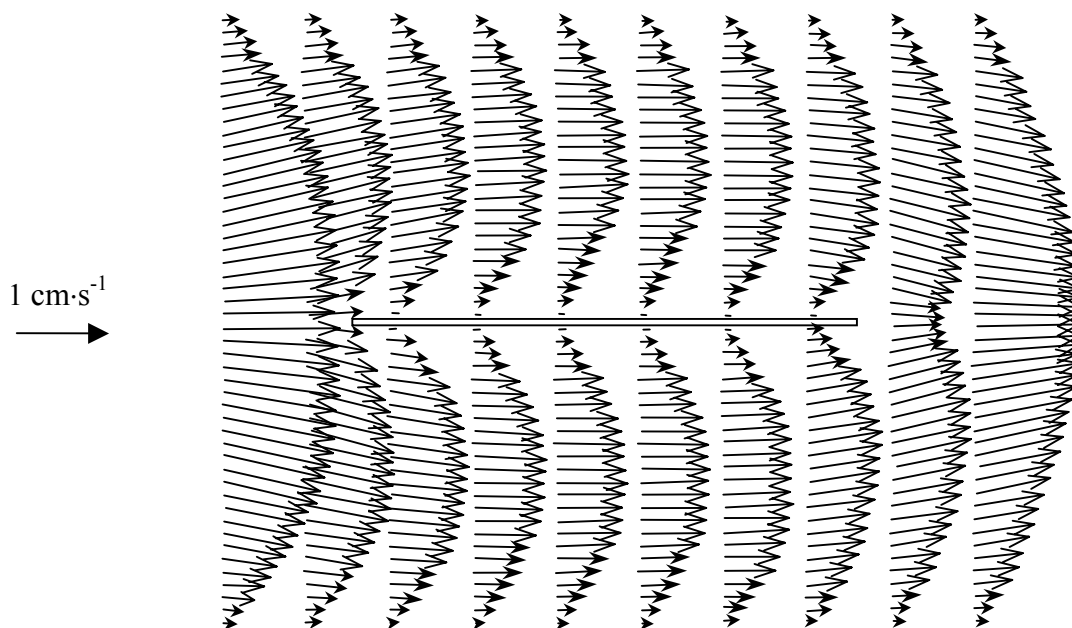


Figure 4.5 Velocity gradient of sucrose-water solution above the glass-cover slip used in the small-cell crystallizer

Table 4.2 Growth and dissolution rate models of sucrose crystals under stagnant and convection conditions (29 °C)

Type of crystallizer	Growth rate model	Dissolution rate model
<i>Stagnant</i>		
Small-cell	$\bar{G} = 0.153 \sigma_G$	$\bar{D} = 0.227 \sigma_D^{1.40}$
Pipe-cell	$\bar{G} = 0.156 \sigma_G$	$\bar{D} = 0.140 \sigma_D^{1.58}$
Batch	$\bar{G} = 0.180 \sigma_G$	$\bar{D} = 0.141 \sigma_D^{1.60}$
<i>Convection</i>		
Small-cell	$\bar{G} = 0.191 \sigma_G$	$\bar{D} = 0.148 \sigma_D^{2.02}$
Pipe-cell	$\bar{G} = 0.303 \sigma_G$	$\bar{D} = 0.860 \sigma_D^{1.30}$
Batch	$\bar{G} = 0.352 \sigma_G$	$\bar{D} = 0.870 \sigma_D^{1.44}$

4.1.2 GRD and DRD results

Both crystal growth and dissolution showed significant rate dispersion. This is common for growth of sucrose crystals but it has only been reported for dissolution recently (Fabian, 1996). The reason that dispersion in dissolution rates is usually not considered is that dissolution is usually believed to be controlled by the diffusion step. Since the diffusion rate depends only on the mass transfer coefficient (dependent on solution properties) and the concentration driving force, there has been no reason to suspect that dissolution dispersion should exist. A possible explanation for this situation that could be considered is that mass transfer coefficients are only well-defined for spheres. For crystal not only is the mass transfer coefficient difficult to calculate but its value will vary both from face to face of the crystal in a way which depends on the orientation of the crystal with respect to the flow field, and over a given face (Garside, 1985b). The magnitude of GRD and DRD can be reported by the value of the coefficient of variation (C.V.) of growth rate distribution defined by

$$(C.V.)_G = \frac{\sigma_G}{\bar{G}} \quad (4.1)$$

$$(C.V.)_D = \frac{\sigma_D}{\bar{D}} \quad (4.2)$$

where	$(C.V.)_G$	= Coefficient of variation of growth rate data
	$(C.V.)_D$	= Coefficient of variation of dissolution rate data
	σ_G	= Standard deviation of growth rate data ($\mu\text{m}\cdot\text{min}^{-1}$)
	σ_D	= Standard deviation of dissolution rate data ($\mu\text{m}\cdot\text{min}^{-1}$)
	\bar{G}	= Average growth rate ($\mu\text{m}\cdot\text{min}^{-1}$)
	\bar{D}	= Average dissolution rate ($\mu\text{m}\cdot\text{min}^{-1}$)

To compare the GRD and DRD results of data from different techniques, the source of the growth and dissolution rate data have to be taken into account. The growth and dissolution rate data of the small-cell and the pipe-cell crystallizer come from the inherent growth and dissolution rates of individual crystal but for the batch crystallizer, similar data cannot be obtained. In the following section therefore comparison between GRD and DRD results obtained from the small-cell and the pipe-cell crystallizer will be discussed. The mean growth and dissolution rates, standard deviation and C.V. of the crystals run in the small-cell and the pipe-cell crystallizer are summarized in Table 4.3.

Table 4.3 Average growth (\bar{G}) and dissolution rates (\bar{D}), standard deviation (σ) and coefficient of variation (C.V.) of sucrose crystals obtained from the small-cell and the pipe-cell crystallizers

	Stagnant				Convection			
	2.20%		3.60%		2.20%		3.60%	
	Small-cell	Pipe-cell	Small-cell	Pipe-cell	Small-cell	Pipe-cell	Small-cell	Pipe-cell
\bar{G}	0.409	0.409	0.535	0.550	0.594	0.727	0.661	1.083
STDEV	0.029	0.033	0.081	0.078	0.115	0.080	0.145	0.104
C.V.	0.070	0.080	0.151	0.141	0.194	0.110	0.219	0.096
D	Stagnant				Convection			
	2.20%		3.60%		2.20%		3.60%	
	Small-cell	Pipe-cell	Small-cell	Pipe-cell	Small-cell	Pipe-cell	Small-cell	Pipe-cell
\bar{D}	0.565	0.592	1.103	1.072	0.733	2.389	1.983	4.526
STDEV	0.083	0.093	0.120	0.136	0.147	0.154	0.388	0.385
C.V.	0.148	0.156	0.109	0.127	0.200	0.064	0.196	0.086

The value of the C.V. of the distribution either in the growth or dissolution data calculated from the two techniques are quite similar under stagnant conditions, confirming that, under stagnant conditions, any crystallizer give accurate results. It is however recommended that the crystals grown in the small-cell crystallizer must be distant from each other to avoid the effect of concentration differences due to the mass transfer limitations. In all conditions involving convection the C.V. values of the small-cell crystallizer are 1.2-1.5 times higher magnitude than those of the pipe-cell crystallizer.

It is believed that the artifact of the small-cell crystallizer is the major cause. In a general experiment, ten to fifteen crystals are mounted on the glass-cover slip in rows. By considering the edge of the cover slip which is in contact with the solution inflow to be the front edge, then crystals near the front edge experience different boundary conditions to those behind them. This is because the crystals near the front edge produce a stagnant or low flow velocity zone behind them, as described in Figure 4.5. The velocity passing to the behind crystals is much lower. This explanation was confirmed by simulating a model of three crystals attached on the glass-cover slip in the small-cell crystallizer using CFX 5.5.1. The simulation result is illustrated in Figure 4.6 showing that the solution velocity was reduced after passing the first crystal to the second crystal. The last crystal, crystal 3, appeared to be in stagnant conditions, since the flow velocity was very low at this point.

An experiment to determine whether the large amount of GRD or DRD is an artifact of the small-cell crystallizer technique was performed. The experiment was studied whether the attachment position of the crystal had an effect on the crystal's growth rate. The method was to change the positions of the crystal in the

cell, i.e. to change the orientation of the glass cover slip by 90° as depicted in Figure 4.7. The crystal 1 is at the same position but in the second position there will be the effect of crystal 3 in front of it, while crystals 2 and 3 change their positions. The solution flow rate passing through the cell was $150 \text{ mL}\cdot\text{min}^{-1}$, which is equivalent to a flow velocity of approximately $1.5 \text{ cm}\cdot\text{s}^{-1}$.

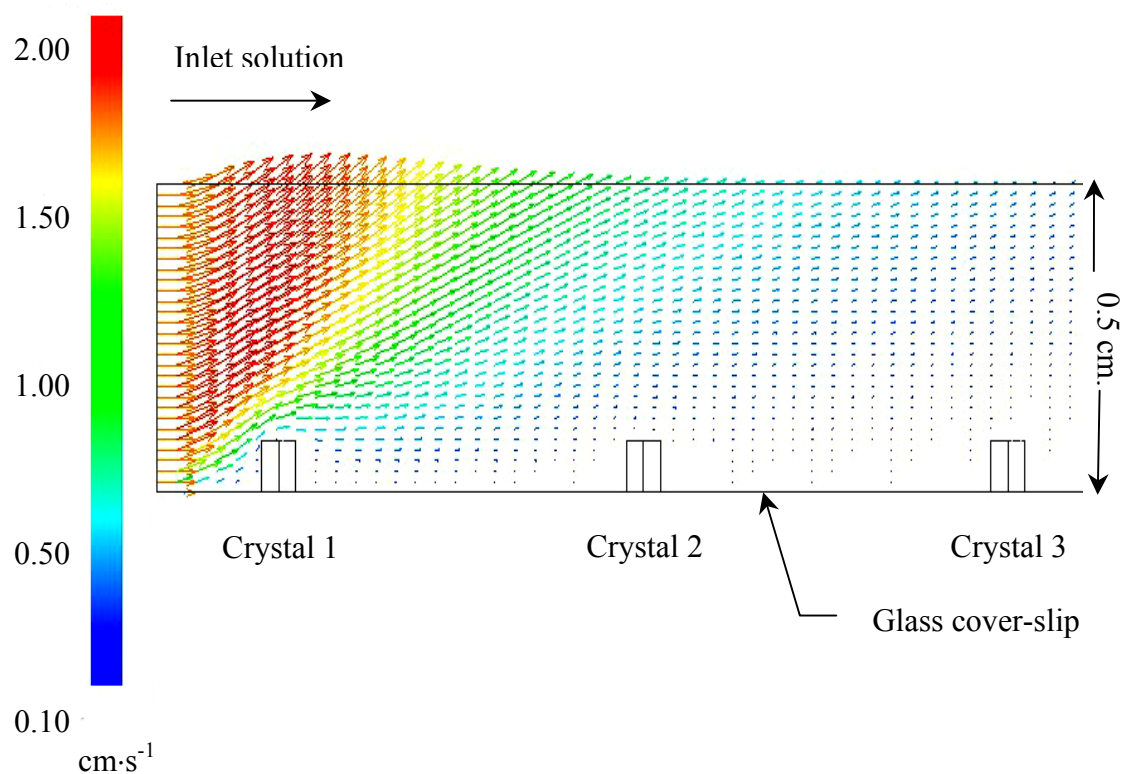


Figure 4.6 Velocity gradient of sucrose-water solution passing three sucrose crystals above the glass-cover slip in the small-cell crystallizer

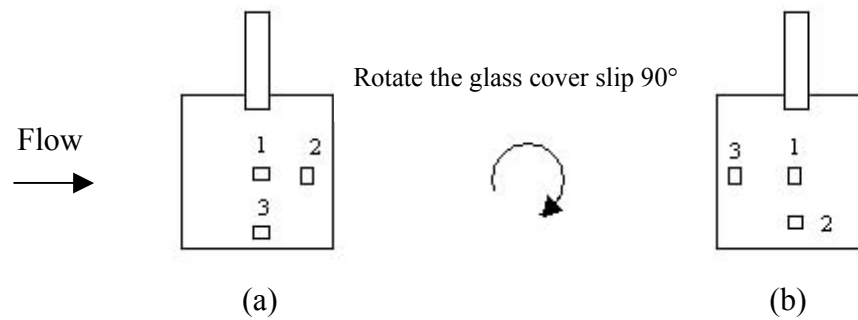


Figure 4.7 Change of the positions of the crystals in the small-cell crystallizer

(a) Position 1 (b) Position 2

The results from five replicate experiments showed a similar trend of the results to the simulation result. The crystal 1 at position 1 grew about 1.2-1.7 times faster than that at position 2. Good agreement results were also found in crystal 2. The growth rates of crystal 2 in Figure 4.7(a) were less than crystal 2 in Figure 4.7(b). No trend of the results was found for crystal 3, though the growth rate data of crystal 3 at different positions yielded different results. Based on these results, there is variation of hydrodynamic conditions found in the small-cell crystallizer, and it must be noted that the individual crystals grew in pipe-cell crystallizer under convection were in a similar hydrodynamic condition because they were mounted at the same position. Hence, it is not surprising that the magnitude of C.V. values in the small-cell crystallizer is very large compared to those in pipe-cell crystallizer. GRD is defined as where seemingly identical crystals grow at different rates under the same environmental conditions including supersaturation and hydrodynamic conditions. The obvious result is that the small-cell crystallizer should not be employed to study GRD under convection conditions. This result appears to invalidate some earlier research in the field of GRD, as the small-cell crystallizer is the most widely used in the study of the phenomenon.

4.2 Study of Which Growth Mechanism or Mechanisms (Mass Transfer and Surface Integration Step) is Responsible for GRD

To study which growth mechanisms are responsible for GRD, the growth and dissolution rates of HMT and sucrose crystals were investigated in the batch crystallizer. In this section, the average growth and dissolution rates of sucrose and HMT crystals will be described first. The GRD and DRD found in the both types of crystals will then be shown and discussed.

4.2.1 Average crystal growth and dissolution rates of HMT and sucrose crystals

The growth and dissolution rates of individual HMT crystal were found to follow constant crystal growth (CCG) and constant crystal dissolution (CCD) models, respectively. The crystals grew and dissolved as a linear function of time, similar to the behavior displayed by sucrose crystals. The crystal growth and dissolution of both solutes depended strongly on both the relative supersaturation (or relative under saturation) and the flow rate of mother liquor (agitation speed). The dependence of the average crystal growth and dissolution rates on these two variables is shown in Figure 4.8 for HMT, and Figure 4.9 for sucrose. The data for each plot are also summarized in Table 4.4. From Figure 4.8 and Figure 4.9, the growth of both crystals followed a typical pattern with both growth and dissolution rates increasing with increasing solution flow, until a plateau is reached; at about 350 rpm for HMT and 400 rpm for sucrose.

In the stagnant case, it is quite interesting that the growth and dissolution rates of HMT crystal are equal; about $0.18 \mu\text{m}\cdot\text{min}^{-1}$ for 0.11% and $0.42 \mu\text{m}\cdot\text{min}^{-1}$ for 0.22% relative supersaturation (or undersaturation), while the average dissolution rates of sucrose crystals under stagnant conditions are larger than the

average growth rates, by approximately 1.5-2 times. Based on the belief that the dissolution process is entirely controlled by the diffusion step, the results found in the HMT crystals case suggest that the growth rates of HMT crystals in aqueous solution under stagnant conditions are controlled by the diffusion step (Mullin, 2001). The growth rate of sucrose crystals (under stagnant conditions) is controlled by the surface integration step (Bourne and Davey, 1976). Therefore, sucrose has lower crystal growth rates than dissolution rates, even under stagnant conditions. However, at the higher agitation speed, the difference in the rates of growth and dissolution of HMT crystals increase, indicating a gradual change in mechanism controlling crystal growth from diffusion to surface integration.

Table 4.4 Average growth and dissolution rates of HMT and sucrose crystals at various agitation speed of the batch crystallizer

Agitation speed (rpm)	Average growth (\bar{G}) and dissolution (\bar{D}) rates ($\mu\text{m}\cdot\text{min}^{-1}$)							
	HMT crystals (35 °C)				Sucrose crystals (29 °C)			
	$\sigma = \pm 0.11\%$		$\sigma = \pm 0.22$		$\sigma = \pm 1.50\%$		$\sigma = \pm 2.20\%$	
	\bar{G}	\bar{D}	\bar{G}	\bar{D}	\bar{G}	\bar{D}	\bar{G}	\bar{D}
0	0.180	0.190	0.426	0.423	0.467	0.562	0.539	1.047
100	0.330	0.492	0.703	1.118	-	-	-	-
200	0.518	0.914	1.303	1.898	0.639	1.184	0.756	3.221
350	0.892	1.733	2.105	3.033	-	-	-	-
400	-	-	-	-	0.759	2.677	1.116	5.329
500	0.904	1.794	2.104	3.157	0.774	2.780	1.107	5.454

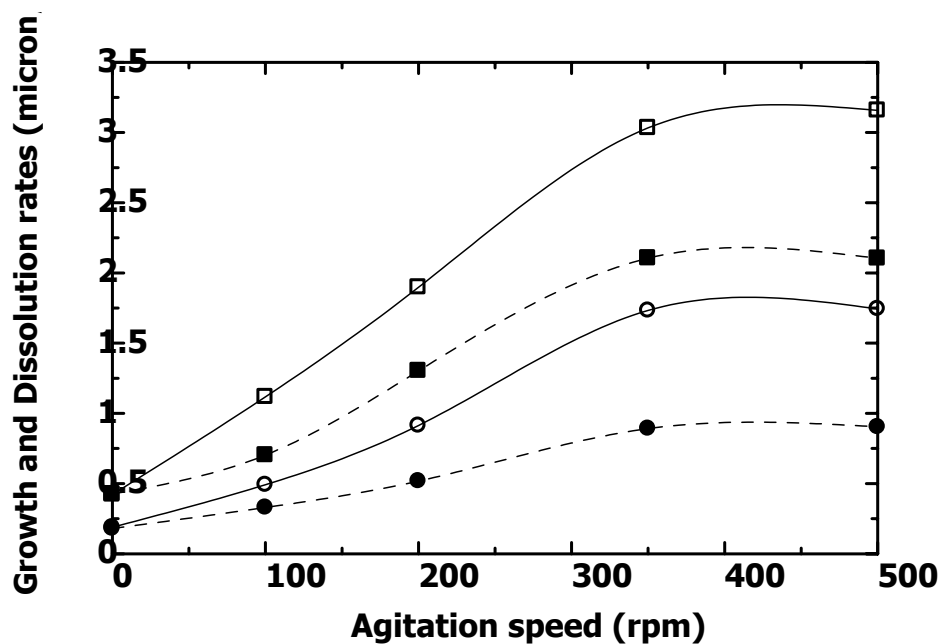


Figure 4.8 Average crystal growth and dissolution rates for HMT grown from aqueous solution. Filled symbols indicate growth rates, and hollow symbols indicate dissolution rates, ● $\sigma = 0.11\%$; ■ $\sigma = 0.22\%$

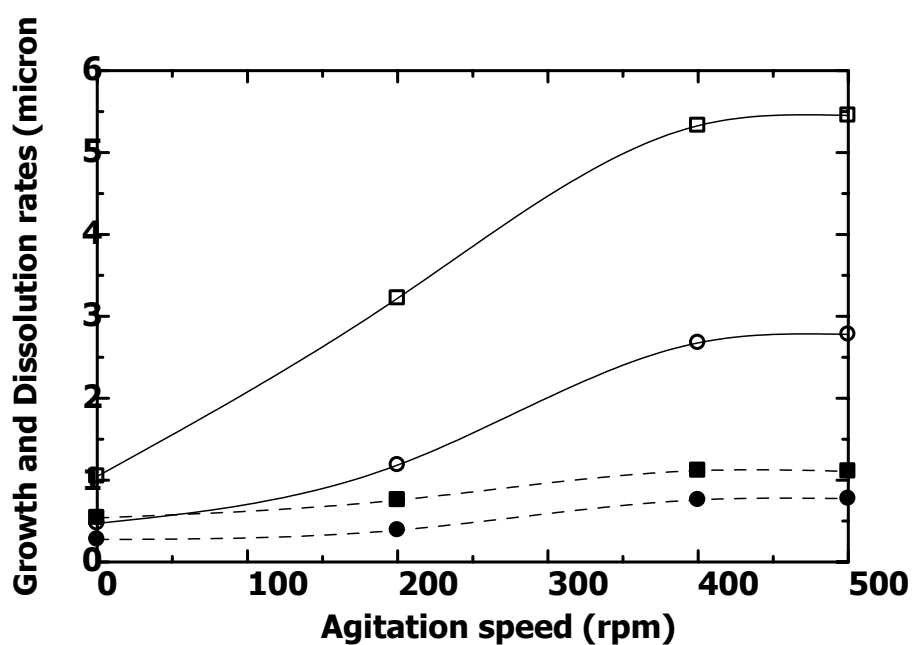


Figure 4.9 Average crystal growth and dissolution rates for sucrose grown from aqueous solution. Filled symbols indicate growth rates, and hollow symbols indicate dissolution rates, ● $\sigma = 2.20\%$; ■ $\sigma = 3.60\%$

4.2.2 GRD and DRD of sucrose crystals

Similar to the results of work in section 4.1, the experiment showed that there was significant dispersion in both the crystal growth rates and dissolution rates of sucrose at every agitation speed. The plots of inherent growth rates (and inherent dissolution rates) of all crystals and agitation speeds are shown in Figure 4.10 (2.20% super-/undersaturation) and Figure 4.11 (3.60% super-/undersaturation). The solid line and dashed line on the figure represents the average growth rate and the average dissolution rate, respectively. From the figures, the magnitudes of the dissolution rate dispersion is much larger than the magnitude of growth rate dispersion, but when the dispersions are measured relative to the average rates, the two are approximately equal since the average dissolution rate is two to six times larger than the average growth rate. By plotting the distribution of the growth and dissolution rates at each flow condition, the distributions were normal distribution as shown in Figure 4.12. Because there are higher values of dissolution rates than the growth rates even in the stagnant solutions, it is possible to conclude there are different mechanisms involved in the growth and dissolution of sucrose (where dissolution is diffusion controlled, but growth is partially controlled by surface integration). It is thus impossible to conclude that the dispersion of growth rates is related to the dispersion of dissolution rates. However, assuming that mass transfer controls the dissolution, it is apparent that there is a significant dispersion in mass transfer rates from crystals, even when the crystals experience apparently identical hydrodynamic and thermodynamic conditions. This indicates that the dispersion of diffusion rates may be a factor influencing crystal growth rate dispersion in system where the growth rate is not entirely controlled by surface integration.

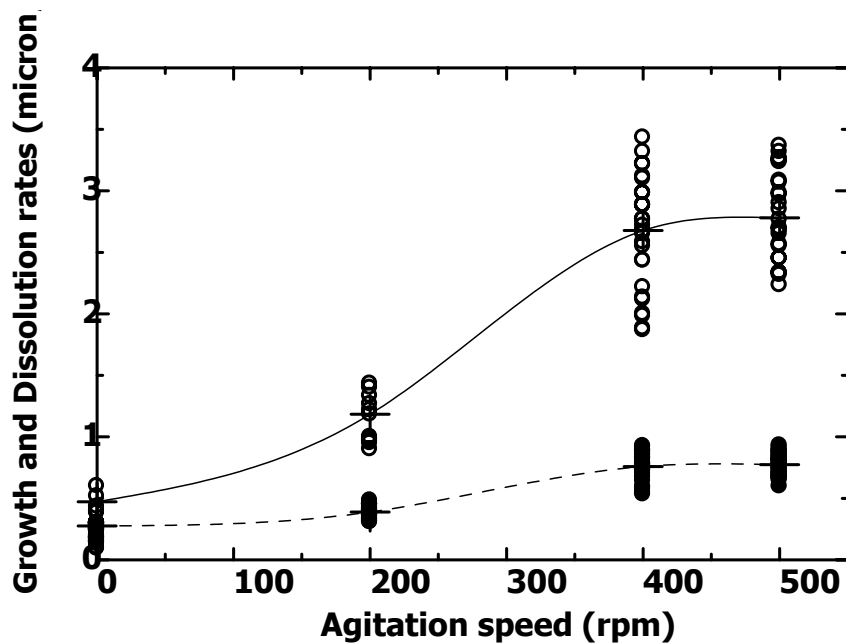


Figure 4.10 Crystal growth rate dispersion (GRD) and dissolution rate dispersion (DRD) for sucrose in 2.20% relative supersaturation. Filled symbols indicate growth rates, and hollow symbols indicate dissolution rates

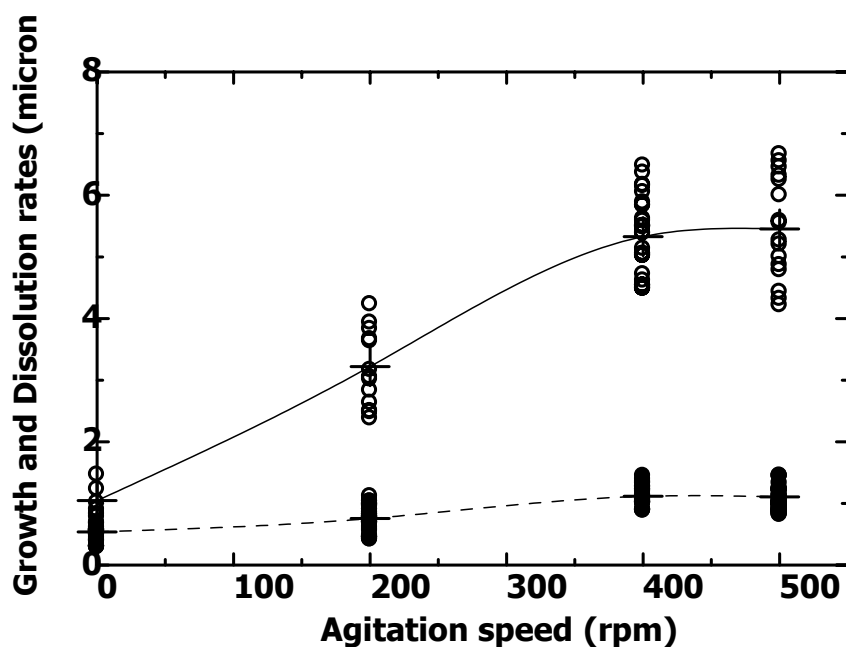


Figure 4.11 Crystal growth rate dispersion (GRD) and dissolution rate dispersion (DRD) for sucrose in 3.60% relative supersaturation. Filled symbols indicate growth rates, and hollow symbols indicate dissolution rates

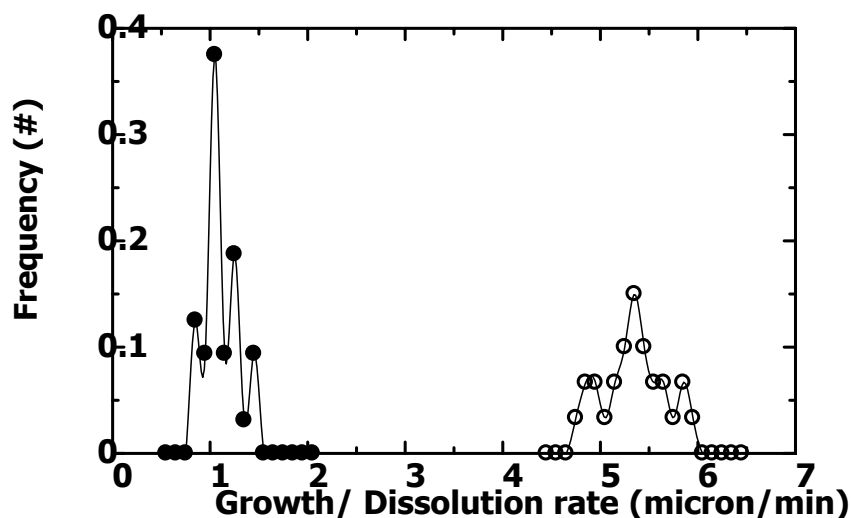


Figure 4.12 Growth rate distribution and dissolution rate distribution of sucrose in 3.60% relative supersaturation under 500 rpm of agitation speed. Filled symbols indicate growth rates, hollow symbols indicate dissolution rates

4.2.3 GRD and DRD of HMT crystals

As discussed previously, HMT has a very low value of the surface entropy factor, indicating that crystal growth in stagnant solutions is almost certainly controlled by diffusion. It is also apparent from the present study that average crystal growth rates and dissolution rates of HMT in stagnant solutions are equal for equivalent driving forces, confirming that the diffusion controls the crystal growth. The growth and dissolution rates of each face of individual HMT crystals are plotted with the speed of agitation as depicted in Figure 4.13 (for 0.11% relative supersaturation) and Figure 4.14 (for 0.22% relative supersaturation). Similar to the results of sucrose, there is significant dispersion in both growth and dissolution rates. The magnitudes of the growth rate dispersion are similar to the magnitudes of the dissolution rate dispersion, particularly at stagnant and low convection conditions.

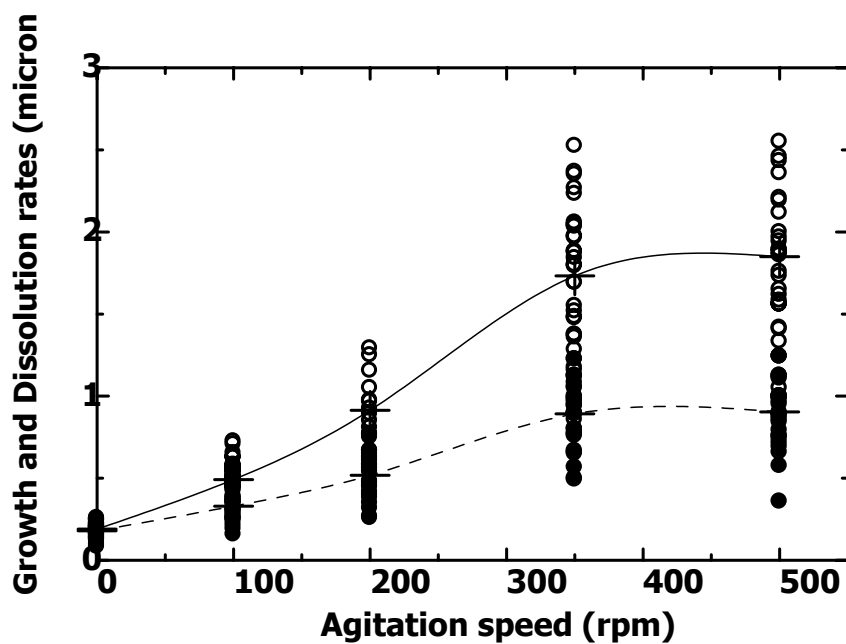


Figure 4.13 Crystal growth rate dispersion (GRD) and dissolution rate dispersion (DRD) for HMT in 0.11% relative supersaturation. Filled symbols indicate growth rates, and hollow symbols indicate dissolution rates

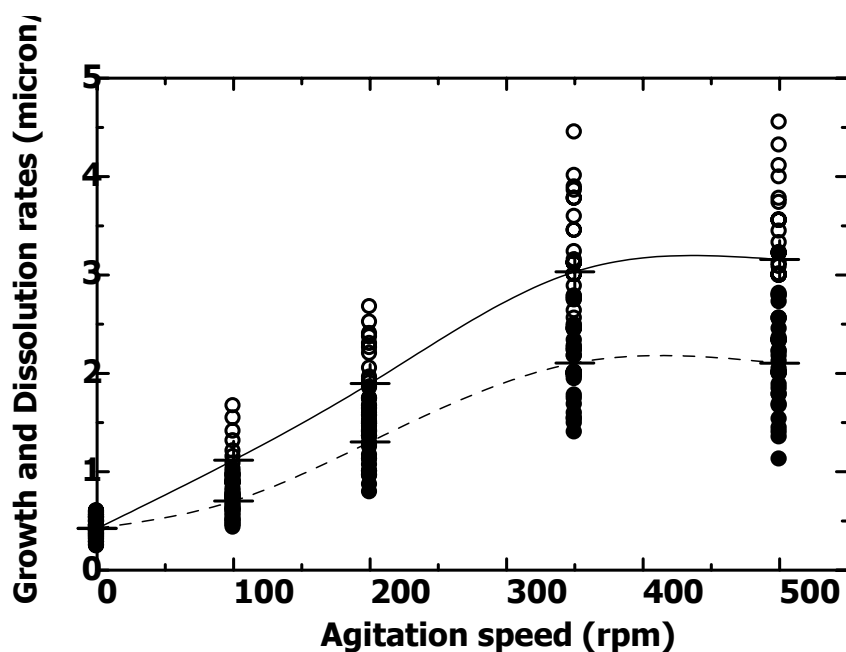


Figure 4.14 Crystal growth rate dispersion (GRD) and dissolution rate dispersion (DRD) for HMT in 0.22% relative supersaturation. Filled symbols indicate growth rates, and hollow symbols indicate dissolution rates

Similar to the growth rate distribution and dissolution rate distribution of sucrose crystal, the distributions of growth and dissolution rates of HMT are also normal distribution as illustrated in Figure 4.15.

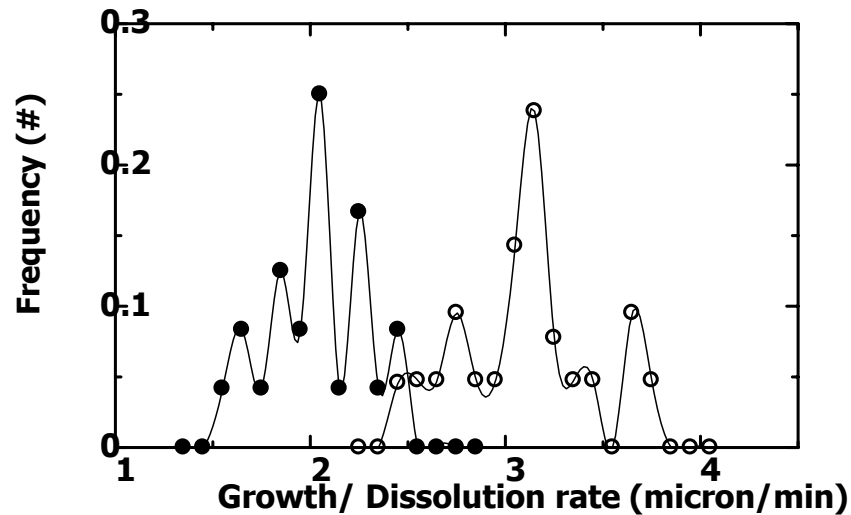


Figure 4.15 Growth rate distribution and dissolution rate distribution of HMT in 0.22% relative supersaturation under 350 rpm of agitation speed. Filled symbols indicate growth rates, hollow symbols indicate dissolution rates

In the crystal growth of both sucrose and HMT, the dispersion in the growth rates is still apparent when the growth mechanism moves away from being diffusion controlled. This shows that dispersion in mass transfer rates can not entirely explain crystal growth rate dispersion. The results clearly show that the dispersion in growth rates is due to a combination of surface integration rate dispersion and diffusion rate dispersion.

4.3 Determination of the Possible Causes of GRD in the Growth Mechanism

4.3.1 Cause of GRD in diffusion step

By considering the effect of flow orientation around the crystal as a possible cause of dispersion in the diffusion step, the two facial growth rates of the single HMT crystals were considered when the solution flow direction was changed. The growth of two faces of a HMT crystal when the solution flow direction was swapped from the left to the right hand side is illustrated in Figure 4.16; a) Direction 1 and b) Direction 2. The increase in the size of the face that was facing into the solution flow was larger than the one at back of the crystal. The facial growth rate of the front face (Face 1) at Direction 1 was $0.67 \mu\text{m}\cdot\text{min}^{-1}$ and that of the back face (Face 2) was only $0.10 \mu\text{m}\cdot\text{min}^{-1}$. When the flow direction was changed to Direction 2, the growth rate of Face 1 decreased to $0.18 \mu\text{m}\cdot\text{min}^{-1}$ but that of Face 2, which was now front face, increased to $0.92 \mu\text{m}\cdot\text{min}^{-1}$. The change of growth rate when the flow orientation changed was from $0.77 \mu\text{m}\cdot\text{min}^{-1}$ to $1.10 \mu\text{m}\cdot\text{min}^{-1}$, or by approximately 1.5 times. This result shows that when the growth process is mostly or entirely controlled by diffusion, the solution flow orientation plays an important role as a cause of GRD. The face of the crystal which is directly introduced to the solution flow has a thinner boundary layer thickness due to the force of solution flow on that face, resulting in a higher mass transfer rate. However, when the solution flow further increases, it can produce the back-mixing at the back face, leading to high mass transfer rates for that face.

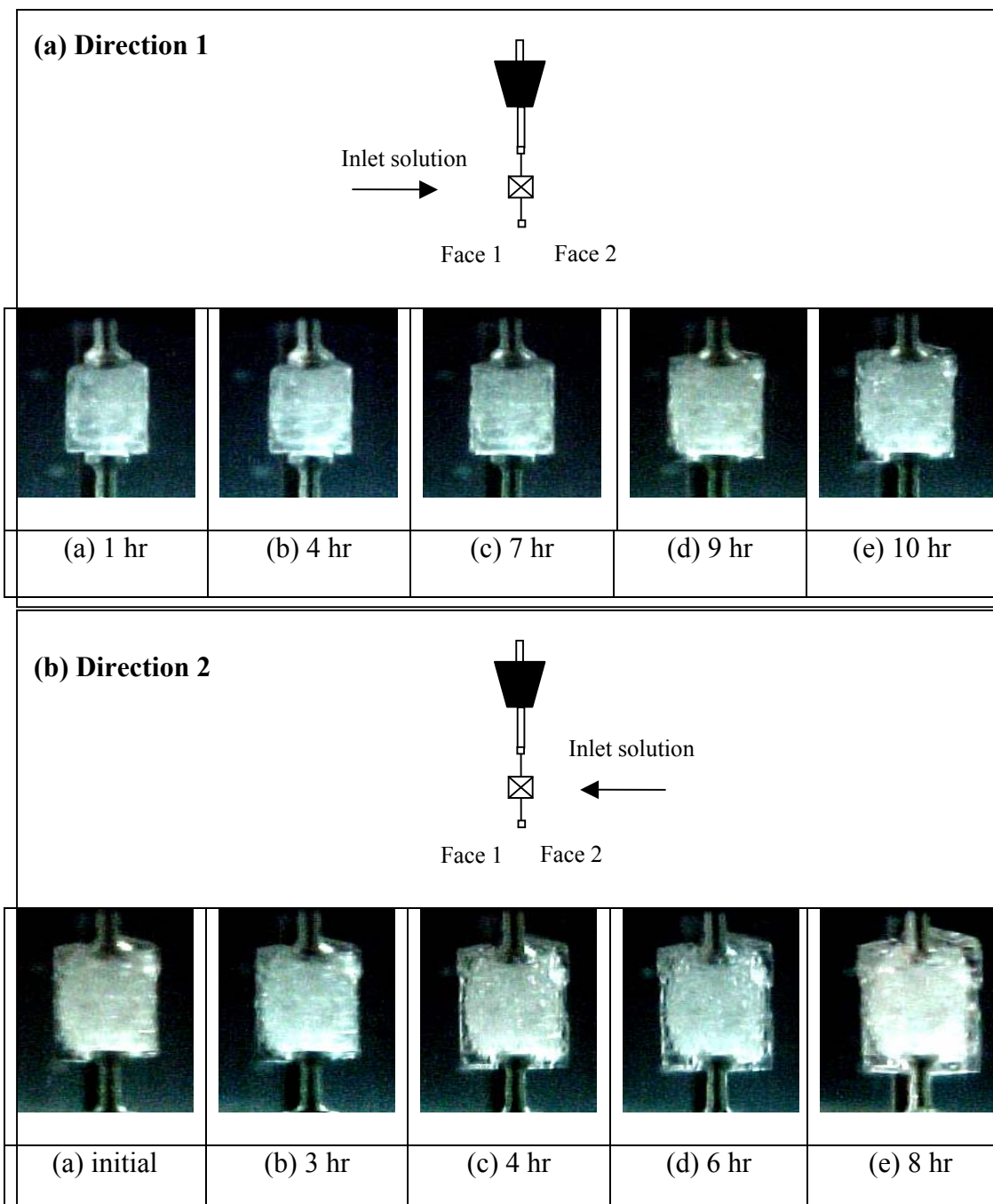


Figure 4.16 Facial growth of a HMT crystal with $0.25 \text{ cm}\cdot\text{s}^{-1}$ solution flow when the flow direction was changed from (a) Direction 1 to (b) Direction 2

4.3.2 Cause of GRD in the surface integration step

4.3.2.1 Determination of the effect of supersaturation levels on the crystal surface

The surface of four sucrose crystals before and after growing in different supersaturation levels, 1.50%, 2.20%, 3.60% and 5.10% supersaturations are illustrated in Figure 4.17. The results demonstrate that the supersaturation levels in which the crystals are grown have significant effect on the surface roughness of the crystal, with the crystals grown more quickly at higher supersaturation having a surface that was significantly rougher on a microscopic level than the seed crystals they are grown from. As shown in Figure 4.17, the seed crystals were randomly chosen, so this had a variable amount of surface roughness at the beginning of the crystal growth. The results suggest that crystals grown at lower saturation became smoother, while those at the highest supersaturation had progressively rougher surfaces. SEM photographs of the product crystals of 2.20 and 5.00% relative supersaturation are shown in Figure 4.18 for comparison. This phenomenon was not only found for sucrose crystals, but also for potash alum and KDP crystals. SEM photographs of the product crystal of the other two crystal types (potash alum and KDP) are also shown in Figure 4.19 and 4.20, respectively.

It should be noted that the scale of the surface roughness observed in this case is on the microscopic level, not the molecular or macroscopic levels. According to the review paper of Garside on industrial crystallization from solution (Garside, 1985a), roughness at the molecular level is related to the nature of solute and solvent as well as their interactions, whilst that at the macroscopic level is about the change in morphology of the crystals. In this experiment, the roughness in

the molecular scale should not vary, because the two crystals are of the same species, such as sucrose, and were grown in the sucrose-water system with identical hydrodynamics and temperatures, but only different supersaturation levels. The SEM micrographs are also unlikely to distinguish roughness at a molecular level. The morphology of the product crystals was also not changed, so it also cannot be explained using the macroscopic scale. At the microscopic scale, on the scale of about $1\mu\text{m}$ up to $100\mu\text{m}$, the roughness is possibly caused by the group of clusters, step bunches or surface nuclei formed on the surface of the crystals.

The results of a study of the surface of potash alum from AFM confirmed that the roughness of the crystals grown in high supersaturation was due to surface nuclei forming on the surface (See Figure 4.21). Figure 4.21 (a) is a region ($50\times 50\mu\text{m}$ in size) of the surface of potash alum scanned by AFM after growth in low supersaturation, and Figure 4.21 (b) is for growth in high supersaturation. The AFM micrographs show that surface nuclei occur at low concentrations on the surface of the crystal even after growth in low supersaturation, but more surface nuclei occur when the supersaturation level is high. In each figure, a line with two triangular marks was used to locate the position for measuring the height of the surface roughness, which is the amplitude between the crystal surface and the tip of the pin scanning in the surface of the crystals. The plots of the height of roughness as a function of distance for each supersaturation are also in the figure.

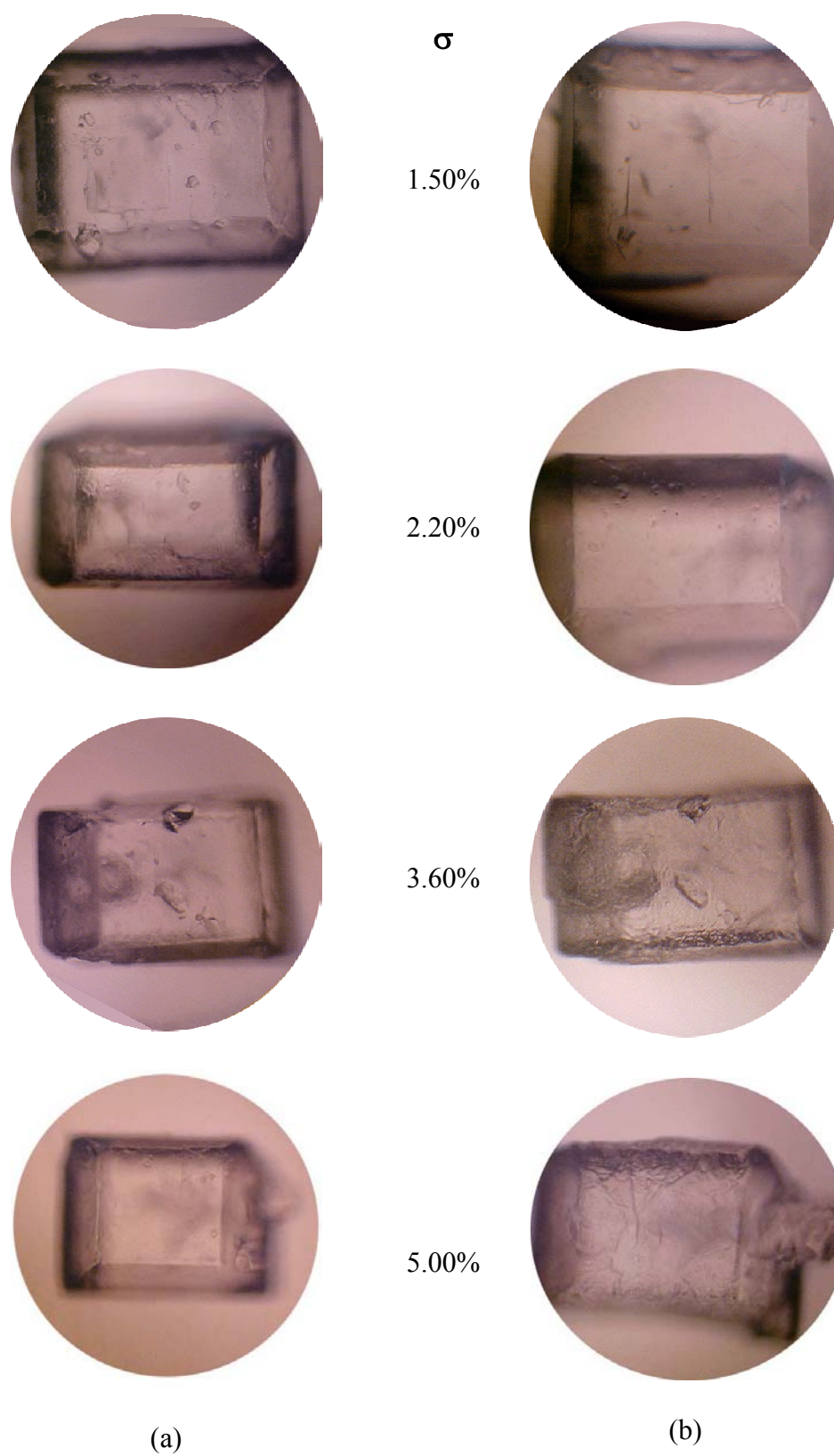


Figure 4.17 The effect of supersaturation during crystal growth on the surface roughness of sucrose crystals (a) before growth (b) after growth

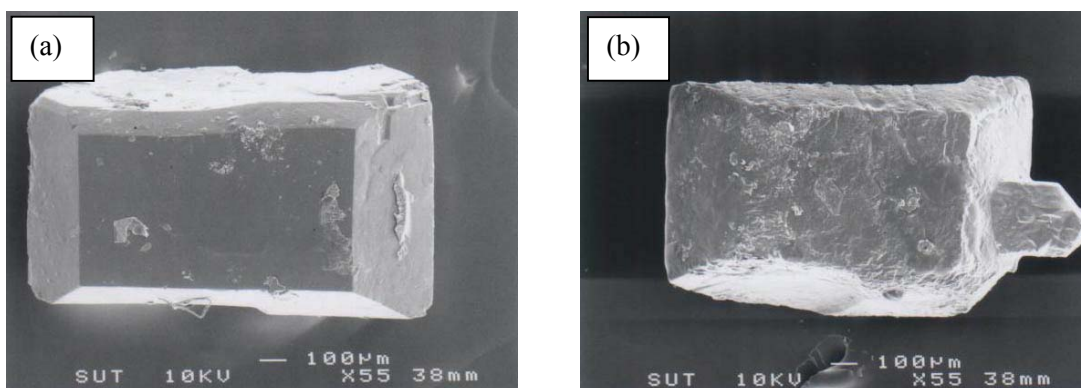


Figure 4.18 SEM photographs of the surface of sucrose (a) after growth at 2.20% relative supersaturation (b) after growth at 5.00% relative supersaturation

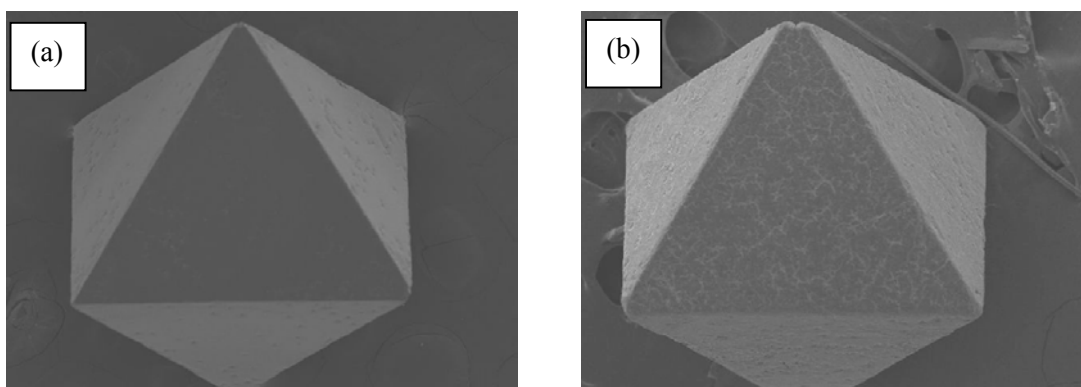


Figure 4.19 SEM photographs of the surface of potash alum (a) after growth at 2.60% relative supersaturation (b) after growth at 7.50% relative supersaturation

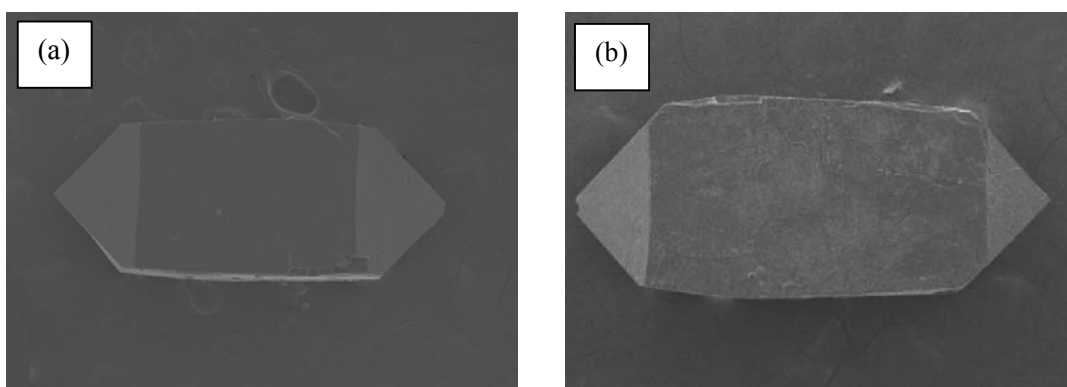


Figure 4.20 SEM photographs of the surface of KDP (a) after growth at 2.00% relative super-saturation (b) after growth at 5.00% relative supersaturation

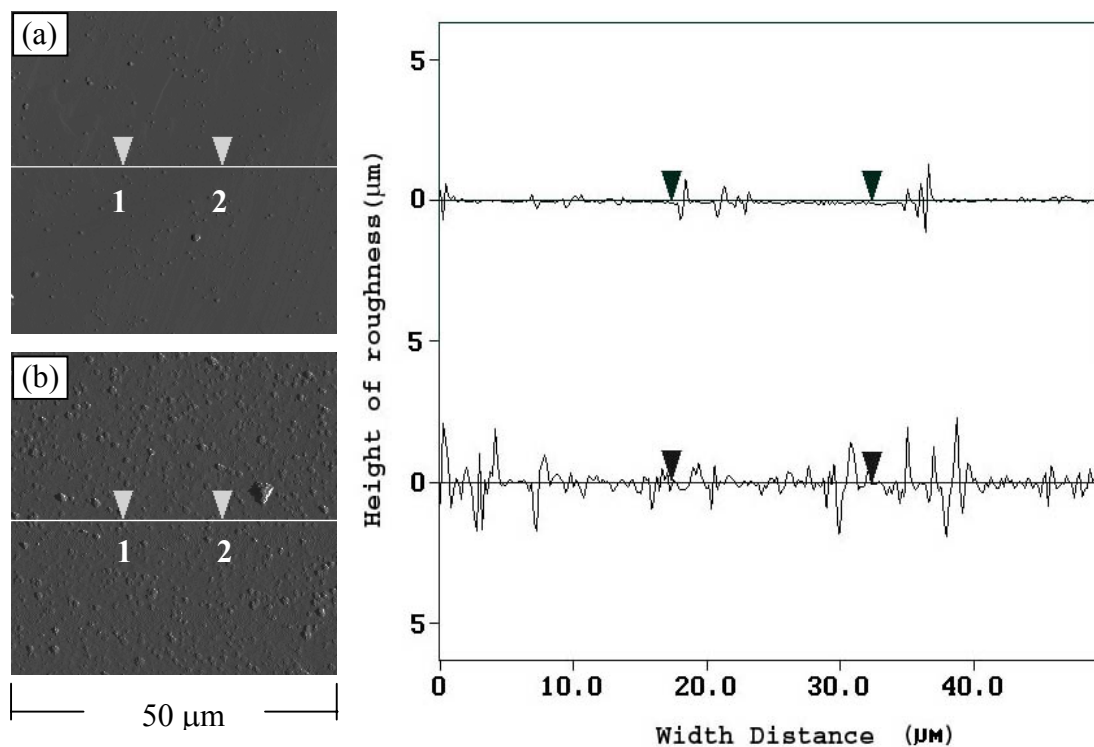


Figure 4.21 50×50 μm area of the surface of potash alum (a) after growth at 2.60% relative supersaturation (b) after growth at 7.50% relative supersaturation. Plots of the height of roughness at each width distance of each crystal are also shown

4.3.2.2 Determination of effect of growth history on the current crystal growth

Results demonstrating the effect of growth history on current crystal growth rates of sucrose are summarized in Table 4.5. The diagonal of the table represents growth at constant conditions for six hours, and these results showed approximately constant rates for the two periods (for instance $1.95 \mu\text{m}\cdot\text{min}^{-1}$ for the first period of two hours and $1.91 \mu\text{m}\cdot\text{min}^{-1}$ for the second period of two hours at 5.00% supersaturation) with the exception of the system at 3.60% supersaturation.

The cause for this discrepancy is not known, but other experiments have shown this to be a rate occurrence. The data above the diagonal represents experiments where the second period of growth occurred at higher supersaturation than the initial period, and vice versa for the data below the diagonal.

Table 4.5 The effect of crystal growth history on current crystal growth rates of sucrose

Growth at σ_1		Growth at σ_2 (%) : G_2 ($\mu\text{m}\cdot\text{min}^{-1}$)			
σ_1 (%)	G_1 ($\mu\text{m}\cdot\text{min}^{-1}$)	$\sigma_2 = 1.50$	$\sigma_2 = 2.20$	$\sigma_2 = 3.60$	$\sigma_2 = 5.00$
1.50	0.48	0.46	0.72	1.19	2.00
2.20	0.74	0.66	0.76	0.92	1.60
3.60	1.25	0.54	0.76	0.94	1.38
5.00	1.95	0.26	0.57	0.84	1.91

There is a clear relation whereby crystals initially grown at a low supersaturation have a higher growth rate during the second period of growth than the crystals initially grown at a high supersaturation. This is illustrated in Figure 4.22, where the growth rate function is plotted for crystals initially grown at very low supersaturation (1.50%), and high supersaturation (5.00%). The growth rates of the crystal grown in the second period of 1.50% supersaturation between the crystal previously grown at 1.50% and 5.00% supersaturations are also plotted in Figure 4.23 to demonstrate their differences. Similar results were also found for potash alum and KDP as shown in Figure 4.24 (a) and (b).

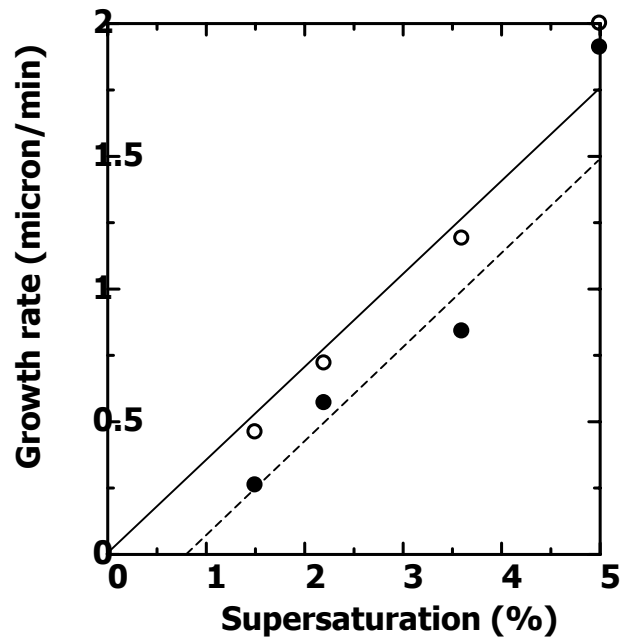


Figure 4.22 The effect of the growth history of sucrose crystals on their current crystal growth. Previous crystal growth under; ● 5.00% supersaturation; ○ 1.5% supersaturation

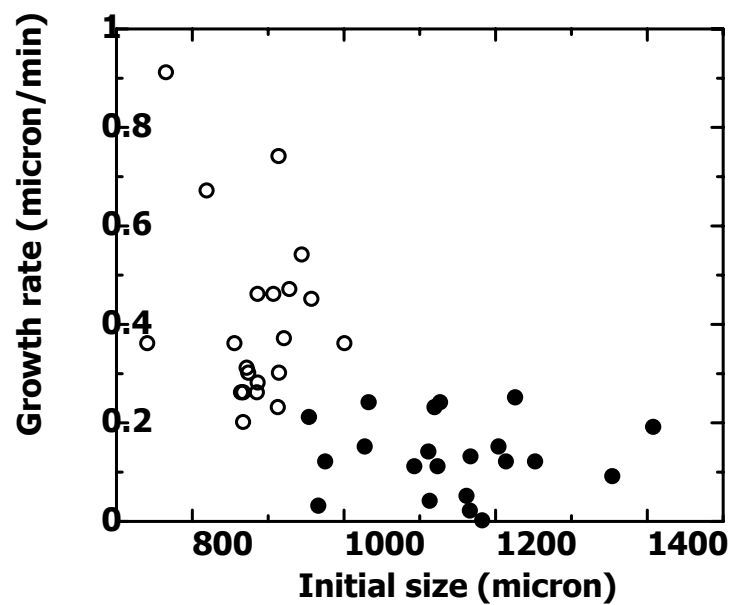


Figure 4.23 Growth rate of sucrose crystals at 1.50% supersaturation. Previous crystal growth under; ● 5.00% supersaturation; ○ 1.50% supersaturation

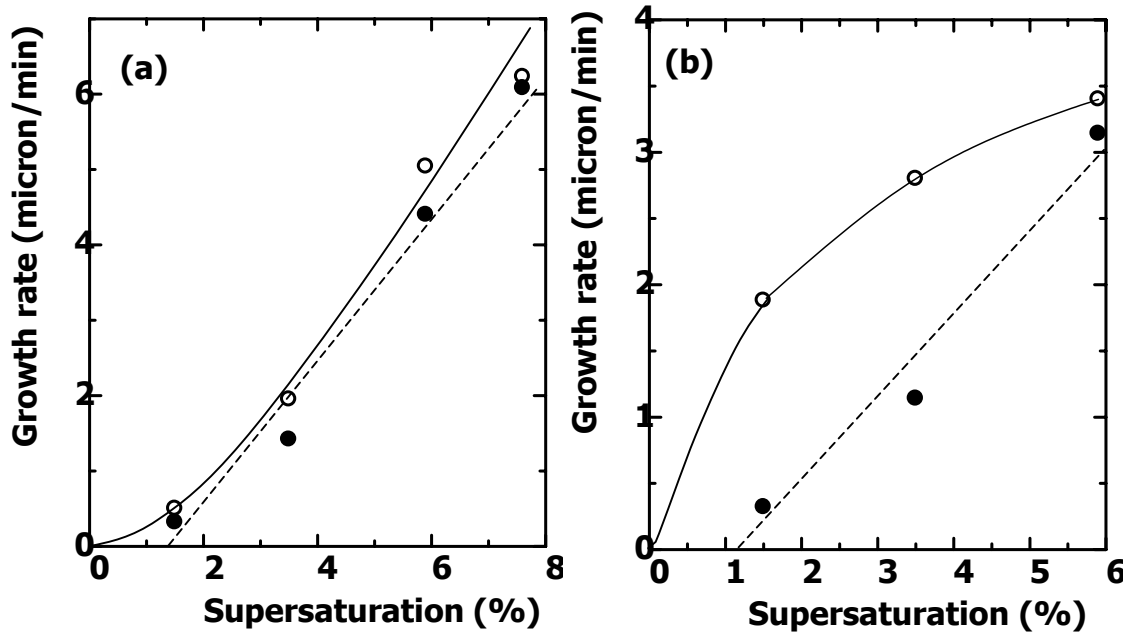


Figure 4.24 The effect of growth history of (a) potash alum; (b) KDP on their current crystal growth. Previous crystal growth under; ● 5.00% supersaturation
○ 1.50% supersaturation

The effect of growth history was studied by initiating sudden step changes in supersaturation in which the initial growth was at a low supersaturation (σ_1), followed by a period at high supersaturation (σ_2), and then returning to the initial supersaturation (σ_1), for a longer period of time. As illustrated in Figure 4.25(a), the size of the crystal increases linearly with time during the initial periods of growth, indicating constant crystal growth. When crystals are returned to a solution of low supersaturation, the growth of the crystal does not follow the typical behavior of constant growth rate under constant supersaturation. The growth rate just after the supersaturation change is essentially zero, but increases with time and approaches a constant growth rate as the crystal heals. As a result, the growth rate is lower than during the initial period of growth at the same supersaturation. However,

the new period of slow growth tends to heal the surface of the crystal, and eventually (typically after more than 2 hours of growth) the crystal growth rate returns to what it was in the initial period of growth. This is demonstrated in a plot of growth rate vs time in Figure 4.25(b).

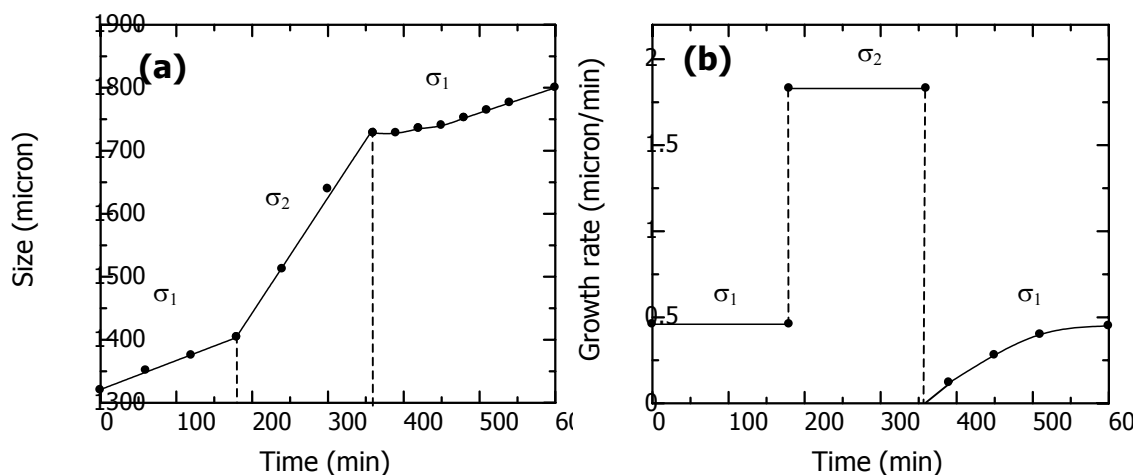


Figure 4.25 Crystal growth behavior of sucrose under varying conditions of supersaturation (a) Crystal size vs time; (b) Growth rate vs time

Experiments were also performed with two sets of supersaturation jumps, having variable growth times at each level of supersaturation (1, 2 and 3 hours of growth), in order to determine if low growth rates can enhance crystal growth rates past 'normal' growth kinetics, and investigate the effect of healing time on subsequent crystal growth. Replicate experiments were performed for each condition. Example results from these experiments are given in Figure 4.26. These experiments demonstrate that growth at high supersaturation has the effect of decreasing subsequent crystal growth rates. Periods of growth at low supersaturation may heal the crystal, thus allowing the crystal to regain 'normal' growth kinetics, but

cannot improve the growth rate beyond this point. Once the surface has been repaired for healing by a period of slow growth, the growth rate is not further enhanced. The time required for healing is of the order of several hours of growth. It is also interesting that the thickness of the crystal layer required to heal the surface (which can be calculated from the growth rate and healing time) is in excess of 100 micron. This is much greater than the magnitude of the surface roughness, which is the order of 10 microns. This suggests that a significant amount of good quality crystal lattice is required at the surface of the crystal for the crystals to grow at their normal rate.

A proposed mechanism for the effect discussed above is the effect of surface roughness on crystal growth. Very rough surfaces present on the crystals grown at high supersaturation is probably caused by the fact that at relatively high supersaturation, the concentration of solute molecules in the adsorbed layer is sufficiently high to form the group of islands or clusters (with a size on the microscopic scale) on the surface. The solidification of these clusters or surface nuclei that do not align perfectly with the underlying crystal lattice might therefore be the major cause of the very rough crystal surfaces apparent in the micrographs. When these crystals are subjected to low supersaturation, where the crystals can grow near-ideal lattice due to the slow growth process, the degraded surface or imperfection lattice is improved by filling and covering of the imperfect layers created by the fast growth periods. This healing period requires significant time, and thickness of improved crystal lattice: the time required depends on how much the surface is degraded. This was investigated using AFM to observe the surface of a potash alum crystal when the supersaturation for crystal growth was changed from 7.50% relative supersaturation (at high supersaturation producing a rough surface) to 2.50% relative supersaturation, where surface healing could occur. The AFM scans of the initial

surface of the crystal (crystallized from 7.50% relative supersaturation), and the surface of the crystal after growth in 2.50% relative supersaturation for 30 minutes and 1 hour are shown in Figure 4.27. The result confirmed the improvement of the degraded surface when the relative supersaturation was changed to the low supersaturation conditions.

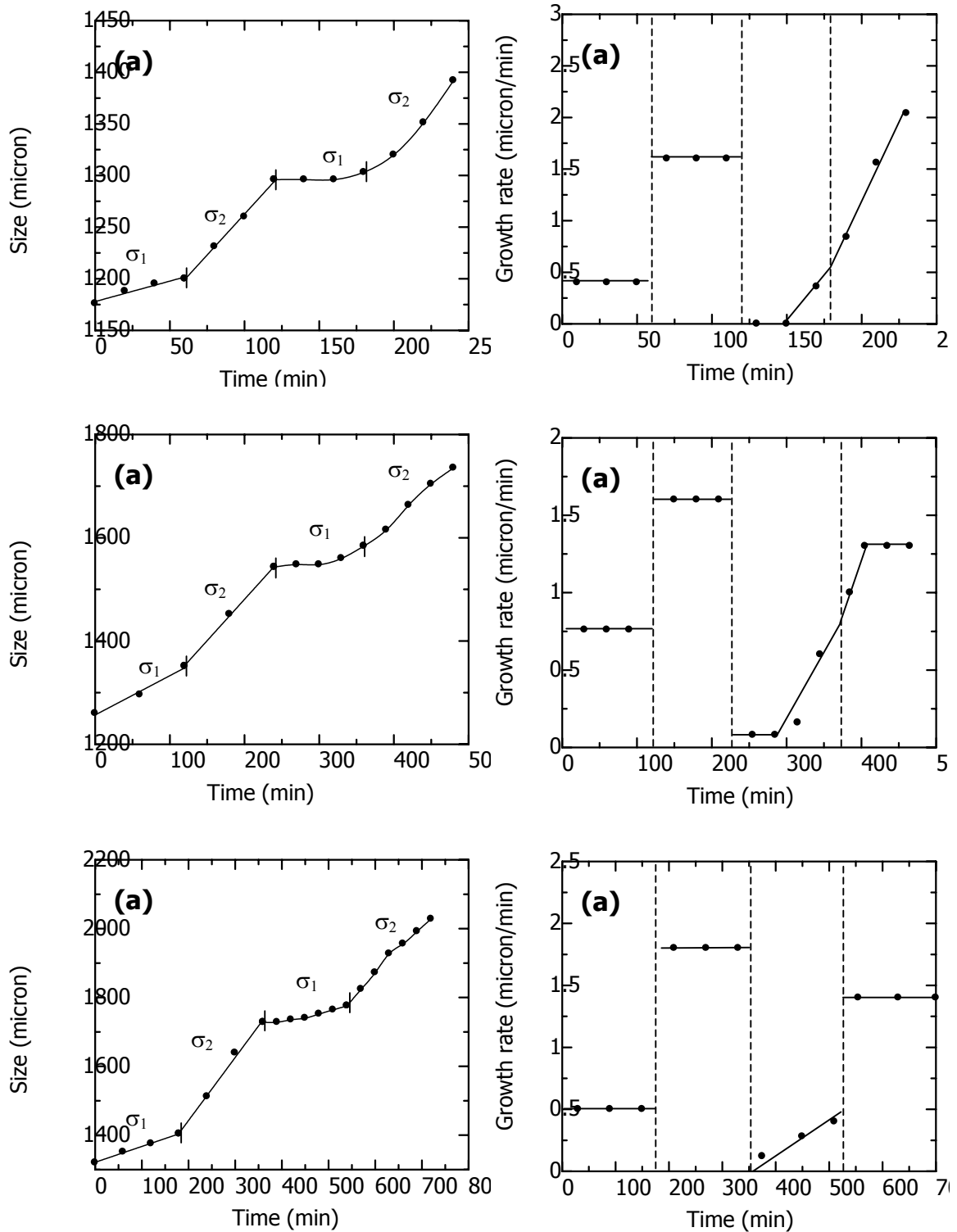


Figure 4.26 The healing period of sucrose crystals demonstrated by three jumps in relative supersaturation (a) crystal size vs time and (b) growth rate during the healing period

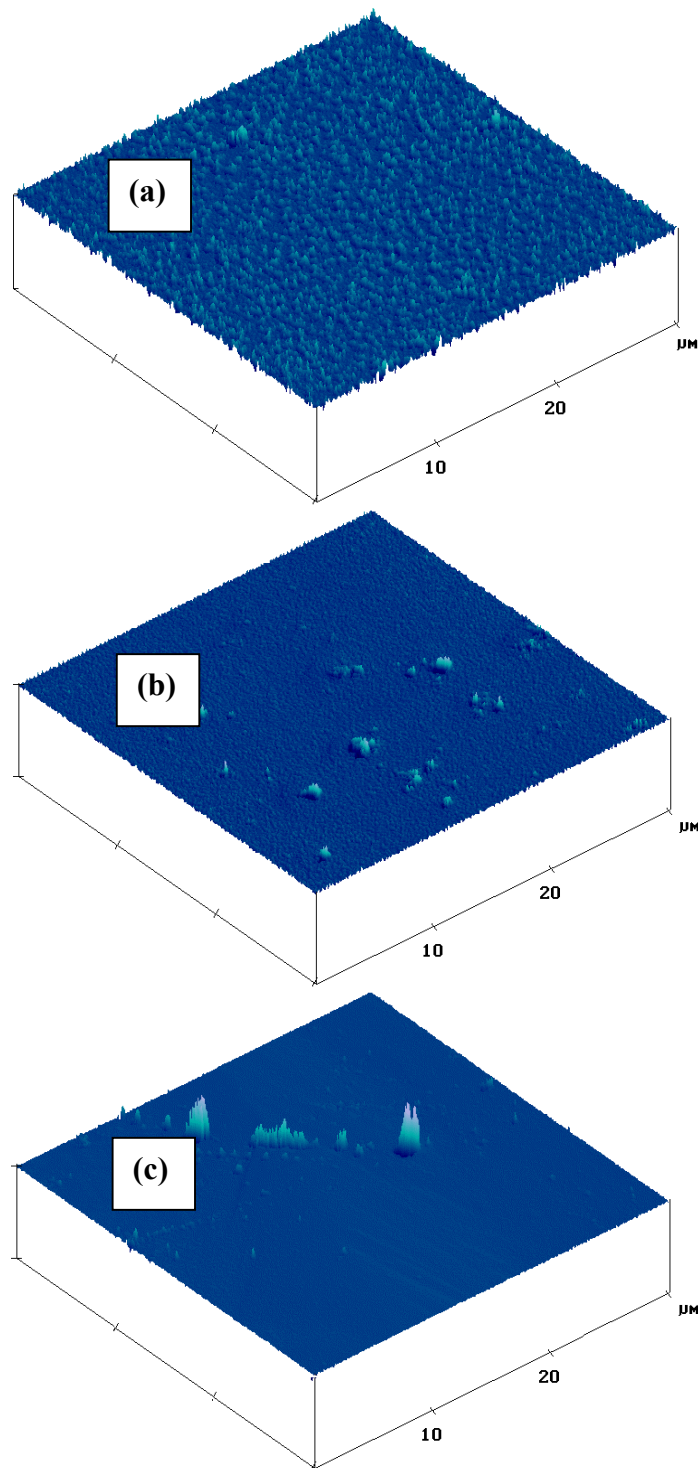


Figure 4.27 $30 \times 30 \mu\text{m}$ area of the surface of potash alum scanned by AFM (a) initial surface 7.50% (b) surface after growth in 2.50% for 30 minutes (c) surface after growth in 2.50% for 1 hour

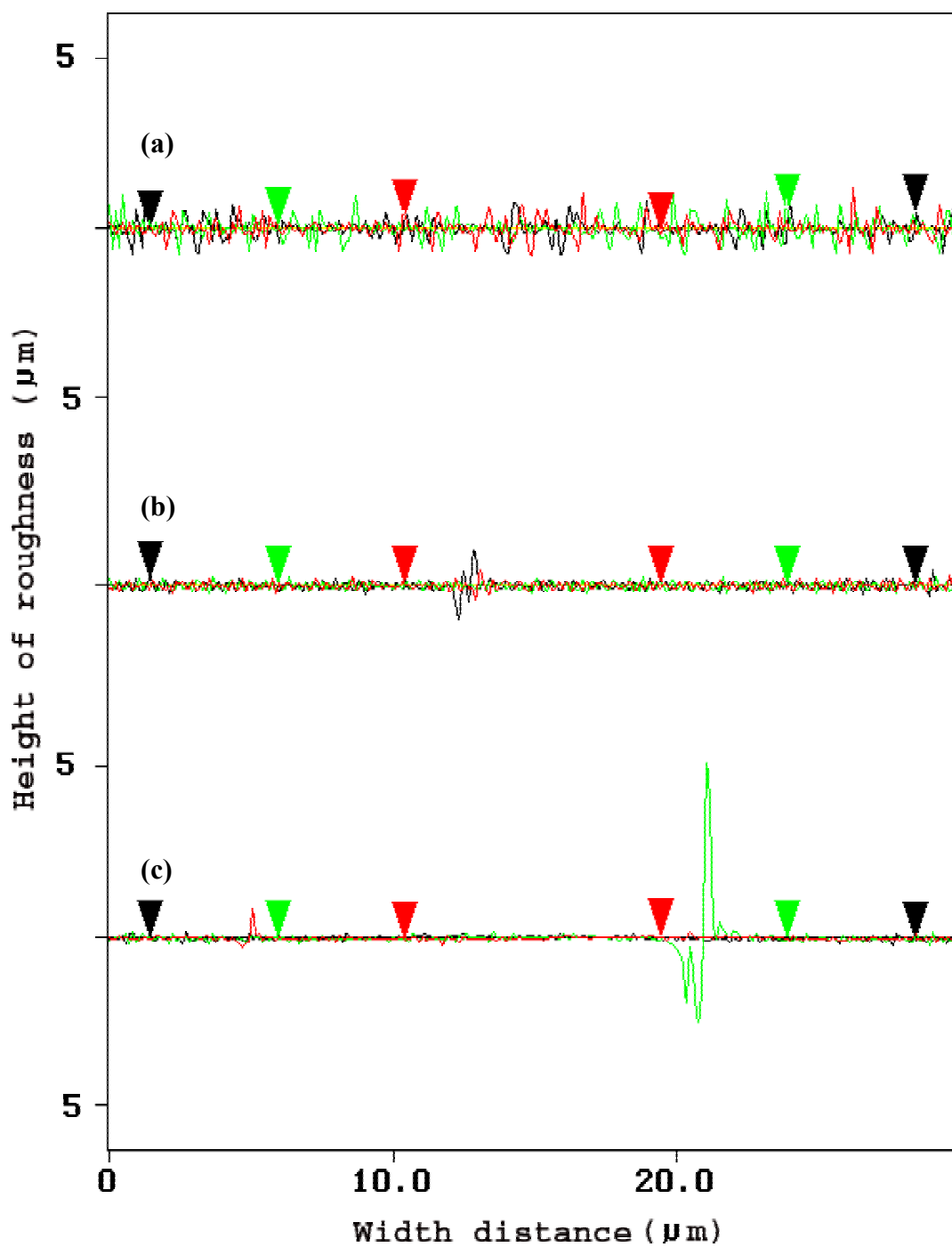


Figure 4.28 Height of roughness of the surface of potash alum scanned by AFM (a) initial surface grown from 7.50% (b) surface after growth in 2.50% for 30 minutes (c) surface after growth in 2.50% for 1 hour

4.3.2.3 Study of the relationship between GRD and crystal surface energy (γ)

According to the plots that demonstrated the effect of growth rate history; Figure 4.22 for sucrose, Figure 4.24 (a) for potash alum and Figure 4.24 (b) for KDP crystals, it is very interesting that although all three crystal types were initially grown at the same supersaturation level, (for preparation of groups of crystals with different surface features) the difference in growth rates between the two-groups of crystals at various supersaturations in the second period of growth were quite different for the three types of crystal. The difference in the two curves (initially 1.5 % supersaturation, and initially 5.0 % supersaturation) in the plot of potash alum was small compared to that in the plot of sucrose and KDP. There is a particularly large difference between the two sets of data for KDP. The plots of relative growth rates, calculated using equation (4.3) of each species as a function of percent relative supersaturation in the second period of growth, are illustrated in Figure 4.29.

$$\text{relative growth rate} = \frac{\bar{G}_{1.5} - \bar{G}_{5.0}}{\bar{G}_{1.5}} \quad (4.3)$$

where $\bar{G}_{1.5}$ = Growth rate of the crystals previous grown in 1.50% supersaturation

$\bar{G}_{5.0}$ = Growth rate of the crystals previous grown in 5.00% supersaturation

The plots on Figure 4.29 represent the sequence of the relative differences from low to high levels, at each supersaturation for potash alum, sucrose and KDP crystals. As discussed earlier, the factor influencing the growth rates is the surface roughness on the microscopic scale, which relates to the clusters or

surface nuclei; therefore, the sequence found in the plots should also be linked with a parameter related to surface nucleation. Surface nucleation in crystallization depends on the surface energy of each crystal. From the literature (Söhnel, 2001 and Bourne and Davey, 1976b), the surface energy of potash alum, sucrose and KDP crystals are 2.5, 4.7 and 12-16 $\text{erg}\cdot\text{cm}^{-2}$ respectively, respectively. The surface energy data of potash alum and KDP were also determined by using the relationship between the primary nucleation rate and the supersaturation level (details are given in Appendix B). In this study, the surface energy of potash alum is $1.27\text{ erg}\cdot\text{cm}^{-2}$ and that of KDP is $9.52\text{ erg}\cdot\text{cm}^{-2}$. There are differences between the measured and literature data but the sequence of them is still similar.

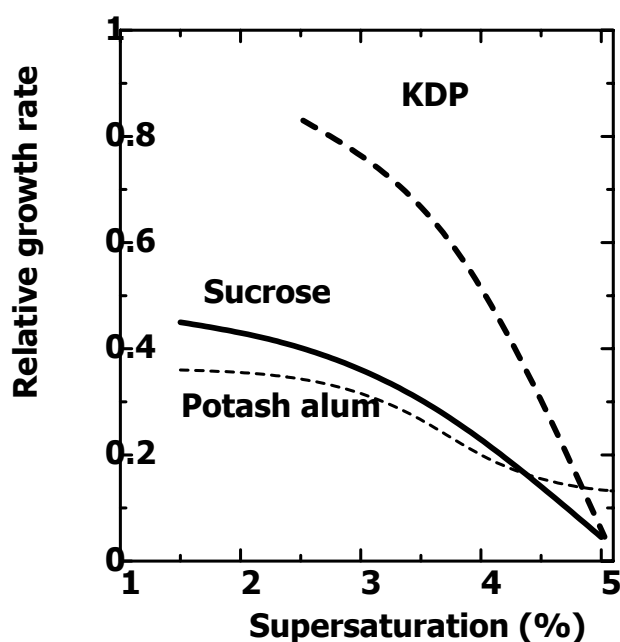


Figure 4.29 The relative difference of the growth rates of crystals that were initially grown in 1.50% and in 5.00% supersaturation

The sequence of the surface energy values seemingly corresponds to that of the relative differences plotted in Figure 4.29. The higher the surface energy the larger the relative differences of the crystals growth rate under high and low initial supersaturation. These results apparently suggest that at the same supersaturation level, the higher surface energy crystals display a rougher surface than the lower surface energy crystals, causing a high difference in growth rate in the second period of growth. For example, at the same conditions for the two crystals, having different surface energy, such as the system that has difference in local supersaturation, the fluctuation of growth rates in the system of higher surface energy crystal should be higher. This suggests to a hypothesis that the crystals which have high surface energy should have high differences in growth rates, or high GRD in the system, particularly if grown at high supersaturation levels, or have a history of growth at high supersaturation levels.

In order to characterize which system has high GRD, the width of crystal size distribution (CSD) is used. The larger the width of the product CSD compared to the seed CSD, the higher the GRD in the system. A study of effect of surface energy on GRD magnitude was performed by comparing the CSD of the final products of three crystals, potash alum, KDP and potassium sulphate (K_2SO_4). The surface of these three inorganic materials are 2.5, 12, 23 $\text{erg}\cdot\text{cm}^{-2}$. All crystals were grown in 2.20% and 5.00% supersaturation for 3 hours. According to our hypothesis, the CSD of K_2SO_4 at the final time should be the widest followed by those of KDP and potash alum respectively. The plots of CSD for initial and final times of all three crystals grown in low (2.20%) supersaturation are depicted in Figure 4.30 and in high (5.00%) supersaturation in Figure 4.31. The magnitude of GRD and

DRD can be reported by using the value of the coefficient of variation (C.V.) and the ratio of the C.V. value at the initial time and the final time are summarized in Table 4.6. The results shown both in the figures and in the table provide a clear illustration that the system of K_2SO_4 has the highest magnitude of GRD while that of potash alum which has the lowest surface energy has the lowest GRD.

Table 4.6 Coefficient of variation (C.V.) values of CSD of sucrose, potash alum and KDP grown in low (1.50%) and high (5.00%) supersaturation

Type of crystal	Coefficient of variation (C.V.) values					
	Low supersaturation (1.50%)			Low supersaturation (5.00%)		
	Initial	Final (3 hr)	$\frac{C.V._{Final}}{C.V._{initial}}$	Initial	Final (3 hr)	$\frac{C.V._{Final}}{C.V._{initial}}$
Potash alum	0.190	0.190	1.00	0.183	0.195	1.10
KDP	0.180	0.197	1.08	0.181	0.221	1.22
K ₂ SO ₄	0.165	0.186	1.12	0.165	0.232	1.40

From the results shown above, it can be noted that GRD in the surface integration step is caused by the effect of crystal growth history. The crystals grown from low supersaturation display very smooth surfaces compared to those grown from high supersaturation. At some level of supersaturation the mechanism of crystal growth changes from smooth addition of solute into the lattice, to imperfect integration of clusters or surface nuclei, with this transition depending on the surface energy of the crystal. The results from AFM also provided a clear image that the high

roughness of a crystal grown from high supersaturation was from the surface nuclei with a size range of 1-10 micrometers generated on the crystal's surface. The effect of this microscopic roughness plays an important role for the current crystal growth. The crystal initially grown from high supersaturation has a high surface roughness on the microscopic scale, and grows at a lower rate than those from low supersaturation (smooth crystals) from a lower supersaturation level. The improvement of the degraded surface at a lower supersaturation (the process of surface healing) was found as the cause of the low growth rates. The effect of growth history is significant for crystallization during both nucleation and growth periods. In nucleation, the set of initial nuclei must be generated from the higher supersaturation levels than that of later nuclei, resulting in differences in surface roughness of nuclei in the system. The effect of microscopic surface roughness in the growth period would also occur in the system that is insufficiently mixed, causing the variation of local concentration.

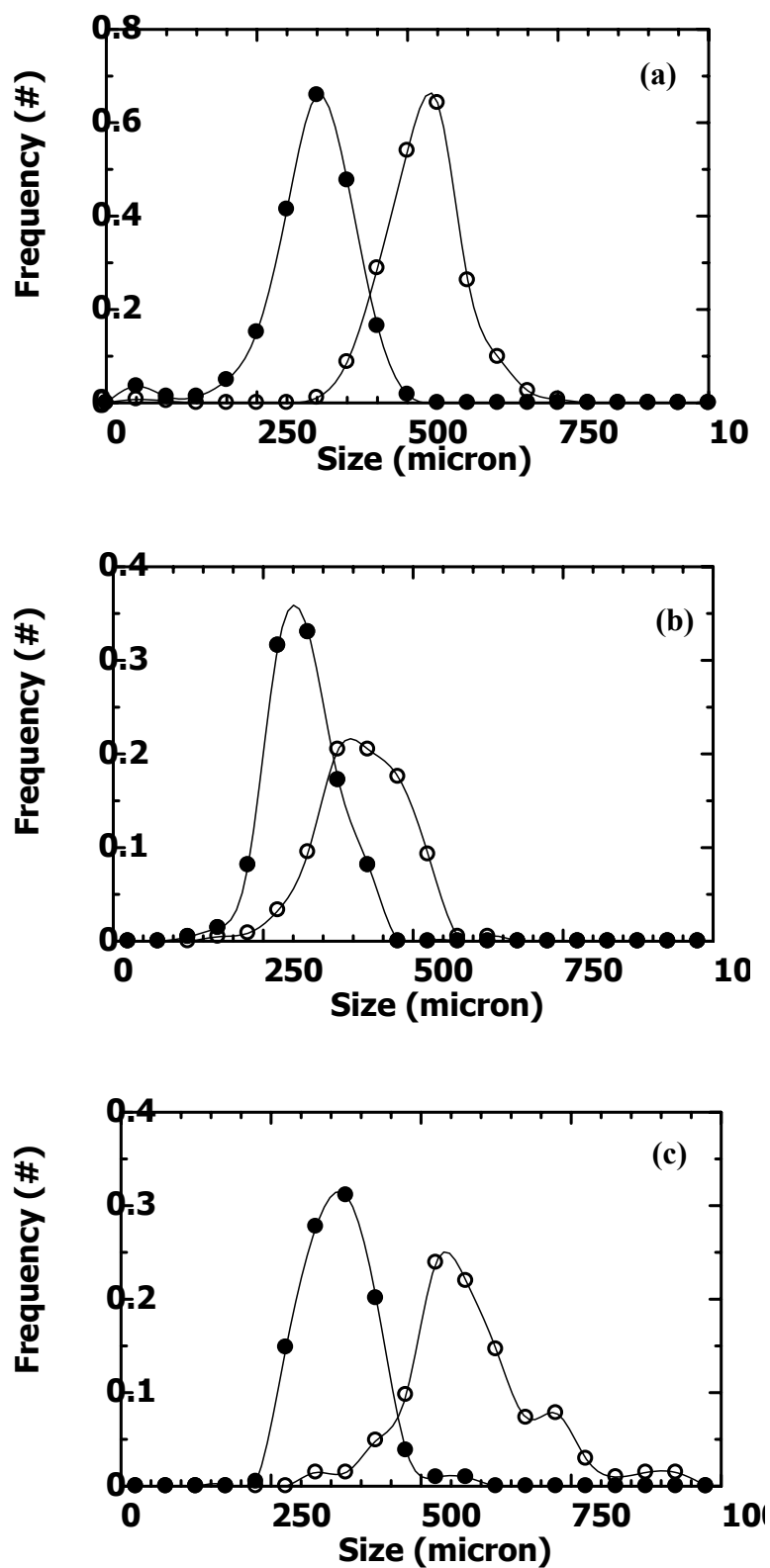


Figure 4.30 CSD of (a) potash alum crystals (b) KDP crystals (c) K_2SO_4 crystals at

2.20% relative supersaturation; ● Initial time; ○ final time

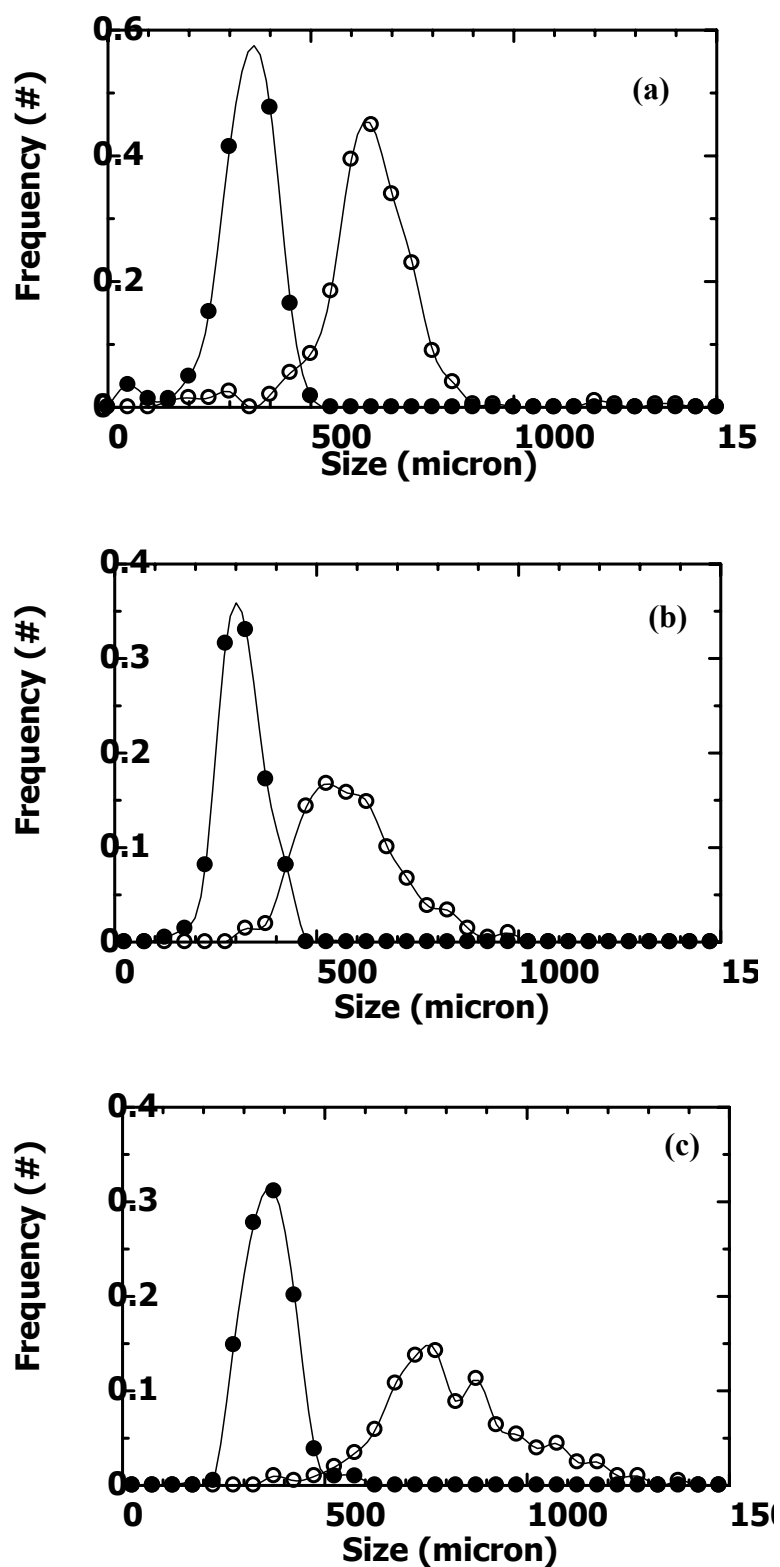


Figure 4.31 CSD of (a) potash alum crystals (b) KDP crystals (c) K_2SO_4 crystals at

5.00% relative supersaturation; ● Initial time; ○ final time

Chapter 5

Conclusions and Recommendation

5.1 Conclusions

5.1.1 There is evidence of growth rate dispersion in all experiments for aqueous system of sucrose, HMT, potash alum, KDP, and K_2SO_4 , showing that individual crystals grown under identical conditions do not have identical growth rates. In each system, the crystals grow at constant rates during the growth period and the growth rates are independent on their initial sizes. This demonstrates that the growth rates correspond to the constant crystal growth (CCG) model, not the random fluctuation (RF) model or the size dependent growth (SDG) model. The dispersion of rate is also found in the dissolution process of crystals, and the model for the dissolution rates is called the constant crystal dissolution (CCD) model.

5.1.2 GRD is apparent in systems which have very different thermodynamic properties, i.e. solubility and metastable limit, different crystal morphology, and different types of molecular bonds which support the idea that GRD occurs more or less in all the crystallizing systems, and this can affect the CSD of product crystals.

5.1.3 The growth rate distributions of all crystals in this study; sucrose, HMT, potash alum, KDP and K_2SO_4 are approximately normally distributed, unless the mean growth rate is very small, which limits the range of spread below the mean growth rate. In this case the distribution may appear more log-normal.

5.1.4 Although the growth rates of the crystals generally followed the CCG model, the crystals, in some conditions, they did not follow the CCG. This case was found only when special conditions were applied to alter the crystal surface. In these cases a healing period occurred before the growth rate became the constant growth rate.

5.1.5 All crystallizer types showed evidence of GRD in all conditions. Thus, it can be concluded that GRD is not only an artifact of crystallizers. Under certain conditions (stagnant solutions) the growth rate distribution was similar for all crystallizers. Under convection conditions, the small-cell crystallizer under-predicted the mean growth rate but over-predicted the dispersion. Very large GRD may be an artifact of the cell, as suggested by the CFD simulation results showing that there is variation in the hydrodynamic conditions in the small-cell crystallizers. The effect of the front-position crystals for the behind-position crystals and the effect of the attachment position of the crystals on the glass-cover slip were also very significant.

5.1.6 Both the diffusion and surface integration mechanisms are responsible for GRD. Significant GRD in growth controlled by diffusion was found in the system of HMT crystals in aqueous solutions under stagnant condition. Under this condition, the mean growth and dissolution rates of HMT are equal, suggesting that the mechanism controlling the two processes are the same, which is the diffusion mechanism. The rate dispersions found both in the growth and dissolution process of HMT represent the GRD and DRD in the diffusion step. The GRD in the surface integration step was confirmed by the results of the growth of sucrose and HMT crystals under strong convection conditions. Under these conditions, the surface integration step is significant for the growth rates of the crystals because the relative

velocity of the solution and the crystal, which maximizes the diffusion step, is very large. In all strong convection conditions, there is evidence of GRD and DRD for HMT and sucrose systems.

5.1.7 The flow orientation around the crystals was investigated as the cause of the GRD in the diffusion step. It was found by varying the crystal orientation in a solution flow that the facial growth rates could be varied. However, this cause is probably found mostly in the equipment where the crystals were fixed such as in the cell crystallizers. It may not be significant for batch crystallizers or other suspension crystallizers where the orientation of the crystal randomly changes due to fluid motion.

5.1.8 A new mechanism has been proposed to explain GRD in the surface integration mechanism; the effect of growth history in terms of microscopic surface roughness on the crystal growth rates. The results showed that the surface of the crystal changed when the supersaturation changed. The higher the supersaturation level used, the rougher the surface of the crystal formed. It was found that the surface roughness has a size range between 0.5-10 micrometer, which is far greater than the size of molecules (where the size is in the nanometer scale), so it is believed that the surface roughness is caused by the group of clusters (more than 100 molecules) integrated on the absorbed layer of crystals. Larger surface features (1 μ m or larger)

5.1.9 The effect of microscopic surface roughness showed that the crystals grown from very high supersaturation, having high surface roughness, will grow at a lower rate than the crystals having smooth surface, which were initially grown in low supersaturation. This is because the degraded surface of rougher surfaced crystals has to be improved before further growth, a process called 'healing'.

5.1.10 The growth during the healing period depends on the type and properties of the crystals. In this study, only the time required for healing of sucrose system was investigated. It is also interesting that the thickness of the crystal layer required to heal the surface (which can be calculated from the growth rate and healing time) is in excess of 100 micrometers. This is far greater than the magnitude of the microscopic roughness, which is of the order of 10 micrometers. This suggests that a significant amount of good quality crystal lattice is required at the surface of the crystal for the crystals to grow at their normal rate.

5.1.11 It was clear from the results that the growth rate history of each type of crystal can be related to the degree of GRD. This can be shown from the values of the relative growth rate, the higher values of relative growth rate relate to the higher magnitudes of GRD. Due to the hypothesis that the larger amount of surface roughness is caused by the higher surface energy, the relationship of the magnitude of GRD in each crystal, and the surface energy value (γ), was also investigated. The important results showed a correlation that the system having higher surface energy also has higher magnitude of GRD.

5.1.12 Although GRD is still not fully understood, the results from this work demonstrate a stronger understanding of the cause and mechanism of GRD than has been understood previously.

5.2 Recommendation

5.2.1 In order to use the small-cell crystallizer in the stagnant case, it is recommended that the crystals attached on the glass cover-slip should be far enough apart to ensure that the local supersaturations are similar. In the case for nucleation

study, it should be noted that the growth rate data may not be accurate enough if the distance between each nuclei formed are very close. This is very difficult to obtain for contact nucleation experiments. The suitable distance to attach the crystal over the glass cover-slip was not studied to obtain an exact value, but about 5 mm. distance is recommended, because the growth rate of each crystal does not change within 5 hours. The cell should not be used for convection conditions if accurate growth rate distributions are required.

5.2.2 To model the GRD phenomenon, three important parameters have to be taken into account including surface energy of the crystal, levels of supersaturation during growth, and the growth temperature.

5.2.3 As this work proposed the mechanism that the microscopic roughness is due to the size of clusters generate on the crystal surface, the work should be further studied as a function of temperature or as a function of degree of supersaturation. The higher temperature increases the thermal energy for the systems which can lead to the smaller size of the clusters formed. In addition, the higher degree of supersaturation forces a higher concentration at the adsorbed layer, resulting in larger sizes of the clusters.

References

- Bennema, P. and van der Eerden, J. P. (1977). On the nature of crystal growth from the melt. **J. Crystal Growth** 42: 201-207.
- Bourne, J. R. and Davey, R. J. (1976a). The growth of hexamethylene tetramine crystals from ethanolic solutions: I. The surface entropy factor. **J. Crystal Growth** 36: 278-286.
- Bourne, J. R. and Davey, R. J. (1976b). The role of solvent-solute interactions in determining crystal growth mechanisms from solution: II. The growth kinetics of hexamethylene tetramine. **J. Crystal Growth** 36: 230-238.
- Bourne, J. R. and Davey, R. J. (1978). α -Factor for solution growth with special reference to glyceryl tristearate. **J. Crystal Growth** 43: 224-228.
- Dirksen, J. A. and Ring, T. A. (1991). Fundamental of crystallization "kinetic effects on particle size distribution and morphology". **Chem. Eng. Sci.** 46: 2389-2427.
- Fabian, J., Hartel, W. R. and Ulrich, J. (1996). **Crystal Growth Org. Mat.** 96: 216-218.
- Garside, J. and Larson, M. A. (1978). Direct observation of secondary nuclei production. **J. Crystal Growth** 43: 694-704.
- Garside, J. (1979). Growth of small crystals. **Industrial Crystallization** 78: 143-151.
- Garside, J. and Ristić, R. I. (1983). Growth rate dispersion among ADP crystals formed by primary nucleation. **J. Crystal Growth** 61: 215-220.
- Garside, J. (1985a). Industrial crystallization from solution. **Chem. Eng. Sci.** 40: 3-26.
- Garside, J. (1985b). Advances in the characterization of crystal Growth **AIChE Symp. Series** 80: 23-35.

- Harding, M. M., Rule, R. J., Oldman, R. J. and Davey, R. J. (1992). Growth rate dispersion in small crystals and its relation to mosaic spread. **J. Crystal Growth** 123: 373-384.
- Herden, A. and Lacmann, R. (1997). The crystallization of potassium nitrate II. Growth rate dispersion. **J. Crystal Growth** 179: 592-604.
- Jackson, K. G., Uhlmann, D. R. and Hunt, J. D. (1967). On the nature of crystal growth from the melt. **J. Crystal Growth** 1: 1-36.
- Janse, A. H. and de Jong, E. J. (1976). The occurrence of growth dispersion and its consequences. **Industrial Crystallization** 75: 145-154.
- Jones, C. M. and Larson, M. A. (1999). Characterizing Growth-Rate Dispersion of NaNO₃ secondary Nuclei. **AIChE J.** 45: 2128-2135.
- Lacmann, R. and Tanneberger, U. (1995). Growth rate dispersion of single potassium alum crystals. **J. Crystal Growth** 147: 194-199.
- Liang, B. M., Hartel, R. W. and Berglund, K. A. (1987). Growth rate dispersion in seeded batch sucrose crystallization. **AIChE J.** 33: 2077-2079.
- Mathlouthi, M. and Cedus, R. (1995). **Sucrose properties and applications** Glasgow: Blackie Academic and Professional.
- McCabe, W. L. (1929). Crystal growth in aqueous solutions: I – Theory. **Industrial and Engineering Chemistry** 21: 30-33.
- Mitrović, M. M., Žekić, A. A. and Petruševski, Lj. S. (1987). Growth rate dispersion of small KDP crystals. **J. Crystal Growth** 198/199: 687-691.
- Mitrović, M. M. (1987). Growth rate dispersion of small rochelle salt crystals. **J. Crystal Growth** 265: 411-416.

- Mitrović, M. M. (1995). Connection between growth rate dispersion of large rochelle salt crystals and growth rate dispersion of their seeds. **J. Phys. Chem.** 99: 5438-5444.
- Mitrović, M. M. (1997). Growth rate dispersion of small KDP crystals. **J. Crystal Growth** 265: 315-319.
- Mullin, J. W. (2001). **Crystallization**, 4th Ed. Oxford: Butterworth-Heinemann Ltd.
- Randolph, A. D. and Larson, M. A. (1988). **Theory of particulate processes: Analysis and techniques of continuous crystallization**, 2nd Ed. California: Academic Press, INC.
- Ristić, R. I., Sherwood, J. N. and Wojciechowski, K. (1988). Assessment of the strain in small sodium chlorate crystals and its relation to growth rate dispersion. **J. Crystal Growth** 91: 163-168.
- Ristić, R. I., Sherwood, J. N. and Shripathi T. (1990). Strain Variation in the {100} growth sectors of Potash Alum single crystals and its relationship to growth rate dispersion. **J. Crystal Growth** 102: 245-248.
- Söhnel, O. and Garside, J. (1992). **Precipitation: Basic principles and industrial applications** Oxford: Butterworth-Heinemann Ltd.
- Tanneberger, U., Lacmann, R., Herden, A., Klapper, H., Schmiemann, D., Becker, R. A., Mersmann, A. and Zacher, U. (1996). The dispersion of growth rate as a result of different crystal perfection. **J. Crystal Growth** 166: 1074-1077.
- Tavare, N. S. (1985). Crystal growth rate dispersion. **Can. J. Chem. Eng.** 63: 436-442.
- Teodossiev, N. (1987). Growth rate dispersion of small ammonium alum crystals. **J. Crystal Growth** 80: 198-202.
- Ulrich, J., and Kruse, M. (1990), **Proceeding of the 11th Symposium on Industrial Crystallization** 1: 361-366.

- Wang, S., Mersmann, A. and Kind, M. (1990). Verification of the constant crystal growth model for attrition particles and its relevance to the modeling of crystallizers. **J. Crystal Growth** 99: 1104-1107.
- Westhoff, G. M., Butler, B. K., Kramer, H. J. M. and Jansens, P. J. (2002). Growth behavior of crystals formed by primary nucleation on different crystallizer scales. **J. Crystal Growth** 237-239: 2136-2141.
- White, E. T. (1967). Enthalpy composition diagram and other data of hexamine-water system. **J. Chem. Eng. Data** 12: 285-288.
- White, E. T. and Wright, P.G. (1971). Magnitude of size dispersion effects in crystallization. **J. Crystal Growth** 67: 81-87.
- Zacher, U. and Mersmann, A. (1988). The influence of internal crystal perfection on growth rate dispersion in a continuous suspension crystallizer. **J. Crystal Growth** 147: 172-180.
- Zumstein, R. C. and Rousseau, R. W. (1987). Growth rate dispersion by initial growth rate distributions and growth rate fluctuations. **AIChE J.** 33: 121-129.

Appendix A
Solubility Data

A.1 Sucrose

The solubility data of sucrose-water system proposed by Mathlouthi and Cedus (1995) is given in Equation (A.1).

$$C_s = 64.47 + 0.10336T + 0.001424T^2 - 0.0000006020T^3 \quad (\text{A.1})$$

where C_s = Saturation conc. (g sucrose/100g solution)

T = Temperature ($^{\circ}\text{C}$)

A.2 Hexamethylene tetramine (HMT)

The solubility data of HMT in water are shown in Table A.1 (White, 1967).

Table A.1 Solubility of HMT (g) in 100 g of solution

T, $^{\circ}\text{C}$	0	10	20	30	40	50	60	70	80	90
X	472	469	466	463	461	459	457	456	456	458

A.3 Potassium aluminium sulphate (potash alum)

The solubility data of potash alum in water are shown in Table A.2 (Mullin, 2001).

Table A.2 Solubility of potash alum in water (g of anhydrous per 100 g of water)

T, $^{\circ}\text{C}$	0	10	20	30	40	60	80
x	3.0	4.0	5.9	8.4	11.7	24.8	71.0

A.4 Potassium dihydrogen phosphate (KDP)

The solubility data of KDP in water are shown in Table A.3 (Mullin, 2001).

Table A.3 Solubility of KDP in water (g of anhydrous compound per 100 g of water)

T, °C	0	10	20	30	40	50	60
x	15.9	18.3	22.6	27.7	33.5	50.0	70.4

A.5 Potassium sulphate (K₂SO₄)

The solubility data of K₂SO₄ in water are shown in Table A.4 (Mullin, 2001).

Table A.4 Solubility of K₂SO₄ in water (g of anhydrous compound per 100 g of water)

T, °C	0	10	20	30	40	50	60
x	7.4	9.3	11.1	13.1	14.9	18.3	21.4

Appendix B

Determination of Surface Energy (γ)

The general equation used to determine the surface energy parameter is the primary nucleation equation as expressed in Equation B.1 (Bourne and Davey, 1976).

$$B = g_k \cdot \exp\left[\frac{-\beta N_o M^2 \gamma^3}{R^3 \rho^2 T^3 \ln^2(x/x_s)}\right] \quad (\text{B.1})$$

$$g_k = k \cdot \ln^{-3}(x/x_s) \quad (\text{B.2})$$

where	B	= Nucleation rate (#·m ⁻³ ·s ⁻¹)
	β	= Geometric factor
	N _o	= Avogadro number (6.023 × 10 ²³ mol ⁻¹)
	M	= Molecular weight (g·mol ⁻¹)
	γ	= Surface energy (J·m ⁻²)
	R	= Gas constant (8.314 J·K ⁻¹ ·mol ⁻¹)
	ρ	= Solid density (kg·m ⁻³)
	T	= Temperature (K)
	x	= Mole fraction of solute in supersaturation solution
	x _s	= Mole fraction of solute in saturation solution
	k	= Constant

By substituting g_k term in Equation (B.2) into Equation (B.1), Equation (B.1) becomes

$$B = \left(k \cdot \ln^{-3}(x/x_s) \right) \frac{\beta N_o M^2 \gamma^3}{R^3 \rho^2 T^3 \ln^2(x/x_s)} \quad (B.3)$$

Then taking logarithm of Equation (B.3) to obtain Equation (B.4) and rearranging Equation (B.5) into Equation (B.6).

$$\ln B = \ln \left(C \ln^{-3}(x/x_s) \right) - \frac{\beta N_o M^2 \gamma^3}{R^3 \rho^2 T^3 \ln^2(x/x_s)} \quad (B.4)$$

$$\ln B = -3 \ln \ln(x/x_s) + \ln C - \frac{\beta N_o M^2 \gamma^3}{R^3 \rho^2 T^3 \ln^2(x/x_s)} \quad (B.5)$$

$$\ln B + 3 \ln \ln(x/x_s) = \ln C - \frac{\beta N_o M^2 \gamma^3}{R^3 \rho^2 T^3 \ln^2(x/x_s)} \quad (B.6)$$

By comparing Equation (B.6) to the linear equation; $Y = a.X + b$, if the term $\ln B + 3 \ln \ln(x/x_s)$ is set as Y and the term $\ln^{-2}(x/x_s)$ is X . The slope of the plot or a is

$$\text{slope} = \frac{\beta N_o M^2 \gamma^3}{R^3 \rho^2 T^3} \quad (B.7)$$

The surface energy parameter (γ) can therefore be calculated as shown in Equation (B.8).

$$\gamma = \left[\text{Slope} \cdot \left(\frac{R^3 T^3 \rho^2}{-\beta N_o M^2} \right) \right]^{1/3} \quad (B.8)$$

To get the plot of $[\ln B + 3 \ln \ln(x/x_s)]$ and $[\ln^{-2}(x/x_s)]$, the primary nucleation rate (B) as a function of supersaturation level (x) must be known. The

primary nucleation rate can be determined by using the relationship of number of surface nuclei and time as written in Equation (B.9)

$$N = B.t \quad (B.8)$$

where N = Number of crystals (#)

t = Time (s)

The number of nuclei at each relative supersaturation when the time progressed of potash alum and KDP crystals obtained from Coulter Counter are depicted in Figure B.1 and Figure B.2, respectively. From the plots, the nucleation rate can be obtained from the slope of the plot after induction period; about 480 sec for potash alum and 240 sec for KDP crystals. The slope or nucleation rate at each condition is reported in Table B.1.

Table B.1 Primary nucleation rate (B) of potash alum and KDP crystals as a function of relative supersaturation levels

Potash alum crystal		KDP crystal	
Ratio of x/x_s	Primary nucleation rate, B ($\# \cdot \text{cm}^{-3} \cdot \text{s}^{-1}$)	Ratio of x/x_s	Primary nucleation rate, B ($\# \cdot \text{cm}^{-3} \cdot \text{s}^{-1}$)
1.086	6.10	1.078	32.63
1.093	25.57	1.087	140.76
1.10	43.19	1.093	408.87

Based on Equation (B.6), the slope of the plot of $\ln B + 3 \ln \ln(x/x_s)$ and $\ln^{-2}(x/x_s)$ have to be used to find the surface energy. The plots for potash alum and

KDP crystals are shown in Figure B.3. The surface energy of each crystal was calculated by using Equation (B.8). By using the physical data in Table B.2, the surface energy of potash alum is $1.27 \text{ erg}\cdot\text{cm}^{-2}$ and KDP is $9.52 \text{ erg}\cdot\text{cm}^{-2}$.

Table B.2 Physical properties of potash alum and KDP crystal for surface energy calculation

Physical properties	Potash alum	KDP
Molecular weight ($\text{g}\cdot\text{mol}^{-1}$)	474.39	136.1
Density ($\text{g}\cdot\text{cm}^{-3}$)	1.3	1.7
Temperature (K)	297.45	297.45
β	32	32

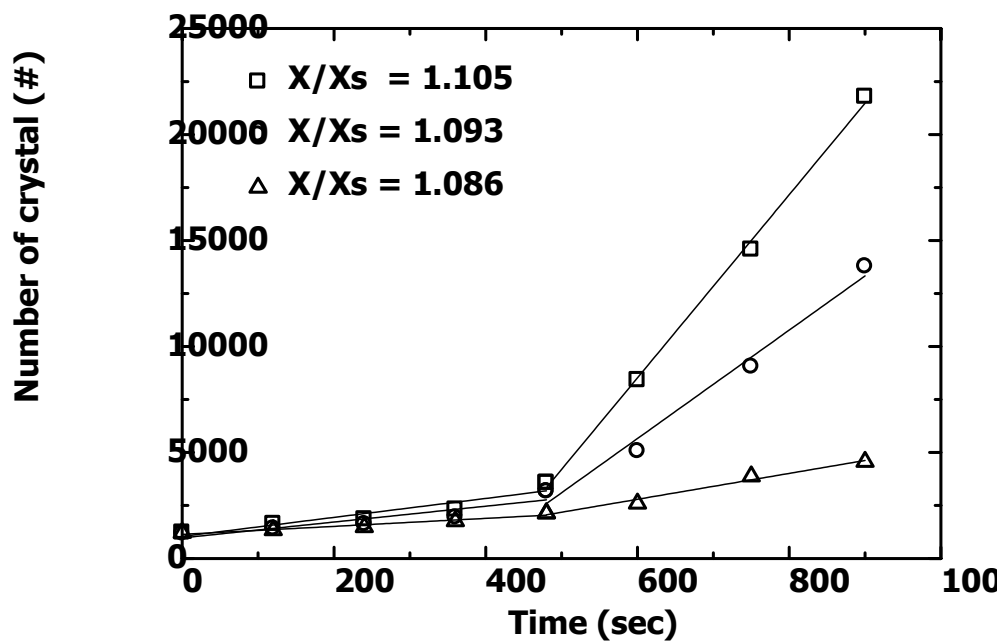


Figure B.1 Number of potash alum nuclei from primary nucleation experiment as a function of time

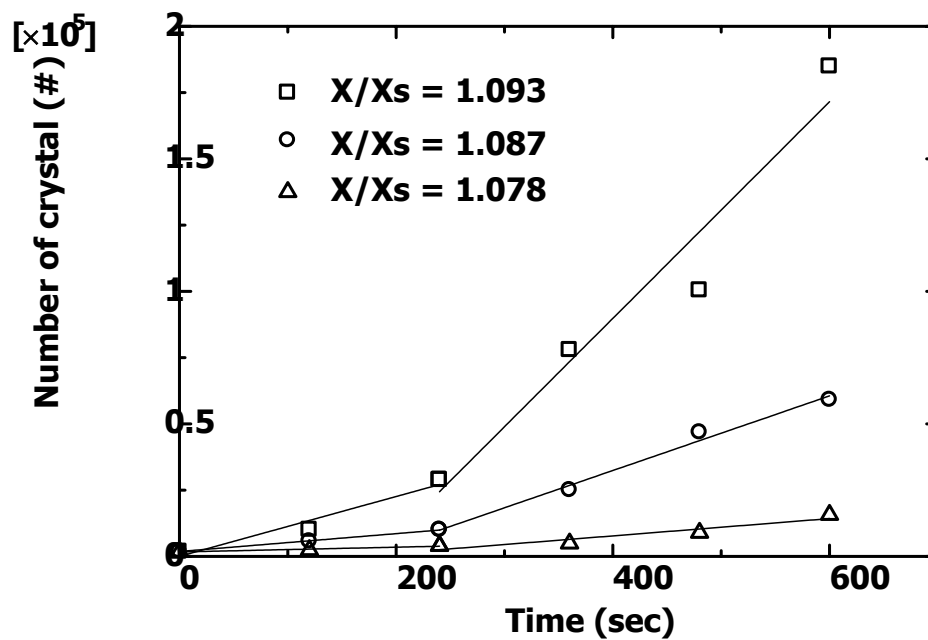


Figure B.2 Number of KDP nuclei from primary nucleation experiment as a function of time

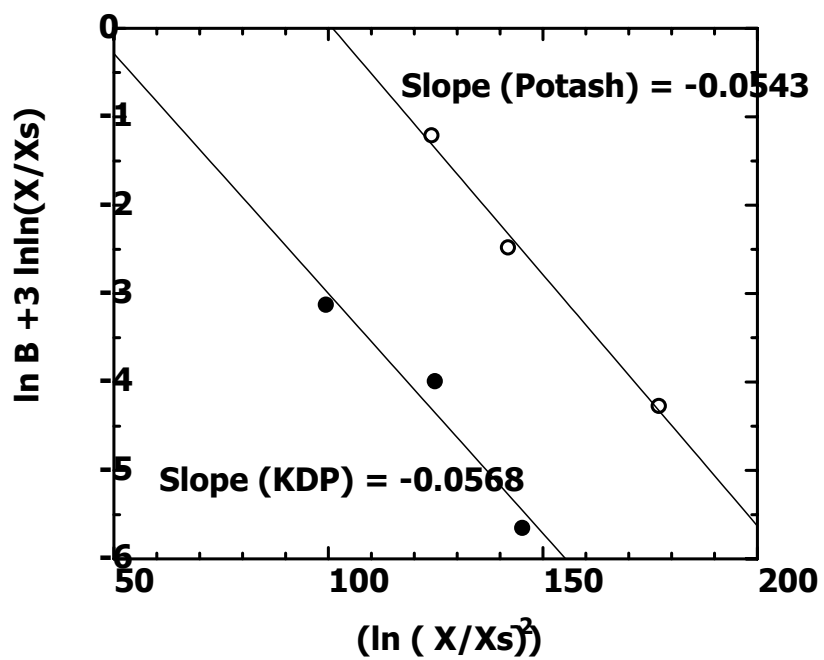


Figure B.3 Plots of $\ln B + 3 \ln \ln(x/x_s)$ and $\ln^{-2}(x/x_s)$ for potash alum and KDP

CD of Experimental Data

Biography

Miss Pareena Pantaraks was born on July, 27, 1977 in Cholburi Province. She graduated with the bachelor degree of chemical engineering with second class honor in 1999 from Suranaree University of Technology (SUT) and the masters degree of chemical engineering in 2001 from the Chemical Engineering Practice School, King Mongkut's University of Technology Thonburi (KMUTT). She has received an RGJ Ph.D. scholarship from the Thailand Research Fund (TRF) to study the doctoral degree of chemical engineering at Suranaree University of Technology since 2001.